



Universidade do Minho
Escola de Engenharia

Emma del Carmen González González

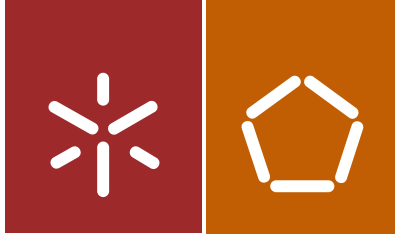
LAOS characterization of
polymer modified bitumens

Emma del Carmen González González LAOS characterization of polymer modified bitumens

UMinho | 2015



July 2015



Universidade do Minho
Escola de Engenharia

Emma del Carmen González González

LAOS characterization of
polymer modified bitumens

Master thesis
European Master's in Engineering Rheology

Work performed under the guidance of
Loic Hilliou, PhD.
Hugo Manuel Ribeiro Dias da Silva, PhD.



July 2015

DECLARAÇÃO

Nome: Emma del Carmen González González

Endereço electrónico: jainnark@yahoo.com.mx

Número do Passaporte: G05975477

Título dissertação: LAOS characterization of polymer modified bitumens

Orientador: Loic Hilliou, PhD.

Co-Orientador: Hugo Manuel Ribeiro Dias da Silva, PhD

Ano de conclusão: 2015

Designação do Mestrado:

European Master's in Engineering Rheology

É AUTORIZADA A REPRODUÇÃO PARCIAL DESTA TESE/TRABALHO (indicar, caso tal seja necessário, n.º máximo de páginas, ilustrações, gráficos, etc.) APENAS PARA EFEITOS DE INVESTIGAÇÃO, MEDIANTE DECLARAÇÃO, ESCRITA DO INTERESSADO, QUE A TAL SE COMPROMETE;

Universidade do Minho, ____/____/____

Assinatura: _____

Acknowledgements

I would like to thank to all the people who helped me during the development this work.

I want to specially thank to my supervisors PhD. Loic Hilliou and PhD. Hugo Manuel Ribeiro Dias da Silva who kindly guided me during the research project; their advice and feedback was key for the completion of this work.

I would like to acknowledge that this master thesis was done in the frame of the project PLASTICROADS (PTDS/ECM/119179/2010). In this regard I want to thank the researcher of this project M. Sc. Liliana Costa for the incommensurable help she gave me during all the stages of the project.

I would like to acknowledge that this Master's thesis is part of the Erasmus Mundus in Engineering Rheology (EURHEO) Program. In this respect, I am very thankful with the EURHEO consortium for its academic and financial support through all the Master's, since my first academic year at KULeuven, Belgium until the closure of my research project at UMinho, Portugal.

I would like to specially thank to the Civil Engineering department at UMinho for its financial support, and to its staff namely Eng. Carlos Palha and Eng. Hélder Torres for its academic support given to this research project, as well as PIEP Institute and Polymers engineering department at UMinho and its staff for the facilities and equipment used during this project.

Finally, I would like to thank to my family and friends, because thanks to their love and advice I got the strength to finish this project.

To my family with love

Abstract

In the present work, large amplitude oscillatory shear (LAOS) coupled with Fourier transform rheology (FTR) were used for the first time to characterize the nonlinear rheology of bituminous binders, including two polymer modified bitumens (PMB) containing EVA and HDPE. Additionally, a brief study in the linear regime was done to complete the rheological characterization along with morphological characterization of PMBs by means of fluorescent optical micrographs. The comparison between the LAOS-FTR characteristics of samples was done using a rheological approach (all binders compared at either same phase shift angle δ or same Deborah number, De) and an experimental approach (all binders compared at same frequency). In all the approaches, EVA PMB had the lowest nonlinear levels compared to HDPE PMB. Furthermore differences in the nonlinearity among PMBs, parent 70/100 pen grade bitumen, and benchmark 35/50 pen grade bitumen were also found. The LAOS-FTR fingerprint of bituminous binders, though unique, held some similitudes with the reported FTR spectra of multiphase and polymeric systems. For characterization of asphalt binder in the nonlinear regime, the strength of LAOS-FTR technique over stress relaxation one was confirmed, not only in terms of the sensitivity but also in terms of the results interpretation. Furthermore LAOS-FTR was used to analyze time sweep data with the aim to propose FTR quantifiers as indices to predict fatigue performance.

Keywords: LAOS, Fourier Transform Rheology, nonlinear rheology, bitumen, PMB, fatigue, FOM.

Resumo

Neste trabalho utilizou-se pela primeira vez a técnica *Large Amplitude Oscillatory Shear* (LAOS) associada à técnica de *Fourier Transform Reology* (FTR), para caracterizar a reologia não-linear de ligantes betuminosos, nomeadamente betumes modificados com polímeros (PMBs), sendo estes polímeros EVA e HDPE. Para além disso realizou-se um breve estudo no regime linear para completar a caracterização reológica, bem como a caracterização morfológica dos ligantes modificados com polímeros por meio de micrografias óticas fluorescentes. A comparação entre as características LAOS-FTR das amostras foi realizada usando uma abordagem reológica (todos os ligantes foram comparados estando no mesmo ângulo de fase δ ou no mesmo número de Deborah, De) e uma abordagem experimental (todos os ligantes foram comparados à mesma frequência). Em todas as abordagens, EVA PMB apresentou níveis mais baixos de não-linearidade quando comparado com o PEAD PMB. Além disso foram encontradas diferenças na não-linearidade entre os PMBs, o betume base de penetração 70/100 e o betume usado como referência com penetração 35/50. O comportamento LAOS-FTR característico dos ligantes betuminosos, embora único, apresentou algumas semelhanças com os espectros FTR de sistemas multifásicos e poliméricos encontrados na literatura. A superioridade da técnica LAOS-FTR, na caracterização em regime não linear de ligantes de betuminosos, em comparação com as técnicas de *stress relaxation* foi confirmada, não só em termos da sensibilidade, mas também em termos de a interpretação dos resultados. Além disso LAOS-FTR foi usado para analisar dados de *time sweep* com o objetivo de propor quantificadores FTR como índices para prever o desempenho à fadiga.

Table of Contents

1. Introduction	1
1.1. Motivation	1
1.2. Objectives	2
1.3. Strategy	3
1.4. Outline	4
2. Literature review	5
2.1. Large amplitude oscillatory shear and Fourier transform rheology	5
2.1.1. Fourier Transform concept	8
2.1.2. The Discrete Fourier Transform (DFT)	10
2.1.3. Fourier transform matters of practicality	11
2.1.4. Fourier Transform Rheology	14
2.1.5. FTR studies of selected classes of materials	21
2.2. Bitumen basics	25
2.3. Polymer Modified Bitumen (PMB)	29
2.4. Bitumen rheology	33
2.4.1. Linear rheology	33
2.4.2. Nonlinear rheology	35
2.5. Test in binders for performance prediction	39
2.6. Morphological characterization of PMB samples	40
3. Materials and methods	43
3.1. Materials	43
3.2. Methods	45
4. Linear viscoelasticity of asphalt binders and morphological characterization	53
4.1. SAOS test	53

4.2. Stress relaxation in linear regime	55
4.3. PMBs morphology (FOM).....	56
5. Experimental method validation of LAOS-FTR test for binders at room temperature.	61
5.1. Linearity range of ARES rheometer	61
5.2. Experimental conditions for repeatability of LAOS test of binders at room temperature. .	65
5.2.1. Storage duration	66
5.2.2. Torsion bar height	67
6. LAOS characterization of asphalt binders	71
6.1. LAOS asaf of frequency	71
6.2. LAOS at same delta (δ).....	93
6.2.1. Bitumen grades at $\delta \sim 57^\circ$	94
6.2.2. PMBs and 35/50 at $\delta \sim 50^\circ$	97
6.3. LAOS at same Deborah number ($De \sim 0.06$).....	101
7. Stress relaxation test of asphalt binders in NLVE region	107
8. LAOS-FTR test to predict fatigue behavior.....	113
9. Results discussion	121
9.1. Linear viscoelasticity of asphalt binders and morphological characterization	121
9.2. LAOS characterization of asphalt binders	124
9.3. Stress relaxation test of asphalt binders in NLVE region	129
10. Conclusions	133
11. References	139
Appendix A. Trigonometric integrals.....	147
Appendix B. Rheology basics	149
Appendix B.1. Shear stress relaxation	153
Appendix B.2. Oscillatory shear	155

Appendix C. Extra Lissajous curves..... 159

List of figures

Figure 2-1 Schematic representation of a LAOS test: time (up) and frequency domain (down), adapted from [1].	5
Figure 2-2 Representation of the four canonical behaviors of G' and G'' in LAOS tests, from [1]	6
Figure 2-3 The four characteristic functions in time domain (from left to right): a sine, a rectangular, a triangular and a saw tooth shaped wave, representing: viscoelastic, strain softening, strain hardening, and shear bands. Adapted from [1]	7
Figure 2-4 Analysis of stress curves in time domain based of curve tilting respect to a pure sinusoidal: stress curves (left) and half cycle comparison with a sinusoidal curve (right). Adapted from [1].	7
Figure 2-5 Lissajous plots: in LVE region (left) and in NLVE region (right).	8
Figure 2-6 Representation of a sinusoidal wave in (left) time domain and in (right) frequency domain.	9
Figure 2-7 Spectra of a square periodic wave composed of several sinusoidal signals, adapted from [4].	9
Figure 2-8 Representation of aliasing. Adapted from [4].	12
Figure 2-9 Periodic signal (up), integer (middle) and non-integer (down) number of cycles windowed, adapted from [4].	13
Figure 2-10 Representation of a symmetric (left) and a non-symmetric wave (right) along with its FT spectra [1]. .	19
Figure 2-11 $I_3/I_1\%$ at 1 Hz for dispersions of PS-PBA coated with AA and ACM: E base suspension undiluted, E.1 and E.2 are water dilutions of E suspension, and A.1 is dispersion of uncoated particles [14].	22
Figure 2-12 Microstructure of PS and iso-dioctyl phthalate	24
Figure 2-13 FTR behavior of entangled PS solutions (linear and branched) in iso-dioctyl phthalate at different weight concentration and at $\gamma = 2$: (left) I_3/I_1 signal and (right) Φ_3 signal asaf of De [13].	24
Figure 2-14 Nonlinear response of a cis- 1,4 polybutadiene loaded with 0.258 volume fraction of carbon black: (upper curve) total harmonicity, (middle curve) $I_3/I_1\%$, different than (lower curve) $I_5/I_1\%$. Adapted from [10].	25
Figure 2-15 Bitumen 35/50 (left) in the liquid state at $T > 60^\circ\text{C}$ and (right) in the semi-solid state at room temperature.	26
Figure 2-16 Colloidal representation of bitumen according to the modified Yen model [25]	27
Figure 2-17 Slabs of asphalt mixes: (up) mineral aggregates covered with binder, (down) cross section of a slab. ..	28
Figure 2-18 Representation of the different failures that road pavement undergo: rutting and cracking [27]	28
Figure 2-19 Schematic representation of physical distillation	31
Figure 2-20 Chemical structure and topology of polyethylene	32
Figure 2-21 Chemical structure of poly ethyl-vinyl-acetate (EVA)	32
Figure 2-22 Mechanical spectra for a 70/100 pen bitumen from vacuum distillation \circ elastic modulus (G'), \blacksquare loss modulus (G''), \blacktriangle loss tangent ($\tan \delta$), $T_{\text{ref}}=0^\circ$, adapted from [22].	34
Figure 2-23 Mechanical spectra for a 70/100 bitumen with 7.2% wt. of (radial) SBS \circ elastic modulus (G'), \blacksquare loss modulus (G''), \blacktriangle loss tangent ($\tan \delta$), $T_{\text{ref}}=0^\circ$, adapted from [22].	34

Figure 2-24 Master curves for (a) 150/200 and (b) 60/700 pen grade bitumen modified with a 50:50 mix of EVA and LDPE. Tref=25°C. Adapted from [24].....	35
Figure 2-25 Stress relaxation modulus of a 70/100 pen grade bitumen at 20°C for various strains (left), and after the vertical shift (right) [34].....	36
Figure 2-26 Stress relaxation modulus of a 200/300 pen grade with 8% wt. EVA at 35°C for various strains [34]... 37	37
Figure 2-27 Stress relaxation modulus of a 70/100 pen grade bitumen with 4% wt LLDPE at various strains [34]. . 37	37
Figure 2-28 Qualitative shapes of the four proposed stress relaxation types: a) SBS, b) EVA, c) SEBS, d) PE, [22].	38
Figure 2-29 Flow curves of a 200/300 pen grade bitumen at different temperatures from [36]......	38
Figure 2-30 Flow curves of the previous 200/300 pen grade bitumen with (left) 4 %wt and (right) 8 % wt of EVA from [36].	39
Figure 2-31 Example of a micrography of a sample (SBS PMB) without optical smoothness [42]	41
Figure 3-1 Comparison of data analysis between Orchestrator (rheometer) and LabView (external) software.	49
Figure 3-2 Stress relaxation data analysis: a) raw data acquired from rheometer, b) data obtained at 98% of target strain, c) raw torque and modulus data acquired at 98% of target strain, d) data acquired above the transducer sensitivity limit, e) same as d) showing saturation of data acquisition at ~ 2 s, f) data clean of experimental pitfalls and used for analysis.	50
Figure 4-1 Mechanical spectra of bitumen binders at T~ 20°C: G' filled symbols and G'' unfilled symbols.	53
Figure 4-2 Phase angle of binders asaf of ω at T~20°C.	54
Figure 4-3 Linear stress relaxation modulus of binders at T~20°C.....	56
Figure 4-4 FOM micrograph of 70/100EVA5 binder (a,b,c) and 70/100HDPE5 (d,e,f), acquired from the top part of the glass slide.	57
Figure 4-5 FOM micrograph of 70/100EVA5 binder (a,b,c) and 70/100HDPE5 (d,e,f), acquired from the bottom part of the glass slide.	59
Figure 5-1 Intervals tested to determine the rheometer linearity range: a) strain, b) torque, and c) motor θ	62
Figure 5-2 Leading nonlinear signal (I_3/I_1) of the ARES motor at different frequencies measured with PP (filled symbols) and TB (crossed symbols).....	63
Figure 5-3 Leading nonlinear signal (I_3/I_1) of the ARES transducer at different frequencies measured with PP (filled symbols) and TB (crossed symbols).....	64
Figure 5-4 $I_3/I_1\%$ asaf of torque at 5 Hz. For both geometries used it is depicted the transducer $I_3/I_1\%$ and the motor $I_3/I_1\%$ that corresponded to the given torque: PP (filled symbols) and TB (crossed symbols).....	64
Figure 5-5 Linearity range of ARES rheometer: (left) motor and (right) transducer signal.	65
Figure 5-6 Nonlinear response at different bar heights for all the binders.	67
Figure 6-1 Pipkin diagram of γ vs ω for Lissajous curves of 70/100 binder. Additionally in the horizontal axis the corresponding De and δ values are given.	72

Figure 6-2 Pipkin diagram of γ vs ω for Lissajous curves of 35/50 binder. Additionally in the horizontal axis the corresponding De and δ values are given.	73
Figure 6-3 Pipkin diagram of γ vs ω for Lissajous curves of 70/100HDPE5 binder. Additionally in the horizontal axis the corresponding De and δ values are given.	73
Figure 6-4 Pipkin diagram of γ vs ω for Lissajous curves of 70/100EVA5 binder. Additionally in the horizontal axis the corresponding De and δ values are given.....	74
Figure 6-5 Example of the nonlinear transient response: (left) stress signal decayed over time and tended to leveled off, and (right) the transient was reflected in a halo in the Lissajous curves. Sample 70/100EVA5 at $I_3/I_1=2\%$	75
Figure 6-6 Comparison of odd (left) and even (right) harmonic signals for 35/50 binder at 2Hz.	76
Figure 6-7 First odd harmonics asaf of strain for 35/50 binder at 0.7 Hz.	76
Figure 6-8 Strain for onset of rising of I_3/I_1 signal, for all binders at all the frequencies tested.	77
Figure 6-9 Harmonicity degree for all samples tested asaf of frequency.	78
Figure 6-10 Example of criteria for valid data in LAOS test: a) raw data, b) fitting of transducer and motor signal, the crossover signaled the valid data without motor noise, which are given in c).	79
Figure 6-11 Pipkin diagrams for $I_3/I_1\%$ signal for all binders.....	80
Figure 6-12 $I_3/I_1\%$ data for all samples at all frequencies tested: (unfilled symbols) data free of motor noise, (filled data) data considered for power law, and (solid lines) power law fitting.	81
Figure 6-13 Exponent of the power law fitting asaf of frequency for all the binders.	83
Figure 6-14 Calculated critical strain for onset of I_3/I_1 for all samples at different frequencies.	84
Figure 6-15 Pipkin diagrams for total harmonicity signal for all binders	85
Figure 6-16 Total harmonicity data for all samples at all frequencies tested: (unfilled symbols) data free of motor noise, (filled data) data considered for power law, and (solid lines) power law fitting.	86
Figure 6-17 Exponent values of the odd sum power law fitting asaf of frequency for all the binders.....	87
Figure 6-18 Calculated critical strain for onset of odd sum for all samples at different frequencies	88
Figure 6-19 Relative phase angle at different frequencies asaf of strain for all samples.	89
Figure 6-20 Strain (left) and stress (right) signals to exemplify the general trend of the stress signal to be tilted to the right. Sample 35/50 at 2 Hz and 25% strain.....	90
Figure 6-21 Example of the 1 st harmonic trend asaf of strain.	90
Figure 6-22 Characteristic relative phase angle asaf of frequency for all the binders.	91
Figure 6-23 Relative 3 rd phase angle asaf of De number for all the binders.	92
Figure 6-24 Odd sum fitting parameters re-plotted asaf of delta value (a) pre-exponent and (b) exponent. Characteristic 3 rd harmonic phase angle (c) re-plotted asaf of delta.	93
Figure 6-25 Relative intensity signals for bitumen grades at $\delta \sim 57^\circ$: (unfilled symbols) data free of motor noise, (filled data) data considered for power law, and (solid lines) power law fitting.....	95

Figure 6-26 Phase angle signal asaf of train for binder grades at $\delta \sim 57^\circ$ condition	97
Figure 6-27 Relative intensity signals for bitumen grades at $\delta \sim 57^\circ$: (unfilled symbols) data free of motor noise, (filled data) data considered for power law, and (solid lines) power law fitting.	99
Figure 6-28 Relative phase angle signal asaf of strain for binders at $\delta \sim 50^\circ$	100
Figure 6-29 Relative intensity signals for bitumen grades at $De=0.06$ (unfilled symbols) data free of motor noise, (filled data) data considered for power law, and (solid lines) power law fitting.	103
Figure 6-30 Relative phase angle for binders at $De \sim 0.06$	105
Figure 7-1 Stress relaxation test in nonlinear regime for all binders at $T \sim 20^\circ C$	107
Figure 7-2 Damping function computed for all the binders at $T \sim 20^\circ C$, lines are only to guide the eye.	108
Figure 7-3 <i>Stress relaxation modulus shifted according to the damping function value for all samples.</i>	110
Figure 7-4 Repetition of the stress relaxation test at 0.05% strain for sample 70/100HDPE5 at $T \sim 20^\circ C$: (left) stress relaxation modulus and torque signals, (right) strain signal.	111
Figure 8-1 Time sweeps at same delta and $I_3/I_1=2\%$ for 35/50 and 70/100EVA5 binders.....	114
Figure 8-2 Time sweeps at same delta and $I_3/I_1=3\%$ for 35/50 binder and PMBs.....	115
Figure 8-3 Time sweeps at same delta and $I_3/I_1=4\%$ for PMBs.	116
Figure 8-4 $I_3/I_1\%$ signal asaf of cycles number for all binders (log-log representation).	117
Figure 9-1 Mechanical spectrum of binder grades: data of 70/100 binder were horizontally shifted by 10Hz to overlap the 35/50 data.	122
Figure 9-2 I_3/I_1 signal for all binders asaf of De at an arbitrary 20.3% strain	126
Figure 9-3 Binders $I_3/I_1\%$ response at specific frequencies that shown a bump in the nonlinear signal.	128
Figure B-1 Schematic representation of simple shear flow (left), and simple shear deformation (right).	149
Figure B-2 Schematic representation of drag and pressure flows.	150
Figure B-3 Geometries available to study shear deformation in rotational rheometers, adapted from [58].	150
Figure B-4 Schematic representation of strain controlled and stress controlled rheometers, adapted from [60].	151
Figure B-5 Schematic representation of a stress relaxation experiment: strain imposed (left), canonical responses per material type (right).....	154
Figure B-6 Schematic representation of a Maxwell model mechanical spectra.	158
Figure C-1 Lissajous curves for binder samples at $\delta \sim 57^\circ$	159
Figure C-2 Lissajous curves for binder samples at $\delta \sim 50^\circ$	160
Figure C-3 Lissajous curves for binders at $De \sim 0.06$	161

List of tables

Table 2-1 Fourier analysis techniques.....	10
Table 2-2 Bitumen composition and basic characteristics according to the SARA fractions [22]	26
Table 3-1 Polymer transition temperatures	43
Table 3-2 PMBs specs	44
Table 3-3 Clamping force used to lock the samples in the rectangular geometry.....	46
Table 3-4 Data acquisition details for FFT computation	47
Table 4-1 Crossover frequency of the different binders at T~ 20°C.....	55
Table 5-1 Experimental conditions studied to determine the linearity range of the ARES rheometer.	62
Table 5-2 Statistical analysis of linear and nonlinear parameters asaf of the days in the freezer	66
Table 5-3 Frequencies used in the LAOS tests for bar height determination.....	67
Table 5-4 Relative standard deviation associated to the experimental repeatability.....	68
Table 5-5 Repeatability results for power law fitting of ATBs at 2.5 cm height	69
Table 6-1 Experimental conditions for LAOS tests at different frequencies	71
Table 6-2 Power law fitting results of I_3/I_1 signal for all binders at different frequencies.....	82
Table 6-3 Power law fitting results of odd sum signal for all binders at different frequencies.....	87
Table 6-4 Characteristic relative phase angle of the 3 rd harmonic for all the samples at different frequencies.	89
Table 6-5 Experimental conditions for $\delta \sim 57^\circ$	94
Table 6-6 Harmonicity degree found in both bitumen grades at $\delta \sim 57^\circ$	94
Table 6-7 Power law fitting results of nonlinear signals for binder grades at $\delta \sim 57^\circ$	94
Table 6-8 Limit condition for nonlinear signal used to compute the critical strains, as well as the sample from which the limiting value was obtained.	96
Table 6-9 Critical strains for nonlinear signals at $\delta \sim 57^\circ$ condition.....	96
Table 6-10 Characteristic relative phase angle data for different harmonics of bitumen grades at $\delta \sim 57^\circ$	97
Table 6-11 Experimental conditions for $\delta \sim 50^\circ$	97
Table 6-12 Harmonicity degree for binders at $\delta \sim 50^\circ$	98
Table 6-13 Power law fitting results of nonlinear signals for binder grades at $\delta \sim 50^\circ$	98
Table 6-14 Critical strains for nonlinear signals at $\delta \sim 50^\circ$ condition.....	100
Table 6-15 Characteristic relative phase angle data for different harmonics of bitumen grades at $\delta \sim 57^\circ$	101
Table 6-16 Experimental conditions for $De \sim 0.06$	102
Table 6-17 Harmonicity degree for binders at $De \sim 0.06$	102
Table 6-18 Power law fitting results of nonlinear signals for binder grades at $De \sim 0.06$	103

Table 6-19 Critical strains for nonlinear signals at $De=0.06$ condition	104
Table 6-20 Relative phase angle for binders at $De \sim 0.06$	105
Table 7-1 Damping function sigmoidal fitting and time validity.	109
Table 8-1 Experimental conditions for time sweep tests in NLVE regime.	113
Table 8-2 Results summary of time sweep tests.....	118
Table 9-1 Computed $53\Phi_3 - \Phi_5$ to support the existence of a relationship between relative phase angles of binders	127
Table 9-2 Frequencies at which binders shown a bump in the $I_3/I_1\%$ signal.....	127
Table 9-3 Comparison between LAOS/FTR and stress relaxation tests for nonlinear characterization.....	131

Nomenclature, abbreviations and acronyms

Nomenclature

Ca	Capillary number [-]
De	Deborah number [-]
G	shear modulus [Pa]
$G(t)$	linear stress relaxation modulus [Pa]
$G(t, \gamma)$	nonlinear stress relaxation modulus [Pa]
G'	elastic or real modulus – real 1 st harmonic intensity [Pa]
G''	viscous or loss or imaginary modulus – complex 1 st harmonic intensity [Pa]
G^*	complex shear modulus [Pa]
i	imaginary number $\sqrt{-1}$
I_n	n^{th} harmonic intensity [Pa]
I_n/I_1	n^{th} harmonic relative intensity [-]
k	k^{th} harmonic idem as n
n	n^{th} harmonic
N	number of data points for FFT
p	viscosity ratio [-]
t	time [s]
t_{dw}	dwelling time [s]
t_{aq}	acquisition time [s]
T	temperature [°C]
T_g	glass transition temperature [°C]

$T_{R\&B}$	ring and ball temperature [°C]
$X_d(k\omega_0)$	k^{th} FT coefficient
γ	shear strain [-]
$\dot{\gamma}$	shear strain rate [1/s]
γ_c	critical strain and critical strain in total harmonicity signal [-]
γ_{c-n}	critical strain in n^{th} harmonic signal[-]
Γ	interfacial tension [N/m]
δ	loss angle, phase shift or phase lag of stress signal respect to strain signal [°]
η	non-Newtonian shear viscosity[Pa.s]
η_m	matrix viscosity
η_d	dispersed phase viscosity
λ	(characteristic) relaxation time [s]
μ	Newtonian viscosity [Pa.s]
σ	shear stress [Pa]
$\dot{\sigma}$	time derivative of shear stress [Pa/s]
ϕ_n	phase angle of n^{th} harmonic respect to a cosine curve that starts a $t = 0$ s [°]
$\phi_n - n\phi_1$	relative phase angle of n^{th} harmonic respect to the signal of the fundamental [°]
Φ_n	abbreviation for $\phi_n - n\phi_1$
ω	frequency [Hz]
ω_0	fundamental frequency [Hz]
ω_c	crossover frequency [Hz]
ω_{max}	maximum frequency to be sampled [Hz]

Abbreviations and acronyms

AA	Acrylic acid
ACM	Acrylamide
ARP	asphalt rich phase
asaf	as a function of
ATB	asphalt torsion bar
DFT	discrete Fourier transform
EVA	Poly ethyl-vinyl-acetate
FFT	fast Fourier transform
FOM	fluorescent optical microscopy
FT	Fourier transform
FTR	Fourier transform rheology
HDPE	High density polyethylene
Im	imaginary part of a complex number
LAOS	large amplitude oscillatory shear
LVE	linear viscoelasticity or linear viscoelastic
MAOS	medium amplitude oscillatory shear
n/a	not available or not applicable
NLVE	nonlinear viscoelasticity or nonlinear viscoelastic
OM	order of magnitude
PBA	polybutylacrylate
PDMS	polydimethylsiloxane
PIB	poly (isobutylene)

PMB	polymer modified bitumen
PP	parallel plates
PS	polystyrene
PRP	polymer rich phase
Re	real part of a complex number
SAOS	small amplitude oscillatory shear
STB	steel torsion bar
TB	torsion bar
VE	viscoelastic

1. Introduction

1.1. Motivation

The study of bitumen is of crucial importance for the production of high performance asphalt roads. This primary idea is justified by the fact that the mechanical properties and performance of the asphalt mixes are clearly influenced by the bitumen, because it is the only deformable component and it conforms the continuous matrix. Furthermore, current traffic loads and economically sustainable trends demand long service life paving roads. In this regard, service life in paving roads is determined by the tendency of the asphalt mix to undergo failures (rutting, fatigue cracking, and thermal cracking) as a consequence of the mechanical history at which it is subjected. In order to increase the service life of road pavements by delaying the emergence of these failures, conventional pen grade bitumens have been modified by the addition of polymers. This process results in polymer modified bitumens (PMBs), which are expected to have improved mechanical properties in comparison with those of the conventional pen grade bitumens they will replace: reflected in asphalt mixes with a longer service life.

Considering above, it can be inferred that characterization of the mechanical properties of binders is of great help in the design of better paving roads. Since a binder is a viscoelastic material, its mechanical properties can be studied by means of rheology. In terms of rheology, microstructure is studied in the linear viscoelastic (LVE) region and microstructural changes due to mechanical fields are studied in the non-linear viscoelastic (NLVE) region.

Linear rheological characterization of binders has been done mainly by means of small amplitude oscillatory shear tests (SAOS), and there is ample information regarding it. In SAOS test the microstructure of the system is preserved due to the low deformations applied. However, SAOS can have limited resolution to distinguish among complex materials with similar microstructure. In fact, linear characterization of asphalt binders has been proven to be unsuccessful in differentiating and predicting performance of PMBs. Furthermore, in service life asphalt is subjected to deformations outside the LVE region. Therefore the LVE characterization is a good starting point to study asphalt binders, but it will lack predictability towards service life performance.

Nonlinear rheological characterization of binders has only recently been reported in more detail. In NLVE characterization the microstructure is changed due to the high deformations applied: it can be more sensitive to small microstructural differences. Furthermore since the deformations applied are large, tests in the nonlinear regime can have a better potential to predict service life performance, as it better simulates limiting service conditions. Non-linear characterization of binders can be done by means of stress relaxation, steady shear flow, creep, and LAOS tests. In current open literature, there is available information for the first two types of tests. Nevertheless, its interpretation for proper ranking and differentiation between bitumens and PMBs has been proven to be difficult, and in most of the cases at most a qualitative differentiation between binders has been done. On the other hand, LAOS test coupled with Fourier transform rheology can yield specific quantifiers of the non-linear behavior of asphalt binders, by means of which a better characterization of bituminous binders could be done.

It is worth to mention that rheological information of binders close to room temperature (20°C – 25°C) is scarce or even null for some rheological tests. Contradictory, room temperature is roughly the mean for service temperature of paving roads in several countries. Furthermore, the reported tests performed around room temperature were done in shearing geometries (parallel plates and cone and plate), which are not suitable for the study of asphalt at room temperature (semisolid material), this could have induced experimental pitfalls and therefore a misinterpretation of the reported results.

Therefore, characterization of asphalt binders at room temperature using a suitable geometry by means of LAOS tests and FTR could provide a better quantitative characterization of the NLVE behavior of asphalt binders. The outputs of this characterization could be potentially more useful not only to differentiate between binders with similar microstructure, but also to give an insight of the service life performance.

1.2. Objectives

The main goal of the present work was to contribute to the bitumen and PMBs rheological characterization under large deformation at service temperature ($T \sim 20^\circ\text{C}$) by means of LAOS-FTR. This as an alternative to published NVLE characterization of bitumen and PMB.

The specific goals were:

To use a torsional bar geometry as an alternative to allow for the NLVE study of binders at room temperature ($T \sim 20^\circ\text{C}$).

To design and validate a LAOS-FTR experimental protocol to study the NLVE behavior of bitumen and PMB.

To establish whether LAOS-FTR outputs can efficiently distinguish between the nonlinear rheological behavior of different bitumens and PMBs.

To relate LAOS-FTR outputs with morphological properties.

To compare LAOS-FTR data with stress relax data for characterization of NLVE behavior of binders.

To explore the possibility to apply LAOS-FTR as a fast technique to characterize binders' fatigue behavior.

Above studies were done using two binder grades: 70/100 pen grade (parent bitumen) and 35/50 pen grade (benchmark bitumen), and two thermoplastic polymer modified bitumens: 70/100 pen grade with 5% wt. of recycled EVA copolymer (70/100EVA5), and 70/100 pen grade with 5% wt. of recycled HDPE copolymer (70/100HDPE5).

Finally in view that LAOS test is currently used to predict fatigue performance in binders, it seemed logical to expand this technique in terms of Fourier transform rheology quantifiers to clarify whether FTR could have some potential for data analysis.

1.3. Strategy

To start a brief characterization of the binders in the linear regime (SAOS and stress relaxation) was first performed. This in view that linear properties are the set point from which nonlinear properties depart and that linear & nonlinear rheology study different aspects of the material. This first characterization was also complemented with morphological studies of PMBs by means of fluorescent optical microscopy (FOM).

Then to avoid experimental pitfalls prior to start the LAOS-FTR characterization, the determination of the linearity range of the rheometer was done and the experimental conditions to obtain repeatable LAOS-FTR experiments in binders were set.

After the baseline, the playground, and the experimental conditions were established, the LAOS-FTR characterization of the mentioned bituminous binders was done. The LAOS-FTR characterization was done in amplitude sweep tests, which were performed using an experimental approach (all binders compared at same frequency) and a rheological approach (all binders compared at either same phase shift angle δ or same Deborah number, De). This was done to compare both approaches in order to select which could have a better potential for binders characterization. The binders FTR fingerprint obtained was compared with literature data of specific materials classes (emulsions, suspensions, polymers, etc.) to link morphological similitudes.

Then considering that time sweep tests are currently used to predict fatigue behavior in binders and that LAOS-FTR is a very sensitive technique, time sweep test data in the nonlinear regime were analyzed by FTR.

1.4. Outline

The present work will begin with a literature review given in chapter 2, and then a description of the materials and methods used in chapter 3. Afterward, in chapter 4 the LVE characterization of asphalt binders is given along with the FOM study. The determination of the rheometer linearity range and the methodology to obtain repeatability in LAOS test are presented in chapter 5. The NLVE characterization of asphalt binders by LAOS-FTR is presented in chapter 6. Subsequently, the nonlinear stress relaxation tests are given in chapter 7. The implementation of LAOS-FTR to predict fatigue behavior is introduced in chapter 8. The discussion of the results is provided in chapter 9 and the conclusions and further work are drawn in chapter 10.

2. Literature review

2.1. Large amplitude oscillatory shear and Fourier transform rheology

Large amplitude oscillatory shear (LAOS) is a useful test for nonlinear characterization of complex fluids, because strain amplitude and frequency are decoupled, and it does not involve any sudden jump in stress or strain: it is a relatively easy flow to generate [1, 2].

As expected, in the NLVE regime the rheological functions (G' , G'' , G^* , δ) depend not only of the frequency (time), but also of the deformation amplitude. This is reflected in the fact that the stress (or strain) output is no longer a pure sinusoidal signal [3], though the LAOS strain (or stress) input is ideally a pure sinusoidal. In fact, the output signal is a sum of several sinusoidal waves: even if not sinusoidal the output stress is yet periodic.

The most common LAOS test mode is a strain sweep, illustrated in Figure 2-1 on which it is clear that the moduli depend on strain and that the stress output is no longer a pure sinusoidal curve. Still, any dynamic test carried out outside the LVE region can be named LAOS test [1], e.g. frequency sweep test at a strain amplitude in the NLVE region.

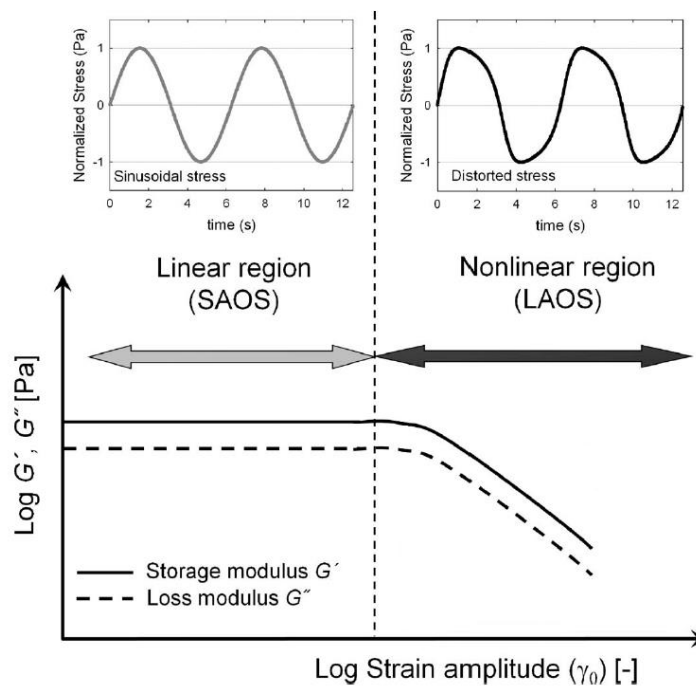


Figure 2-1 Schematic representation of a LAOS test: time (up) and frequency domain (down), adapted from [1].

In LAOS strain sweep test, there were reported four canonical responses for G' and G'' which are shown in Figure 2-2: type I, strain thinning (G' and G'' decreasing); type II, strain hardening (G' and G'' increasing); type III, weak strain overshoot (G' decreasing, G'' increasing followed by decreasing); type IV, strong strain overshoot (G' and G'' increasing followed by decreasing). Each type has been related to specific types of materials. Type I is the most common behavior in polymer solutions and melts. Since asphalt has shown similar rheology to a low molecular weight polymer this behavior was the one expected.

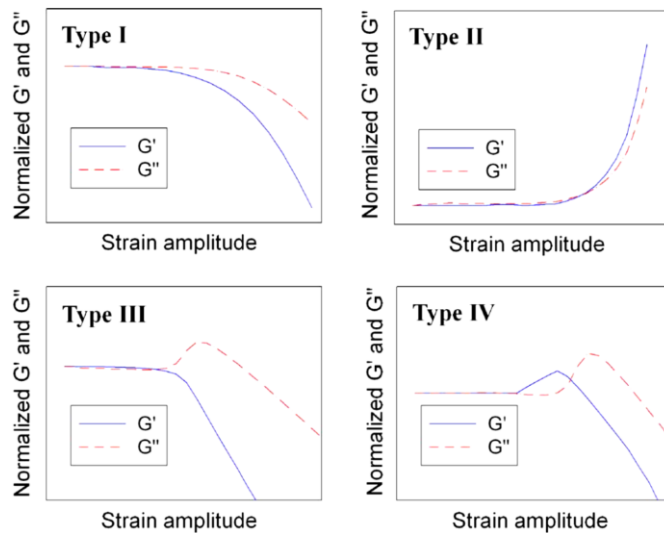


Figure 2-2 Representation of the four canonical behaviors of G' and G'' in LAOS tests, from [1]

Considering the above, for a strain sweep test in LAOS (which in the following will be referred only as LAOS test) the frequency at which the test is performed is also important (because the material is viscoelastic). The frequency to perform the test can be chosen to be either below, at, or above the crossover point between G' and G'' . To have a more complete analysis LAOS tests can be carried out at several frequencies to evidence the viscoelastic nonlinear response. Furthermore, some other modes of comparison are used, e.g. test the samples at the same value of $\tan \delta$ i.e. test samples mechanically equivalent, test the samples at the De number i.e. test samples at same relaxation state.

Since in LAOS the response of the material becomes more complex as compared to SAOS, the results analysis has also to be done in a different way. In general LAOS test analysis can be done either in time, or in deformation, or in frequency domain.

Data analysis in the time domain is done by means of stress curve shapes. Reported stress curve analysis are based on the departure from a pure sinusoidal shape, and their canonical forms are shown in Figure 2-3, while the tilting degree analysis is shown in Figure 2-4, among others [1].

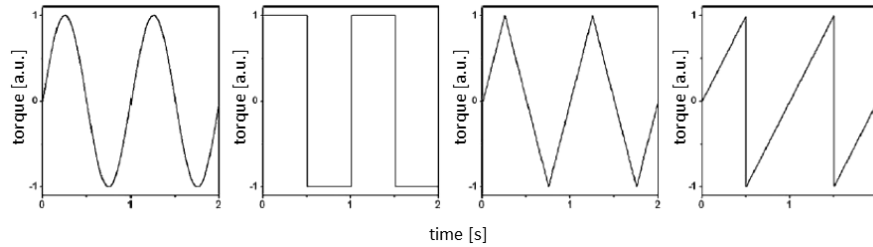


Figure 2-3 The four characteristic functions in time domain (from left to right): a sine, a rectangular, a triangular and a saw tooth shaped wave, representing: viscoelastic, strain softening, strain hardening, and shear bands. Adapted from [1].

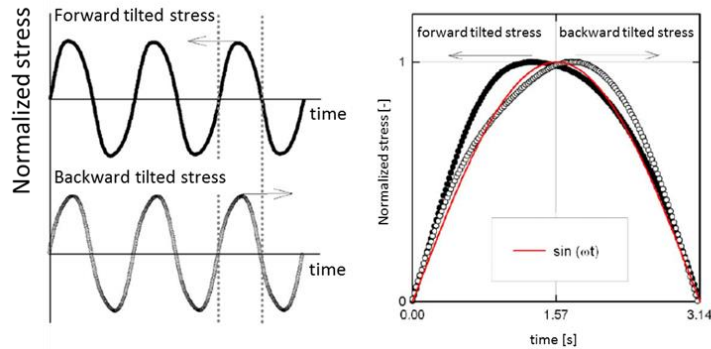


Figure 2-4 Analysis of stress curves in time domain based of curve tilting respect to a pure sinusoidal: stress curves (left) and half cycle comparison with a sinusoidal curve (right). Adapted from [1].

However one of the most used data analysis is Lissajous plots which correspond to the deformation domain. Lissajous plots are closed loop plots of σ vs γ (or σ vs $\dot{\gamma}$) which canonical forms for elastic, viscous, and viscoelastic materials in the LVE region are shown in Figure 2-5. In the nonlinear regime, the shape of the canonical forms is deformed, shown in Figure 2-5 as well.

Analysis of Lissajous plots can be done by visual inspection of the curves deformation (qualitative), and by quantification of the deformation by means of integration of the curve area (quantitative). The former analysis is a good method for rapid qualitative evaluation.

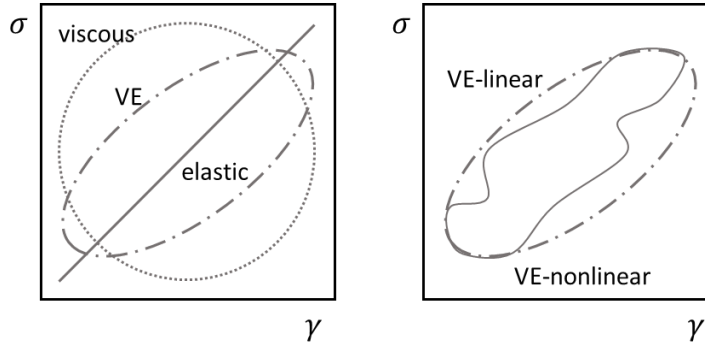


Figure 2-5 Lissajous plots: in LVE region (left) and in NLVE region (right).

Even though these plots do not yield any information regarding microstructure, they demonstrate how nonlinearity can affect the output signal of a VE material. Despite the fact that these visual analysis is useful, quantitative methods are also needed to fully analyze the nonlinear response of the material. In this regard Fourier Transform Rheology (FTR) is the preferred quantitative method to analyze stress curves in the nonlinear region, and it is done in the frequency domain. Fourier transformation is described in the next section.

2.1.1. Fourier Transform concept

Fourier analysis techniques consist in transforming a signal in the time domain to a signal in the frequency domain. The frequency domain representation can give a different insight about the time signal. Hence time and frequency representation describe the same signal, but from a different point of view [4].

To illustrate this time-frequency correspondence, a sinusoidal wave is shown in Figure 2-6, and in the frequency domain this signal is represented in magnitude and phase charts, also shown in Figure 2-6.

In the magnitude plane the amplitude of the sinusoidal wave is given along with the frequency at which each cycle occurs. In the phase plane, the phase delay respect to time equal to zero is given along with the frequency at which each cycle occurs. With this data from the frequency domain (frequency, amplitude and phase angle) the wave can be reconstructed in the time domain [4].

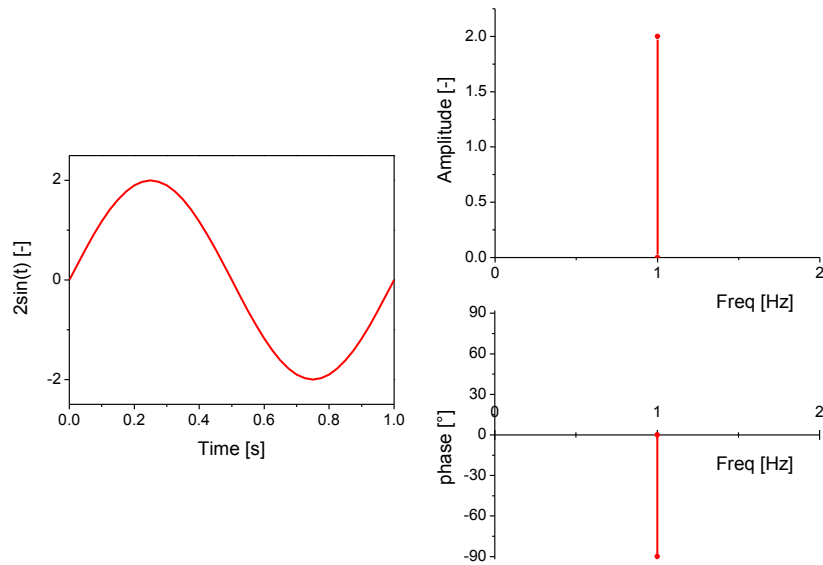


Figure 2-6 Representation of a sinusoidal wave in (left) time domain and in (right) frequency domain.

Fourier analysis is spectrum analysis, and different wave shapes have different spectra. More complicated periodic functions will be composed of the sum of several waves. In the spectra each wave (or spectral component) is represented by a single line or impulse which are located in the frequency axis at integer multiples of the fundamental frequency. Each of these Fourier terms is referred as a harmonic. Each harmonic will have a spectral line in the magnitude and in the phase diagram, shown in Figure 2-7.

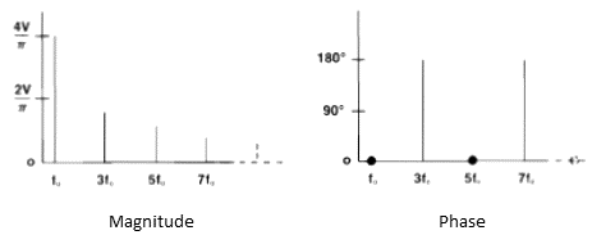


Figure 2-7 Spectra of a square periodic wave composed of several sinusoidal signals, adapted from [4].

Fourier analysis is intended for several types of function (continuous, discrete, periodic, and non-periodic). Therefore, in Fourier analysis there are three types of transformations: Fourier series, Fourier Integral, and discrete Fourier transform. The main characteristics and differences between these techniques are given in Table 2-.

In the case of the Fourier series and the Fourier integral, the function to be transformed must be described by a mathematic expression. In other words, if the function cannot be set to an equation,

then the classic Fourier techniques cannot be applied. This is impractical for real waves acquired in an experiment (e.g. in oscillatory shear). On the other hand, considering that a real wave is continuous then by definition is not suitable for Discrete Fourier Transform (DFT) analysis. However, a real wave can be sampled in a set of discrete points, and then the DFT can be used to analyze the signal in the frequency domain.

Table 2-1 Fourier analysis techniques

Fourier technique	Transformation pairs	Function type in t domain	Function type in ω domain
Fourier series	$x(t) = a_0 + \sum_{n=1}^{\infty} (a_n \cos n\omega_0 t + b_n \sin n\omega_0 t)$ $a_0 = \frac{1}{T} \int_0^T x(t) dt$ $a_n(n\omega_0) = \frac{2}{T} \int_0^T x(t) \cos n\omega_0 t dt$ $b_n(n\omega_0) = \frac{2}{T} \int_0^T x(t) \sin n\omega_0 t dt$	continuous periodic function	frequency charts (magnitude and phase) at specific discrete frequencies
Fourier transform (integral)	$X(\omega) = \int_{-\infty}^{+\infty} x(t) e^{-i2\pi\omega t} dt$ $x(t) = \int_{-\infty}^{+\infty} X(\omega) e^{i2\pi\omega t} d\omega$	continuous non periodic function	continuous spectra respect to ω
Discrete Fourier Transform (DFT)	$X_d(k\omega_0) = t_{dw} \sum_{n=0}^{N-1} x(nt_{dw}) e^{-i2\pi k\omega_0 nt_{dw}}$ $x(nt_{dw}) = \omega_0 \sum_{k=0}^{N-1} X_d(k\omega_0) e^{i2\pi k\omega_0 nt_{dw}}$	discrete sets of data points evenly spaced on time during a finite period of time	frequency charts (magnitude and phase) at specific discrete frequencies

2.1.2. The Discrete Fourier Transform (DFT)

The DFT transformation pairs are given on Table 2-1. An alternative representation of above equations can be yielded by means of the Euler's equation

$$e^{ix} = \cos(x) + i\sin(x) \tag{2.1.2-1}$$

in terms of cos and sin series, where the coefficients for the cos series give the real part coefficients and the coefficients for the sin series give the imaginary part coefficients. For the DFT

$$X_d(k\omega_0) = Re(k\omega_0) + i Im(k\omega_0) \quad (2.1.2-2)$$

and considering that any complex pair can be represented in a vectorial form (Argand diagram). Above result can be further expressed as

$$|X_d(k\omega_0)| = \sqrt{Re(k\omega_0)^2 + Im(k\omega_0)^2}$$

$$\tan \delta = \frac{Im(k\omega_0)}{Re(k\omega_0)} \quad (2.1.2-3)$$

which yields the harmonic magnitude and phase angle.

Therefore any data in the frequency domain can be described either by real and imaginary (G' and G'') or by magnitude and phase (G^* and δ) coefficients.

By using above expressions, it is straightforward to compute the DFT for any string of waveform samples. The values of $x(n)$ are taken directly from the experimental data. Nevertheless the classical DFT algorithm is lengthy and not easy to implement. Because of this, nowadays the so called Fast Fourier transform (FFT) algorithm is used. The FFT algorithm is a fair approximation of the strict DFT one that is capable to yield the same harmonic coefficients in shorter time [4].

2.1.3. Fourier transform matters of practicality

Data acquisition and analysis

Windowing and sampling.

To be analyzed in FFT, a wave has to be windowed and sampled. Windowing is the delimitation of the time period over which the signal analysis will be done. Sampling is the decomposition of the continuous wave in discrete evenly spaced data points. In practice, windowing and sampling is done by an analog to digital converter (ADC) [4].

Signal averaging.

Time-domain noise transforms to frequency-domain noise. In the case that the noise is random, it will have a zero mean. Therefore signal averaging will eliminate the noise and lead to sharper signals, and this is done by analyzing several cycles of the same response. For truly mean-zero noise, the improvement in signal-to-noise ratio for M cycles acquired is \sqrt{M} [4, 5].

Aliasing.

Aliasing is the representation of a high-frequency component by a lower frequency component, shown in Figure 2-8.

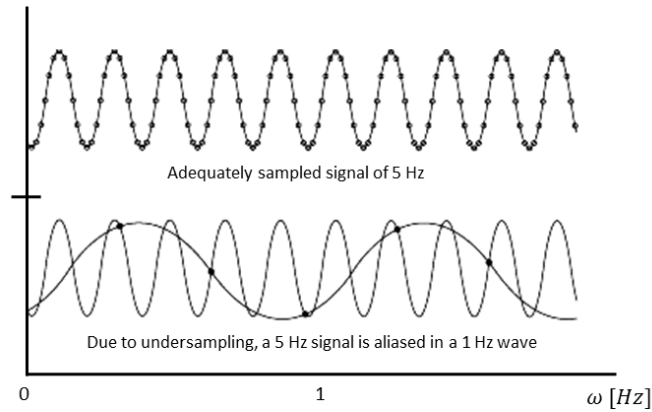


Figure 2-8 Representation of aliasing. Adapted from [4].

To explain aliasing time-frequency relationship of the sampled data points will be introduced. Each data point in time is acquired at a fixed time increment t_{dw} or dwelling time over a total time t_{aq} or acquisition time

$$t_{aq} = Nt_{dw} \quad (2.1.3-1)$$

Hence, from N real data points by means of FFT a discrete spectrum of N complex points is generated. Time and frequency hold a reciprocal relationship. Therefore, the spectral width or maximum frequency is given by

$$\omega_{max} = \frac{1}{t_{dw}} \quad (2.1.3-2)$$

and frequency resolution is given by

$$\Delta\omega = \frac{1}{t_{aq}} \quad (2.1.3-3)$$

The Nyquist theorem governs the proper sampling: it states that the sampling rate has to be at least twice the maximum frequency contained in the function to be analyzed [4].

$$\frac{1}{t_{dw}} = 2\omega_{max} \quad (2.1.3-4)$$

In other words, there must be at least two points per cycle for any frequency component contained in the wave. If there are less points then aliasing occurs. Therefore, equation (2.1.3-2) is correct for the reciprocal relationship of time and frequency, but due to the Nyquist theorem, equation (2.1.3-4) is the one that defines the real spectral width.

In real world aliasing is unavoidable, the better is to set the Nyquist frequency at a value high enough so that the signal of the highest frequency component falls beyond the noise. Therefore, in any experiment one should first estimate the maximum possible harmonic contribution (of the maximum harmonic that one wishes to acquire) and adjust the sampling rate accordingly [5].

The major issue with aliasing is that sometimes the high frequency components that are aliased can be erroneously added to low frequency signals, and this will mislead the results [4].

Leakage.

The FFT assumes periodicity in all cases, i.e. the windowed signal will be repeated all over again (shown in Figure 2-9).

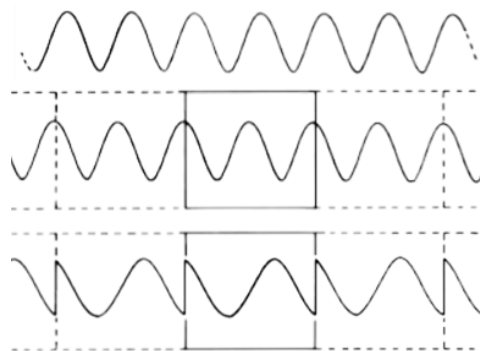


Figure 2-9 Periodic signal (up), integer (middle) and non-integer (down) number of cycles windowed, adapted from [4].

In the case where a non-integer number of cycles occur in the window, leakage will smear the frequency-domain information: error will be introduced.

Rheometer equipment

To perform FTR of LAOS data strain controlled rheometers are preferred in order to have a more monochromatic excitation [1]. By supplying a “monochromatic” strain, it is possible to conclude that any stress output at frequencies other than the fundamental is associated with nonlinearities in the system response. To ensure this, a FFT of the motor signal can be done to determine the linear operational range of the motor. In this frame, the transducer linear range has also to be determined [6]. The rheometer used for FTR has to be modified to allow the collection of the raw data signal from motor and transducer by an ADC card [1]. This data can be analyzed with a FFT in many commercial software (Matlab, Mathematica, LabView, etc).

2.1.4. Fourier Transform Rheology

Fourier Transform Rheology (FTR) is the analysis in the frequency domain of a periodic signal coming from oscillatory experiments. In FTR a discrete, complex, half sided FT is commonly used. It is discrete because the DFT technique with a FFT algorithm is used. It is complex because the FT is inherently complex, but also to make the difference that neither only sine nor cosine FT are used. It is half sided because only the positive axis of the frequency is analyzed.

In an oscillatory experiment a sinusoidal strain excitation is used

$$\gamma(t) = \gamma_0 \cos(\omega t) \tag{2.1.4-1}$$

whose FT is given by the Fourier series

$$C_n(n\omega_0) = \frac{2}{T} \int_0^T x(t) e^{-in\omega_0 t} dt \tag{2.1.4-2}$$

Substituting eq. (2.1.4-1) in eq. (2.1.4-2)

$$C_n(\omega_0) = \frac{2}{T} \int_0^T \gamma_0 \cos(\omega_0 t) e^{-in\omega_0 t} dt \tag{2.1.4-3}$$

and by means of Euler's equation (2.1.2-1)

$$C_n(n\omega_0) = \frac{2}{T} \left[\int_0^T \gamma_0 \cos(\omega_0 t) \cos(n\omega_0 t) dt - i \int_0^T \gamma_0 \cos(\omega_0 t) \sin(n\omega_0 t) dt \right] \quad (2.1.4-4)$$

Considering the properties of sine and cosine integrals given in Appendix A, only for $n = 1$ above integral is different than zero. Thus equation (2.1.4-4) is further simplified to

$$C_1(\omega_0) = \gamma_0 \quad (2.1.4-5)$$

whose magnitude and phase angle are computed according to eq. (2.1.2-3), and given by

$$|C_1(\omega_0)| = \gamma_0$$

$$\tan \delta = \frac{0}{\gamma_0} = 0 \rightarrow \delta = 0^\circ \quad (2.1.4-6)$$

which is the FT of a cosine strain wave.

In the LVE region, the stress output is given by

$$\sigma(t) = \sigma_0 \cos(\omega_0 t + \delta) \quad (2.1.4-7)$$

According to above procedure the FT is given by

$$C_n(n\omega_0) = \frac{2}{T} \int_0^T \sigma_0 \cos(\omega_0 t + \delta) e^{-in\omega_0 t} dt$$

or

$$C_n(n\omega_0) = \frac{2}{T} \left[\int_0^T \sigma_0 \cos(\omega_0 t) \cos(\delta) e^{-in\omega_0 t} dt - \int_0^T \sigma_0 \sin(\omega_0 t) \sin(\delta) e^{-in\omega_0 t} dt \right] \quad (2.1.4-8)$$

By means of Euler's equation (2.1.2-1)

$$C_n(n\omega_0) = \frac{2}{T} \left[\int_0^T \sigma_0 \cos(\omega_0 t) \cos(\delta) \cos(n\omega_0 t) dt - i \int_0^T \sigma_0 \cos(\omega_0 t) \cos(\delta) \sin(n\omega_0 t) dt \right. \\ \left. - \int_0^T \sigma_0 \sin(\omega_0 t) \sin(\delta) \cos(n\omega_0 t) dt + i \int_0^T \sigma_0 \sin(\omega_0 t) \sin(\delta) \sin(n\omega_0 t) dt \right] \quad (2.1.4-9)$$

Considering the integrals in Appendix A, above equation is different than zero only for $n = 1$:

$$C_1(\omega_0) = \frac{2}{T} \left[\int_0^T \sigma_0 \cos(\omega_0 t) \cos(\delta) \cos(\omega_0 t) dt + i \int_0^T \sigma_0 \sin(\omega_0 t) \sin(\delta) \sin(\omega_0 t) dt \right]$$

or
$$C_1(\omega_0) = [\sigma_0 \cos(\delta) + i \sigma_0 \sin(\delta)] \quad (2.1.4-10)$$

whose magnitude and phase lag are given by

$$|C_1(\omega_0)| = \sigma_0 \quad (2.1.4-11)$$

$$\tan(\delta) = \frac{\sin(\delta)}{\cos(\delta)} \quad (2.1.4-12)$$

Based on above analysis, the FT of $\sigma(t)/\gamma(t)$ is given by

$$FT \left[\frac{\sigma(t)}{\gamma(t)} \right] = G^*(\omega) = \frac{\sigma_0}{\gamma_0} \cos(\delta) + i \frac{\sigma_0}{\gamma_0} \sin(\delta)$$

or
$$G^*(\omega) = G'(\omega) + iG''(\omega) \quad (2.1.4-13)$$

with

$$G'(\omega) = \frac{\sigma_0}{\gamma_0} \cos(\delta) \text{ and } G''(\omega) = \frac{\sigma_0}{\gamma_0} \sin(\delta) \quad (2.1.4-14)$$

whose magnitude and phase lag are given by

$$|G^*(\omega)| = \sqrt{G'^2(\omega) + G''^2(\omega)} \quad (2.1.4-15)$$

$$\tan(\delta) = \frac{G''(\omega)}{G'(\omega)} \quad (2.1.4-16)$$

Above set of equations define the material functions of a SAOS test in the Fourier space. This derivation is valid no matter the type of fluid under study, since no constitutive equation was used

during its derivation [7, 8]. By means of this derivation it is clear why G' is the real modulus associated with in-phase or elastic response, and G'' is the complex modulus related to the out of phase or viscous response. Besides, since no higher harmonics are present, it supports the concept of uniqueness of G' and G'' as proper material rheological functions to describe the viscoelasticity in the LVE region.

In the NLVE region the stress output is given by

$$\sigma(t) = \sum_{n=1}^N \sigma_n \cos(n\omega_0 t + \delta_n) \quad (2.1.4-17)$$

which is the superposition of several sinusoidal waves. Considering that the FT is a linear operator, the FT of above equation will be given as a sum of the FT of the different waves, i.e.

$$C_n(n\omega_0) = \frac{2}{T} \int_0^T \sum_{n=1}^N \sigma_n \cos(n\omega_0 t + \delta_n) e^{-in\omega t} dt \quad (2.1.4-18)$$

Using the same analysis as before, in this case C_n higher than one will exist. Therefore, a C_n function can be determined for each n harmonic, and its magnitude $|C_n|$ and phase lag δ_n can also be computed.

Notice that in this case the FT of $\sigma(t)/\gamma(t)$ will yield more than one real and imaginary pair (G'_n and G''_n), and the usage of G' and G'' (1st harmonic real and imaginary coefficients) to fully describe the stress response in the Fourier space is no longer valid. Therefore, in the nonlinear regime the analysis of higher harmonics is required. The FT of the nonlinear signal $\sigma(t, \gamma_0)/\gamma(t)$ is given by

$$FT \left[\frac{\sigma(t, \gamma_0)}{\gamma(t)} \right] = \sum_{n=1}^N \frac{\sigma_n}{\gamma_0} \cos(\delta_n) + i \frac{\sigma_n}{\gamma_0} \sin(\delta_n)$$

or

$$FT \left[\frac{\sigma(t, \gamma_0)}{\gamma(t)} \right] = \sum_{n=1}^N G_n^*(\omega, \gamma_0) = \sum_{n=1}^N G_n'(\omega) + i G_n''(\omega) \quad (2.1.4-19)$$

similarly

$$|G_n^*(\omega)| = \sqrt{G_n'^2(\omega) + G_n''^2(\omega)} = \left| \frac{\sigma_n}{\gamma_0} \right| \quad (2.1.4-20)$$

$$\tan(\delta_n) = \frac{G_n''(\omega)}{G_n'(\omega)} \quad (2.1.4-21)$$

and $|G_n^*(\omega)|$ can also be expressed as

$$|G_n^*(\omega)| = \frac{I_n}{\gamma_0} \quad (2.1.4-22)$$

where I_n is the intensity signal of the n^{th} stress harmonic, (notice that $I_n = \sigma_n$ following above nomenclature). However the δ_n defined above is the phase lag between the strain and the n^{th} stress signal, i.e.

$$\delta_n = \phi_n - \phi_\gamma \quad (2.1.4-23)$$

where ϕ_n is the phase angle of the n^{th} stress harmonic respect to a cosine wave (i.e. $\cos(\omega_0 t) = 0$ at $t=0$), idem for ϕ_γ . In the frame of FT analysis, $t=0$ is the time at which windowing starts. In the case where at $t=0$ the strain signal is starting then $\delta_n = \phi_n$. However, in practice this is difficult to achieve. Therefore in the nonlinear regime, the analysis of higher harmonics is commonly done by intensities (I_n) and phase angles (ϕ_n) based on the stress output rather than $|G_n^*(\omega)|$ and δ_n .

The intensity signals are normally reported as relative intensities respect to the intensity of the fundamental (I_n/I_1), because this quantity is less vulnerable to non-systematic errors and as an intensive quantity is more useful to make comparisons between samples [1]. The relative intensity signals can be either odd ($I_3/I_1, I_5/I_1, I_7/I_1, \dots$) or even ($I_2/I_1, I_4/I_1, I_6/I_1, \dots$). In the frame of FTR odd harmonics are related to nonlinear reversible phenomena and correspond to a no sinusoidal but symmetric wave, shown in Figure 2-10. On the other hand even harmonics are related to nonlinear irreversible phenomena and correspond to a no sinusoidal non symmetric wave, i.e. even harmonics arise when shearing to the right is different than shearing to the left, shown in Figure 2-10. Therefore odd harmonics correspond to reversible microstructure deformation, while even

harmonics can correspond to nonreversible microstructure deformation but also to experimental pitfalls such as wall slip [1].

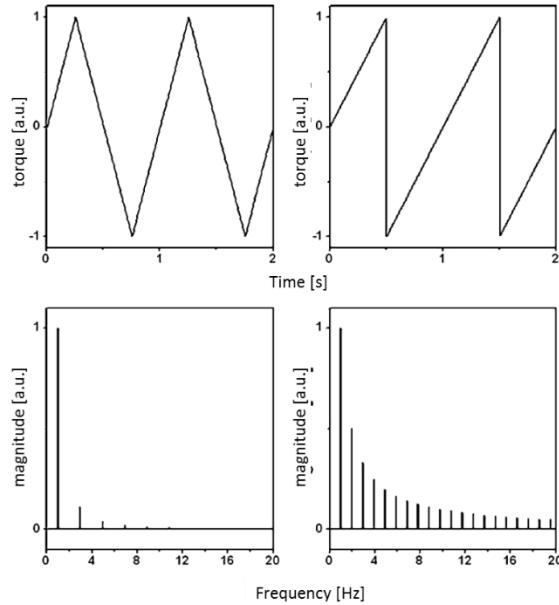


Figure 2-10 Representation of a symmetric (left) and a non-symmetric wave (right) along with its FT spectra [1].

The I_3/I_1 of many materials has been reported to follow a power law dependence as a function of strain described by

$$I_3/I_1 = a\gamma^b \quad (2.1.4-24)$$

which is only valid in a narrow region at the beginning of the nonlinear response which has been called medium amplitude oscillatory region (MAOS) [1]. This region, as well as the LVE region, is reported to be sample dependent. At higher strains, i.e. in LAOS region, the power law dependence is lost and for some samples the I_3/I_1 value levels off to a constant value [1, 9].

For polymeric systems the value of the exponent has been reported to be close to $b = 2$, in agreement with the nonlinear model

$$\sigma = \eta(\dot{\gamma})\dot{\gamma} \quad (2.1.4-25)$$

with

$$\eta(\dot{\gamma}) = \eta_0 + a\dot{\gamma} + b\dot{\gamma}^2 + \dots \quad (2.1.4-26)$$

by substituting equation (2.1.4-25) in equation (2.1.4-26)

$$\sigma = \eta_0 \dot{\gamma} + a\dot{\gamma}^2 + b\dot{\gamma}^3 + \dots \quad (2.1.4-27)$$

Considering that the stress response of viscoelastic materials is typically independent of the shear direction, and that the sign of the shear stress changes as the sign of the shear strain does, then only odd terms of the above expression are valid [1].

$$\sigma = \sum_{n=1}^N a_n \dot{\gamma}^n \quad n = \text{odd} \quad (2.1.4-28)$$

In the Fourier space such equation will yield

$$I_{2n+1}/I_1 = a\gamma^{2n} \quad (2.1.4-29)$$

Since the Taylor series is expanded around zero strain rate value (Maclaurin series), the predictions of such constitutive equation will only be valid in the vicinity of low strains. This explains why the power law trend of equation (2.1.4-29) is only valid in the MAOS regime.

Deviations from this trend do exist and have been reported [9] i.e. not all materials follow the Taylor expansion at low strains. In simply words this is equivalent to detect or not a Newtonian plateau in a flow curve, some materials will have it and some others not, and some others will only have it at specific experimental conditions, i.e. $T, \dot{\gamma}$.

In the case of materials where harmonic signals higher than the 3rd one are significant, the usage of higher harmonics 5th, 7th, ... is common [10, 11, 12] along with the definition of total harmonicity [10]

$$\text{total harmonicity} = \sum_{n_{\text{odd}}}^N \frac{I_n}{I_1} \quad (2.1.4-30)$$

as the sum of the significant odd components.

Phase angle signals (ϕ_n) are normally reported as relative phase angles respect to the fundamental ($\phi_n - n\phi_1$). The derivation of this quantity comes from a variable change ($t = t' - \phi_1/\omega$) to

displace the fundamental signal to have zero degrees, i.e. $\phi_n - n\phi_1 = 0$ for $n = 1$. In the case of the relative phase angle of the 3rd harmonic, the $\phi_3 - 3\phi_1$ quantifies the balance of the softening versus the hardening behavior of the stressed material [13]. A value of $\phi_3 - 3\phi_1 \sim 0^\circ$ or 360° is shear thickening, and $\phi_3 - 3\phi_1 \sim 180^\circ$ shear thinning. Besides, it has been reported that the value of $\phi_3 - 3\phi_1$ is characteristic of materials morphology [1, 2]. Geometrically it is related to the curves tilting, $\phi_3 - 3\phi_1 < 180^\circ$ corresponds to stress curves tilted to the left and $\phi_3 - 3\phi_1 > 180^\circ$ corresponds to stress curves tilted to the right.

2.1.5. FTR studies of selected classes of materials

In the frame of FTR, several studies of specific systems have been reported, e.g. polymer melts, polymer solutions (linear, branched, polysaccharides), suspensions close to the glassy transition, emulsions of Newtonian in Newtonian fluid, rubber with fillers, etc. In the following pages a brief review of those studies will be given.

Dispersion systems

Dispersion systems are systems where interfaces are present as a result of the coexistence of several phases, of which suspensions, emulsions, and bicontinuous blends are examples. These systems have been studied with LAOS-FTR technique, and the common characteristic of those systems rich in interface is a spectrum with a high number of significant harmonics [1].

Suspensions

FTR has been reported to be sensitive to particle softness, solids content (volume fraction), differences in particle surface (hydrophobically coated or with electrostatic charges), particle size, etc. [1, 12, 14]. For the systems reported in [14], an increase in either the solids content or the particle size led to higher harmonic magnitudes. In the case of solids content, the harmonics relative intensity was proven to be very sensitive to this parameter: the I_3/I_1 signal decreased one decade by decreasing in 13% the solids content, shown in Figure 2-11.

Therefore, dispersion systems have been studied mainly at high concentrations and close to the colloidal glassy state [12, 15]. In the linear regime those systems are characterized by $G' > G''$ over the experimentally accessible frequencies, and in the nonlinear regime they commonly exhibited the type III behavior (overshoot in G'') shown in Figure 2-2.

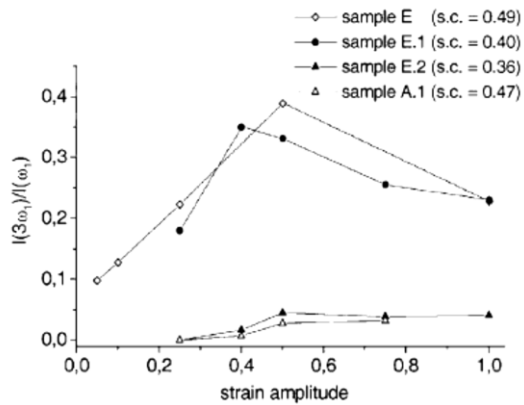


Figure 2-11 $I_3/I_1\%$ at 1 Hz for dispersions of PS-PBA coated with AA and ACM: E base suspension undiluted, E.1 and E.2 are water dilutions of E suspension, and A.1 is dispersion of uncoated particles [14].

For colloidal suspensions close to or beyond the point of dynamical arrest (predominantly elastic in character) the mode coupling theory was used in [12] to predict the behavior under LAOS. One of the model outputs was significant odd harmonics (reported up to the 9th one), in which I_n/I_1 had a power law increase at low strains, with a slope lower than 2, followed by a plateau at high strains.

Emulsions

FTR of polydimethylsiloxane (PDMS) dispersed in poly (isobutylene) (PIB) has been reported in [11, 16, 17] for a range of experimental conditions where both polymers exhibited pure Newtonian behavior. The idea underlined in those studies was that an emulsion formed from two immiscible Newtonian fluids would exhibit a viscoelastic response due to the interfacial tension, and this response would become nonlinear when sufficiently large shear was applied to the emulsion droplets. Consequently emulsion morphology (droplet size and size distribution), physicochemical properties (interfacial tension), and rheological parameters (viscosities of both dispersed and continuous phases) were proven to affect the harmonics intensity in the FTR spectra [17].

For these model emulsions (Newtonian phases, low volume fraction, and buoyancy free), the Maffettone and Minale model (for droplet deformation under flow) coupled with the Batchelor theory (for interfacial effects and behavior of individual phases) were used in order to predict the emulsion response under LAOS conditions at low droplet deformations [11, 16, 17]. The principal

outputs were the existence of significant odd harmonics (reported until the 7th one), which followed a power law of the type

$$I_{2n+1}/I_1 \sim \gamma^{2n} \quad (2.1.5-1)$$

at low strains, and which magnitude was related to both the capillary number (Ca) and the viscosity ratio (p)

$$Ca = \frac{\eta_m \omega \gamma a}{\Gamma} \quad \text{and} \quad p = \eta_d / \eta_m \quad (2.1.5-2)$$

where η is the viscosity of the medium or the dispersed phase, a is the characteristic droplet size, and Γ is the interfacial tension. The characteristic droplet size, a , was replaced by different moments of the average radius depending on both the harmonics considered (3rd, 5th or 7th) and the type of emulsion studied (monodispersed or polydispersed). Therefore, FTR parameters were proposed to be sensitive to the emulsion morphology (droplet size and its distribution) and to the material parameters embedded in Ca and p . This was proven to be valid in the above mentioned model emulsions of PDMS in PIB [17].

In the case of concentrated commercial emulsions (before phase inversion) [17], which fall beyond the model validity, the above mentioned power law relationship held over narrow interval at very small strains for the 3rd, 5th, and 7th harmonics; after that point the power law trend leveled off. Furthermore the ratios of I_5/I_3 and I_7/I_5 in the power law region were proven to be sensitive to droplet size and its distribution.

Polymeric systems

In the case of polymeric systems the information available is broad, but most of the reported studies were restricted to the 3rd harmonic (intensity and phase angle) [1, 13, 3, 5, 6, 9], because higher harmonics were reported as not significant. In polymers, I_3/I_1 in most of the cases followed a square dependence on strain independent of frequency [18], as in equation (2.1.4.29). However this dependence was restricted to only a narrow interval of strains. In this regard, many polymeric systems had a slope different than 2, either higher or lower [9]. Deviations from this “ideal” trend are not uncommon [2, 9] and they can be understood as normal as having deviations from the $G' \sim \omega^2$ and $G'' \sim \omega$ trends in the terminal regime.

Among the several case studies of polymer systems available in the literature, those given in [13, 19] for entangled solutions of linear polystyrene (PS) in iso-dioctyl phthalate (chemical structures are presented in Figure 2-12) reported an analysis of I_3/I_1 and $\phi_3-3\phi_1$ respect to δ and De number. Such scope is relevant for the present study because the bituminous binders were studied with respect to those rheological parameters.

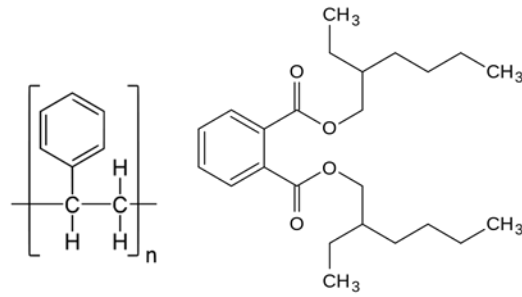


Figure 2-12 Microstructure of PS and iso-dioctyl phthalate

The polymer solutions were analyzed both at frequencies below and above the crossover point ($G' = G''$). The I_3/I_1 signal followed a power law trend asaf of strain, which exponent was lower than 2 and between 1.4-1.5 for different δ values and entanglement density below the crossover point [19]. Even though no specific trend of the exponent or pre-exponent respect to δ was given, for $\delta > 45^\circ$ the I_3/I_1 signal decreased with respect to δ . The dependence of I_3/I_1 and $\phi_3-3\phi_1$ in the De number were also studied and are given in Figure 2-13 [13].

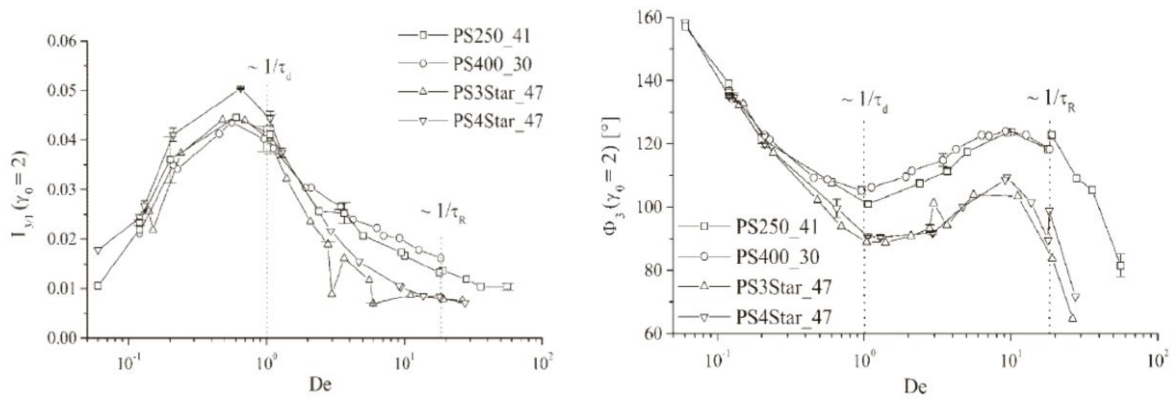


Figure 2-13 FTR behavior of entangled PS solutions (linear and branched) in iso-dioctyl phthalate at different weight concentration and at $\gamma = 2$: (left) I_3/I_1 signal and (right) Φ_3 signal asaf of De [13].

Also the values for $\phi_3-3\phi_1$, $\phi_5-5\phi_1$, and $\phi_7-7\phi_1$ were reported for the two δ values studied in that work [19]. The relative phase angles reached plateau values, which held a relationship of $\phi_3-3\phi_1 < \phi_5-5\phi_1$ irrespective of the sample type (entanglement density) or delta value.

Dispersion systems with polymeric matrix

Under this material class only rubbers loaded with solid particles will be revisited. The systems reported [10] were natural rubber or polybutadiene mixed with carbon black. In such systems there exists a high interaction between the dispersed phase and the viscoelastic matrix: carbon black inclusions interact with rubber by means of Van de Waals forces, chemical interactions (reaction between carbon black functional group and free radicals on polymer chains), and adhesion [20].

In the FTR spectra of such systems, besides significant harmonics higher than the 3rd, there was a bump in the I_3/I_1 signal at low strains (see red arrow in Figure 2-14) after which the power law behavior was recovered, as shown in Figure 2-14.

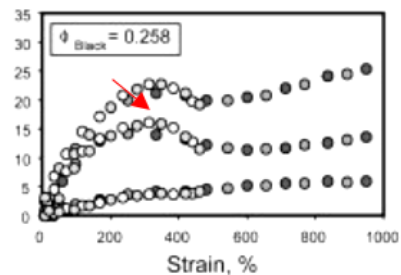


Figure 2-14 Nonlinear response of a cis- 1,4 polybutadiene loaded with 0.258 volume fraction of carbon black: (upper curve) total harmonicity, (middle curve) I_3/I_1 %, different than (lower curve) I_5/I_1 %. Adapted from [10].

This bump was clearly associated with the inclusion of carbon black, because pure rubbers did not have it and an increase in the inclusion concentration led to more pronounced bumps.

2.2. Bitumen basics

Bitumen is a complex material, and only one definition cannot encompass all its characteristics, and thus bitumen has been described from a physical, rheological or chemical point of view.

Physically, bitumen at room temperature is a black, virtually involatile, adhesive and waterproofing material, with a very high viscosity such as it is nearly solid [21].

Rheologically, bitumen is a thermoplastic and viscoelastic material that changes from viscous liquid at high temperatures ($T > 60^\circ\text{C}$) to glassy solid at low temperatures (T_g of -20°C), as shown in Figure 2-15 [21]. At room temperature it is considered as a semi-solid material with viscoelastic properties, which viscosity is around 10^8 Pa.s, i.e. 11 OM higher than water [7].



Figure 2-15 Bitumen 35/50 (left) in the liquid state at $T > 60^\circ\text{C}$ and (right) in the semi-solid state at room temperature.

Chemically, bitumen is a mixture of saturates, aromatics, resins, and asphaltenes. This comprises the so called SARA fractions, shown in Table 2-2, in which the polarity and molecular weight increase from saturates to asphaltenes [21].

Table 2-2 Bitumen composition and basic characteristics according to the SARA fractions [22]

Component	% wt.	Appearance	Tg [$^\circ\text{C}$]	Mn [g/mol]	Density [g/cm ³]
Bitumen	100	black viscous liquid	-20°C	600-1500	1.01-1.04
Saturates	5-15	colorless or lightly colored liquid	-70°C	600	0.9
Aromatics	30-45	yellow to red liquid	-20°C	800	<1.0
Resins	30-45	black solid at room temperature	---	1100	1.07
Asphaltenes	5-20	black powder	---	800-3500	1.15

The first three fractions are commonly grouped as maltenes [22]. Maltenes are by far the most numerous components (up to 95% wt) [21, 23], but asphaltenes are the most studied molecules because of the viscosity building role, the bonding performance, and the temperature stability that they confer to bitumen [22, 23]. In this work the words asphalt or bitumen will be used interchangeably unless specified.

The physical and rheological properties of asphalt were reported to principally be affected by temperature, excitation frequency, and composition [21, 23], but other factors such as aging can also play an important role.

A general picture of bitumen microstructure is that of a colloidal material where asphaltene aggregates are dispersed into maltenes [24], shown in Figure 2-16. The two limiting behaviors of bitumen, i.e. Newtonian liquid and glassy solid, have been associated with this structure. At high temperatures, the contribution of asphaltenes Brownian motion to the viscosity is dominant. Whereas at low temperatures, the transition to a glassy state as a consequence of maltenes vitrification is prevalent [21].

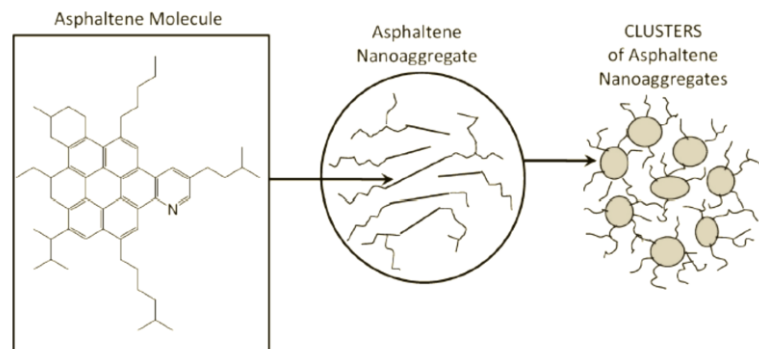


Figure 2-16 Colloidal representation of bitumen according to the modified Yen model [25]

Although bitumen can be found in natural deposits, it is usually produced by crude oil distillation, but independent of its origin the most important usages of bitumen are in road pavement and in waterproof roofing. Only the former usage will be considered in the present work. In a road pavement, bitumen is used as a binder for the mineral aggregates (stones), in order to produce asphalt mixes as those shown in Figure 2-17. Bitumen is added in these mixes at low concentrations (typically around 5% wt.), but it clearly influences the mechanical properties and

performance of the asphalt mixture, because it is the only deformable component and it forms the continuous matrix [24, 26].

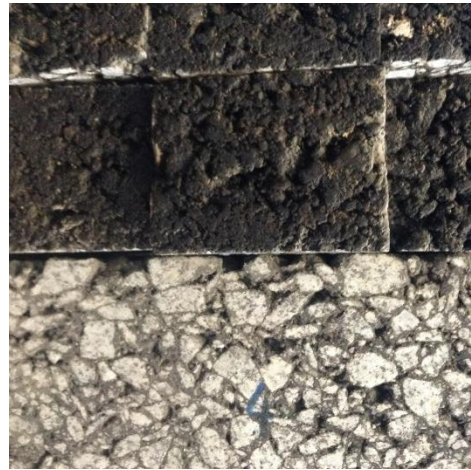


Figure 2-17 Slabs of asphalt mixes: (up) mineral aggregates covered with binder, (down) cross section of a slab.

Nevertheless, during service the asphalt mixes undergo failures such as: rutting, thermal cracking and fatigue cracking, shown in Figure 2-18.



Figure 2-18 Representation of the different failures that road pavement undergo: rutting and cracking [27]

Rutting is a plastic deformation that is more prone to happen at high service temperatures ($T > 40^{\circ}\text{C}$) where the viscous component is dominant against the elastic recovery [22, 24, 28]. Rutting leads to channels formation in the traffic direction [24]. Thermal cracking is a brittle fracture that occurs at low service temperatures ($T < 0^{\circ}\text{C}$) where the glassy behavior of the binder is more prevalent and stress relaxation cannot occur [22, 24, 28]. Thermal cracking is characterized by

cracks formation perpendicular to traffic direction [22, 28]. Fatigue cracking is a long term fracture that occurs at standard service temperatures as a consequence of cumulative stress relaxation cycles during traffic load [22, 24, 29]. In principle, the stress applied is less than needed for immediate fracture, but it is up to stress/relaxation cycling that fracture occurs. Fatigue cracking is present either as transversal, longitudinal or spider web cracks on the pavement [22, 28]. Fatigue cracking is the most common failure mechanism in asphalt roads. Therefore, the service life of a road pavement is given by its susceptibility to undergo fatigue cracking.

The occurrence of these failures is strongly associated with the binder mechanical properties. Hence, mechanical characterization of bitumens is critical to better evaluate and predict the performance of road pavements. Mechanical characterization tests of bitumens can be divided in fundamental and empirical tests. The fundamental tests measure well-defined rheological parameters (shear viscosity, extensional viscosity, dynamic moduli, etc.). The empirical tests measure non fundamental rheological parameters, but they are found to be related to the performance of the binder from practical experience.

Empirical tests are normally considered as an index to rank bitumens. In empirical tests the deformation profile is complex, hence it is difficult to extract fundamental information. Due to this complex kinematics the result depends on geometrical aspects and specific conditions for rate, torque and time. As a consequence, in the case of widely accepted empirical tests there are norms to regulate the conditions and methodology of testing. For instance bitumen classification in Europe is done by the needle penetration test which is reported in the so called *pen grade* and described in ASTM D5 or EN 1426. Other common empirical quantifiers are the ring and ball softening temperature ($T_{R\&B}$), described in ASTM D36 or EN 1427, and Brookfield viscosity, described in ASTM D4402 or EN 13302.

The fundamental rheological tests are described in Appendix B and in section 2.1.

2.3. Polymer Modified Bitumen (PMB)

Current traffic loads and economically sustainable trends demand high performance paving roads, and modified bitumens became a possible solution for this problem. The most common modification types are by acids, by mineral fillers, and by polymers [21]. Only the latter was studied in the present work.

Bitumen modification by polymers has the purpose to enlarge the service temperature and to prevent the most common failures of road pavement, this by enhancing the mechanical properties of the binders [21, 24]. Specifically an increase in the high temperature viscosity and, sometimes, a decrease in the modulus at low temperatures will prevent rutting and thermal cracking respectively [24]. The changes are more evident at high temperatures [22, 30]. Besides, an improvement in resistance to abrasion and aging has been reported [22]. A further advantage of polymer modified bitumens (PMBs) is that with very few amount of polymer added (4-7% wt. of bitumen) significant changes in performance are achieved [22].

The most common polymer types used for asphalt modification are: thermoplastics with elastomer-like properties (e.g. SBS), thermoplastics (e.g. PE, PP, EVA), and reactive polymers (GMA) [22]. The latter can form a chemical network in the bitumen, leading to a chemically cross-linked material which is useless for pavement applications because it is infusible [22]. The thermoplastics with elastomer-like properties are the more widely used. In general this type of polymers confer a more elastic behavior to the binder on top of an increase in the mechanical properties. Nevertheless, the high cost and the limited recyclability (due to oxidation) are negative aspects of its usage [22]. . Thermoplastics are used as an alternative, and they were the type of polymer modifiers used in this work. Therefore they will be described in more depth.

Thermoplastics are a good alternative for bitumen modification due to the low cost, and wide polymer grades availability, furthermore it is an option for polymers recycling [31]. Nevertheless, the low polarity of the polymer as well as the high difference in densities between polymer and asphalt lead to immiscibility and phase separation at high temperatures. These aspects have delayed the widespread usage of thermoplastics as bitumen modifiers.

Thermoplastic PMBs are multiphase mixtures [24] on which the polymer will have different solubility in each of the SARA fractions. For instance it has been reported that the polymer will mix preferentially with the maltenes, and in the case of the aromatics the more polar the polymer the higher the compatibility [21, 22]. This causes a depletion of maltenes in the binder, and this effect is known as physical distillation, shown in Figure 2-19. This phenomenon gives rise to a polymer rich phase (PRP) and an asphalt rich phase (ARP). As a consequence the bitumen rich phase is enriched in asphaltenes which causes an increase in mechanical properties, and in the polymer rich phase a solution is formed changing as well its mechanical properties. Since the

polymer is swollen its volume fraction is increased [22]. Furthermore, depending upon the swelling and the initial volume fraction it is possible to have either a polymer in bitumen, or a co-continuous, or a bitumen in polymer system. In general, polymer mass fractions higher than 7% wt. will lead to phase inversion [22, 24].

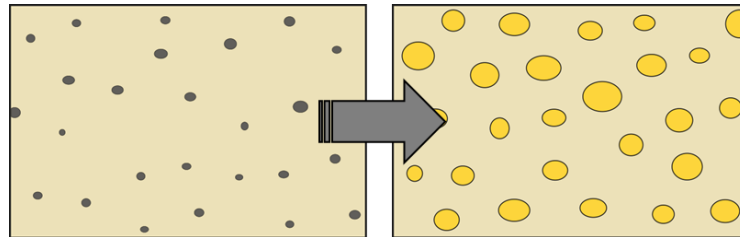


Figure 2-19 Schematic representation of physical distillation

It is worth to mention that PMB are complex mixtures. The bitumen matrix is a colloidal system, and the dispersed phase can be either a liquid or a solid depending upon temperature and swelling degree. Hence it is hard to categorize a PMB as a suspension or an emulsion.

The degree of swelling is a quantifier of the degree of compatibility between polymer and bitumen. However neither absence of miscibility or total miscibility are desired. What is desired is an intermediate miscibility or solubility [22], so that the PMB is a blend of both materials keeping certain characteristics of each of the phases and producing an enhanced mix like in polymer blends.

The most common thermoplastics used for bitumen modification are polyolefines (PE, PP), PVC, PS and EVA. Industrially many grades of these polymers are available. However commonly for binders modification, it is only specified polymer chemistry, molar mass (MM), glass transition temperature (T_g), and crystallization temperature (T_c). The recycled thermoplastic polymers used in this work were high density polyethylene (HDPE), shown in Figure 2-20, and poly ethyl-vinyl-acetate (EVA), shown in Figure 2-21.

High density polyethylene is a semi-crystalline thermoplastic polymer, which is synthesized by chain growth. Polyethylene is the most commonly used plastic and is manufactured in more than 60 million tons/year worldwide. The chemical structure of polyethylene consists only of carbon and hydrogen, which confers to the molecule a non-polar nature. The glass transition temperature is around -133– -143°C, and the melting temperature is around 118 – 146°C. The degree of crystallinity varies form 35-90% depending on molecular weight, crystallization conditions, and method of measurement [32].

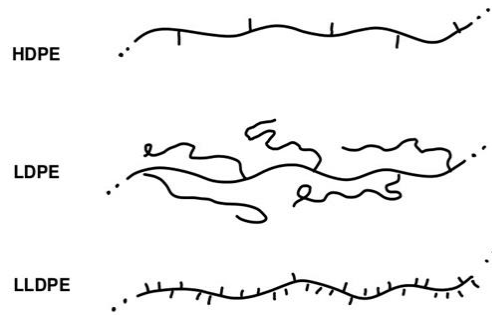
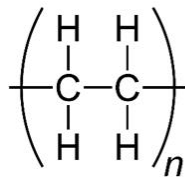


Figure 2-20 Chemical structure and topology of polyethylene

Poly ethyl-vinyl-acetate (EVA) is a semicrystalline thermoplastic copolymer, which is synthesized by chain growth. EVA is the copolymer of ethylene and vinyl acetate, the presence of the acetate group confers a higher degree of polarity respect to PE. The weight percent vinyl acetate usually varies from 10 to 40%, with the remainder being ethylene. It is a polymer that approaches elastomeric materials in softness and flexibility, yet can be processed like other thermoplastics. The glass transition temperature is around -42 – -38 °C, and the melting temperature is around 45 – 72 °C [32].

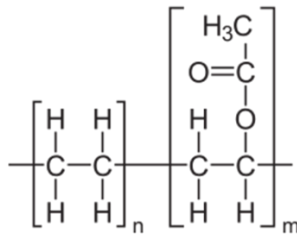


Figure 2-21 Chemical structure of poly ethyl-vinyl-acetate (EVA)

Due to the differences in chemical structure, HDPE and EVA copolymer will mix in a different degree with asphalt. It was reported that the swelling degree of PE is twice less than the one of EVA [21], the main responsible being the low polarity of PE. Hence, in the case of EVA copolymer the higher the content of VA group the better the compatibility with bitumen. In the case of EVA copolymer, the VA group is the one that is swelled by the bitumen maltenes, and the ethylene groups due to a lack of swelling at service temperatures will be in a semi-crystalline state. The latter is also true for HDPE, hence it will swell few and at service temperature its majority will remain in the semi-crystalline state [21, 22].

In general PE PMB will increase the rigidity of the bitumen and reduce significantly the deformations of the pavement road. Besides the lack of miscibility, the density difference with

bitumen triggers separation at high temperature storage. The latter is the unresolved problem that has delayed the industrial application of PE PMB.

In the case of EVA PMB the final performance relays on the relative content of ethylene and vinyl acetate groups. If the ethylene content is high the swelling will be poor and the mechanical properties will resemble those of PE PMB. By increasing the VA content the miscibility will increase, but there is a balance, because the existence of PE crystalline nodes has been reported to be needed to confer better mechanical properties to the PMB [22].

The PMB impact in mechanical properties will be further described in section 2.4.

2.4. Bitumen rheology

2.4.1. Linear rheology

In the LVE region, bitumen and PMB rheology depend upon time and temperature [21]. In this case the time dependence is referred to the VE nature of the binders. For both bitumen and PMB, a viscous behavior characterizes the rheology at high temperatures ($T > 60^{\circ}\text{C}$), a VE behavior characterizes the rheology at intermediate or service temperatures ($20^{\circ}\text{C} < T < 60^{\circ}\text{C}$), and a glassy behavior characterizes the rheology at low temperatures ($T \sim -20^{\circ}\text{C}$).

Rheological characterization of bitumen has been done by flow curve at high temperatures [21, 24], SAOS test for LVE at service temperatures [30], and flexural creep test or uniaxial extension test at low temperatures ($T \sim -20^{\circ}\text{C}$) [24]. Nevertheless, most of the reported literature on rheology is focused on SAOS test [21, 22, 24, 26, 30, 33].

Bitumen rheology is very similar to that of a low molar mass polymer (i.e. no entanglements) [22] as schematically shown in Figure 2-22. There is the absence of a rubbery plateau, nevertheless a glassy and a terminal region are present.

The mechanical spectra in Figure 2-22 was obtained using time temperature superposition (TTS) principle, which has been reported sometimes valid for bitumen (though this is still a matter of debate in the literature [26]) but rarely valid for PMB [22].

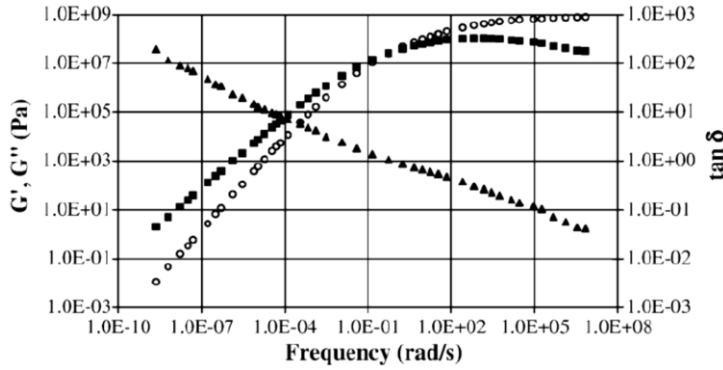


Figure 2-22 Mechanical spectra for a 70/100 pen bitumen from vacuum distillation \circ elastic modulus (G'), \blacksquare loss modulus (G''), \blacktriangle loss tangent ($\tan \delta$), $T_{ref}=0^\circ$, adapted from [22].

In bitumen, the transitions from Newtonian liquid to VE material and eventually to glassy solid have been related to the colloidal nature of the bitumen. In PMBs above those behaviors stand, but in the VE region some departures from the common master curve shape, Figure 2-23, have been reported [30].

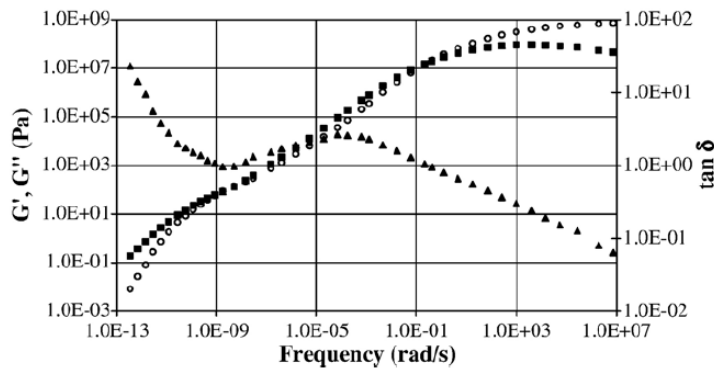


Figure 2-23 Mechanical spectra for a 70/100 bitumen with 7.2% wt. of (radial) SBS \circ elastic modulus (G'), \blacksquare loss modulus (G''), \blacktriangle loss tangent ($\tan \delta$), $T_{ref}=0^\circ$, adapted from [22].

Master curves of bitumen have been divided into three sections [22, 24]. First, at low frequencies a terminal regime with $G^* \sim \omega$ and $G'' \sim \omega$, was reported. However the scaling $G' \sim \omega^2$ was not reported in the literature consulted. Then, at intermediate frequencies a crossover region. Finally, at high frequencies a glassy region characterized by $G^* = 1 \text{ GPa}$ and $\delta = 0^\circ$ [21]. In PMBs these three regions are still present. However, the crossover point related to the longest relaxation time shifts towards lower ω , and the terminal region exponents can notoriously deviate from the standard values. Notice that in Figure 2-23 there are two crossover points: one at high frequencies

related to the glassy transition and other at low frequencies related to the longest relaxation time. The existence of this second relaxation mechanism indicates that another structure was formed, which is of higher size than that of the initial asphaltene aggregates. In contrast, the high frequency region is usually not affected, and at most a slight decrease in the plateau modulus is observed [22, 30]. Nevertheless, when phase inversion occurs the mechanical spectrum will reflect the polymer behavior, [22].

Rheological characterization of bituminous binders in the linear region has the advantages of being a noninvasive technique to study the microstructure of materials. In this regard SAOS characterization has been proven useful to differentiate between bitumen grades and between parent and modified bitumen [24]. However, this approach had limitations in pinpointing differences different PMBs [22, 24], as shown for instance in Figure 2-24.

This limitation is not restricted to asphalts, since it is known that different complex materials with similar microstructure are difficult to differentiate in the linear regime [1]. In contrast, rheological characterization in the nonlinear region has been proven to be sensitive enough to differentiate between materials of similar microstructure [13].

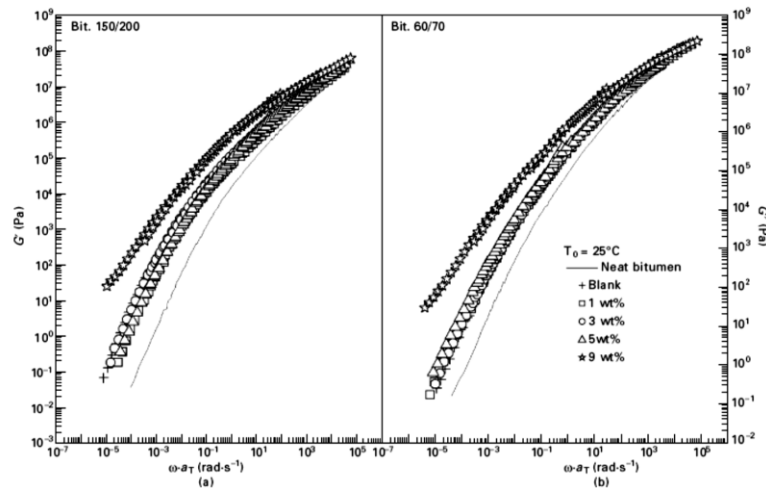


Figure 2-24 Master curves for (a) 150/200 and (b) 60/700 pen grade bitumen modified with a 50:50 mix of EVA and LDPE. $T_{ref}=25^{\circ}\text{C}$. Adapted from [24]

2.4.2. Nonlinear rheology

Even though most of the reported work on bitumen rheology has been done in LVE region, specifically in SAOS characterization, recently some literature on non-linear tests has been reported [22, 30, 34, 35, 36]. The nonlinear characterization of bituminous binders has been

focused, so far, on flow curves at high temperatures ($T > 40^\circ\text{C}$) and stress relaxation tests both in shear mode.

Stress relaxation test in the NLVE region¹ has been reported for bitumen and PMB, the latter comprising several types of polymers. The reported measurements were performed using rotational rheometers, namely Stresstech by Rheologica Instruments (stress controlled) for PE PMB and ARES A-33A (strain controlled) for EVA PMB. In both cases the geometry used was parallel plates [34], which is probably not the best option to test bitumen close to room temperature, see Figure B-3. The tests were carried out at different temperatures for each sample, due to experimental constraints (e.g. sample stiffness), and in the case of PMB also at different % wt [30, 34]. Nevertheless some general observations were reported. In the case of bitumen, the stress relaxation modulus in the NLVE region was described in terms of the product of the linear stress relaxation modulus and the damping function, shown in Figure 2-25. The damping function reported decreased as a function of increasing strain, meaning that bitumen had a softening behavior when deformed in shear. This was reported to be valid for several bitumen grades. The curve shape resembles the one of a LMW polymer [8].

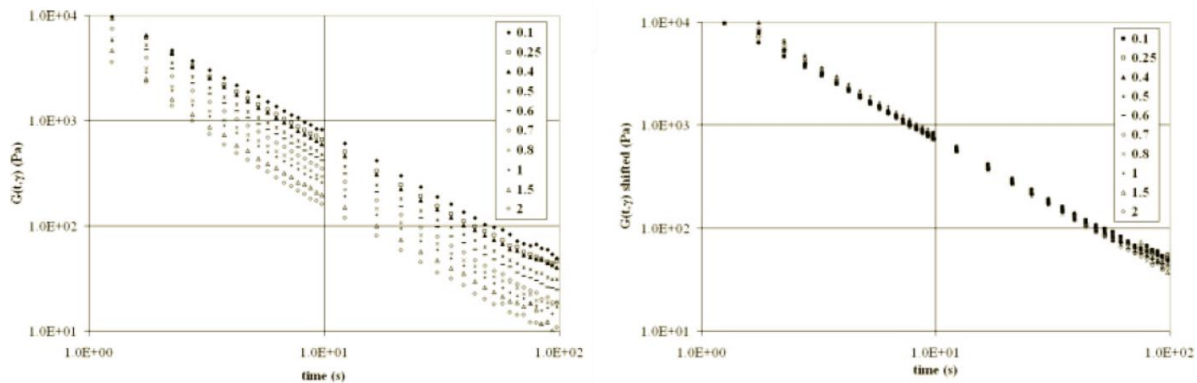


Figure 2-25 Stress relaxation modulus of a 70/100 pen grade bitumen at 20°C for various strains (left), and after the vertical shift (right) [34]

Stress relaxation of EVA PMB was reported for two concentrations 6% and 8% wt. [34], each one tested at different temperatures. The curve shape was reminiscent of a monodispersed linear entangled polymer i.e. sigmoidal shape. The curves were also superposable by means of a damping function between 0.1 s – 100s, as shown in Figure 2-26.

¹ An introduction to stress relaxation tests is given in Appendix B.1

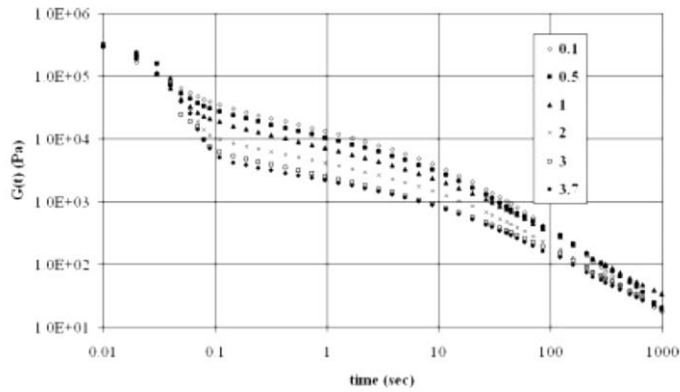


Figure 2-26 Stress relaxation modulus of a 200/300 pen grade with 8% wt. EVA at 35°C for various strains [34].

Stress relaxation of PE PMB was reported for three concentrations, 2%, 4%, and 6% wt [34], all of them showed qualitatively the same curve shape. The $G(t, \gamma)$ curves had a power law decrease on time, but the slope varied respect to the strain: curves superposition and damping function computation was not possible, as shown in Figure 2-27.

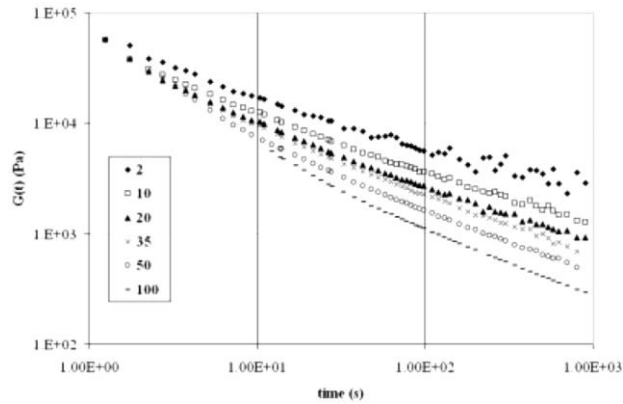


Figure 2-27 Stress relaxation modulus of a 70/100 pen grade bitumen with 4% wt LLDPE at various strains [34].

At the tested conditions for both PE and EVA PMBs none of the samples leveled off at high times, meaning that the samples had a viscoelastic liquid nature, and not a viscoelastic solid one.

Depending on the polymer used for the modification some canonical shapes of the stress relaxation were proposed in reference [22], and are reproduced in Figure 2-28 for further reference.

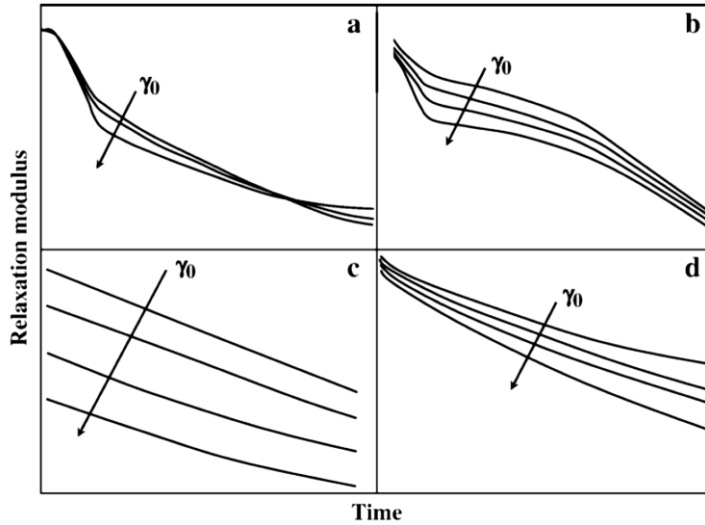


Figure 2-28 Qualitative shapes of the four proposed stress relaxation types: a) SBS, b) EVA, c) SEBS, d) PE, [22].

Flow curves have been reported for several bitumens and PMBs. The reported tests were carried out in ARES A-33A rheometers [35, 36] at high temperatures due to the soft-solid behavior of bitumen at room temperature [22]. Geometries used were parallel plates and cone and plates [35, 36].

The reported flow curves of unmodified binders had a Newtonian plateau at low shear rates followed by a steep shear thinning which in some cases approaches an slope of -1 [35]. The critical shear rate for onset of shear thinning shifted towards higher shear rates as the temperature was increased (see for instance Figure 2-29). The presence of a critical shear rate for onset of shear thinning was regarded as the start of the modification of the asphaltene aggregates by shear [22].

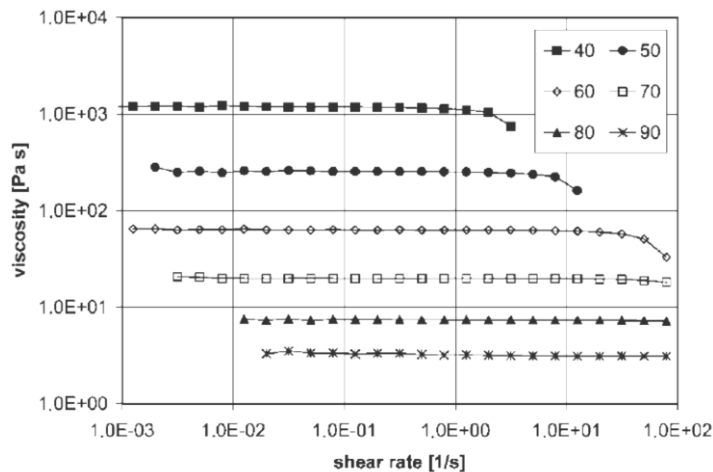


Figure 2-29 Flow curves of a 200/300 pen grade bitumen at different temperatures from [36].

In the case of PMB with either EVA or PE, also a Newtonian plateau followed by a shear thinning region was reported [30, 35, 36] in most cases, as shown in Figure 2-30.

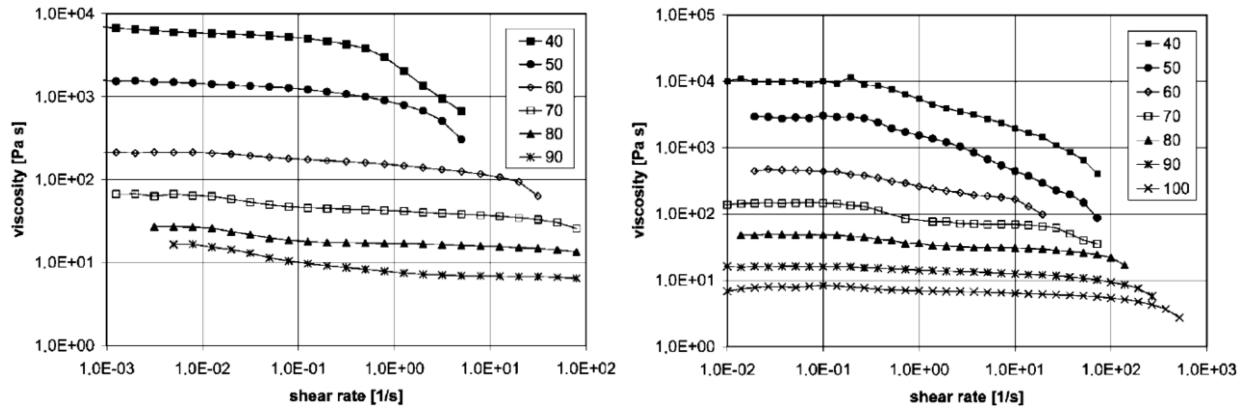


Figure 2-30 Flow curves of the previous 200/300 pen grade bitumen with (left) 4 %wt and (right) 8 %wt of EVA from [36].

However, the onset of the shear thinning occurred at much lower shear rates than the ones of unmodified bitumen [30, 35, 36], and the length of the shear thinning region spanned several decades in shear rate. In some conditions for EVA PMB a steep change in the shear thinning slope was reported at high shear rates [36]. For a given polymer, the slopes and the critical shear rate were reported to change depending on polymer content and temperature [30, 35, 36].

In the case of creep test no publication was found so far where the creep test was carried out to characterize the nonlinear behavior of asphalt binders. However creep tests had been used to assess the zero shear viscosity at high temperatures [37, 38], and this value has been successfully related to the rutting performance of asphalt road materials [39]. Nevertheless in asphalt binders the most common usage of creep test has been in the so called multiple or repeated creep test. Though this method has been applied to predict rutting behavior at high temperatures, the procedure is far from a standard creep test and the results are difficult to interpret with viscoelastic linear and nonlinear models and theories.

2.5. Test in binders for performance prediction

The most notorious standard for binders' evaluation and performance prediction is the one developed by the Strategic Highway Research Program (SHRP) in the US. They developed a series of tests to correlate the binder properties to mixes performance, and the final outputs were evaluation factors for each of the common failures. These factors have been used to rank binders

and to predict its performance [29, 39]. These factors are based on rheological characterization of the binders.

In the case of fatigue cracking the proposed factor is based on SAOS test, and it is

$$G^* \sin \delta < 5000 \text{ kPa @ } 10 \text{ rad/s} \quad (2.5-1)$$

This factor is measured in artificially aged binders (rolling thin film oven and the pressure aging vessel tests). This factor was originally designed to rank bitumens of different grades and origins [39]. Nevertheless, it has been reported that the usage of this factor to predict the fatigue performance of PMBs is poor, and most of the times it underestimates the real performance of the binders [29, 38, 39, 40]. The failure of this parameter is not surprising, since it is based in LVE functions, while the fatigue cracking phenomena is intrinsically non-linear.

An alternative test to characterize the fatigue behavior is based on time sweeps in oscillatory mode [29, 40]. The test consists of individual time sweep measurements at different amplitudes of either stress or strain [29, 40]. The test ends when the value of G^* reaches half of its initial value. The results are presented in a log-log plot of strain (or stress) amplitude vs number of cycles to failure. Then the so called fatigue law of the material is obtained

$$\gamma = aN^{-b} \quad (2.4.2-2)$$

Better fatigue performance will correspond to lower values of b (the closer to zero the better) and high values of a [40]. The conditions for the test in terms of the LVE or NLVE region are not reported. The samples are tested at the same value of G^* and at a standard frequency of 10 Hz. Therefore binders are tested at different temperatures [29].

2.6. Morphological characterization of PMB samples

The polymer inclusions dispersed in bitumen absorb aromatic components of the maltenes, during the physical distillation process. As a consequence of the higher concentration of aromatic compounds in the polymer rich phase as compared to the bitumen rich phase, the polymer inclusions will fluoresce when irradiated with UV-light. The aromatic rings by themselves do not cause fluorescence, but if electron donating groups (amino, hydroxy, ...) or electron accepting

groups (cyano, carbonyl, ...) are added to the ring structure fluorescence may occur [41]. This kind of compounds are found in bitumen. Therefore, fluorescent optical microscopy (FOM) can be used as a contrast technique to study the morphology of PMB samples [22, 30, 41, 42].

In fact, this technique has been shown to be the least invasive technique to study morphology on asphalt samples, e.g. in SEM the increase in temperature caused by the exposure of the sample to the electron beam is enough to modify the microstructure of the samples [22]. Nevertheless, the biggest challenge in FOM for PMBs relies on the correct sample preparation, fact that is sometimes underestimated. Currently, there are two main methods for sample preparation: drop of hot sample over a glass slide and brittle fracture of frozen binder [42]. The first method has the disadvantage that a drop, due to the curvature, will lack optical smoothness at the microscope, as shown in Figure 2-31. This can be solved by the usage of cover slides, but in this case the pressure exerted to flat the sample deforms the size and shape of the inclusions [42]. It is also worth to mention that either reheating the sample or the glass slides also affect the morphology. Brittle fracture of frozen samples can avoid morphology deformation, but the optical smoothness problem is unavoidable. Mechanical techniques have been used to smooth (flatten) the surface of the fractured sample [43], however the morphology integrity is again compromised. Based on this a new method for the production of microscopy samples was suggested on the materials and methods section.



Figure 2-31 Example of a micrography of a sample (SBS PMB) without optical smoothness [42]

The principal output of FOM is the morphology of the PMB sample, i.e. polymer/bitumen, bi-continuous, or bitumen/polymer dispersion. However, also the particle size distribution can be obtained, provided that the correct sampling is done. This in general requires the analysis of a large enough amount of pictures as to reach reliable statistics [42].

3. Materials and methods

In this chapter the materials used during the experimentation as well as the methodologies used during their study will be introduced.

3.1. Materials

Bitumens

In order to minimize the variability inherent to different bitumen sources and batches, only bitumens produced by crude distillation in La Rábida refinery of CEPSA in Huelva, Spain were used. Two different paving grades were used. A 70/100 pen grade (75 dmm EN1426) bitumen with $T_{R\&B}$ of 49°C (EN1427), and a 35/50 pen grade (35 dmm EN1426) bitumen with $T_{R\&B}$ of 54°C (EN1427). The first bitumen was chosen as the one to be modified, and the second one was chosen as the benchmark for the PMBs. In other words the 70/100 pen grade bitumen was polymer modified with the aim to obtain mechanical properties similar or better than those of 35/50 bitumen in order to produce asphalt mixtures with longer service life.

Polymers

Two different thermoplastic polymers were chosen as representatives of this category of polymer modifiers. One was a high density polyethylene, HDPE, (non-polar structure) and the other was an ethyl vinyl acetate, EVA, copolymer. Following the global trend of recyclability both HDPE and EVA were recycled polymers obtained from the company Gintegral – Gestão Ambiental, S.A. The origin of the waste polymers as well as the pre-treatment prior to pelletization were not disclosed by the company. The glass transition and melting temperatures of the polymers are given in Table 3-1

Table 3-1 Polymer transition temperatures

Polymer	T_g [°C]	T_m [°C]
EVA copolymer	-25.3	69.7
HDPE	-	131.2

These parameters were determined according to the methodology described in [44]. The measurements were done by the research team of Civil Engineering at MINHO University who kindly shared these data.

Polymer modified bitumens

The binder 70/100 pen grade was modified with each of the polymers mentioned above. The polymer percent weight used was set to 5% wt. The identification code for each of the samples was: parent binder + polymer + percent weight, i.e. 70/100HDPE5 and 70/100EVA5. Their empirical characterization is given in Table 3-2.

Table 3-2 PMBs specs

PMB	Pen value [dmm]	T_{R&B} [°C]
70/100HDPE5	32	69
70/100EVA5	37	61

These results can be evaluated in comparison with those of unmodified bitumens. The modified bitumens were able to obtain pen values similar to those of 35/50 bitumen, then it was expected that these materials would be stiffer than 70/100 at service temperatures. The R&B temperatures increased to values clearly higher than those of 35/50 bitumen.

Bitumen classification in Europe is given in *pen* grades (EN 1426). This classification is also adopted in this work. For a detailed description of the test refer to EN 1426. Briefly, the test consists in measuring the depth (expressed in tenth of millimeters) at which a standard needle penetrates an asphalt sample after 5 s loading time with a 100 g load at 25°C. The penetration grade is given in intervals, i.e. an asphalt with 85 1/10 mm of penetration will correspond to a 70/100 pen grade [26].

The other parameter reported in Table 3-2 is the ring and ball temperature (T_{R&B}). A detailed explanation of the test can be found in the EN 1426. Concisely, the test consists of pre-forming asphalt binders in metal rings to give cylinders of 8 mm thick and 16 mm diameter. Two asphalt cylinders are placed inside a water bath, and over each asphalt sample a standard steel ball of 3.5 g (9.5 mm diameter) is placed. The water bath temperature is increased at a rate of 5°C/min from a starting temperature of 5°C. The test ends when the bitumen, deformed by the action of the steel weight, touches the vessel bottom. This corresponds to a longitudinal deformation of 25 mm [26].

Calibration standards

Steel torsion bar (STB) provided in the torsion rectangular bar ARES tool kit of TA instruments

(SN 400.02589) and viscosity standard Wacker® siliconel AK 100 000 batch 0H25156 were used to set the experimental protocol for LAOS FTR.

3.2. Methods

PMBs manufacturing

PMB samples were produced by common methods. For 1 kg total sample bitumen was placed in a 2 kg container under mild agitation, while increasing the temperature by means of an electrical jacket up to 160 °C. At this temperature the already weighted polymer pellets were added.

After polymer addition, the hot mix was transferred to a high shear IKA rotomixer set-up to make the proper dispersion of the polymer in the bitumen matrix. In this set-up the mixing was done at 7200 RPM and 160 – 165°C for 20 min. In some cases the temperature dropped during the samples transfer from one device to another, in those cases the sample was heated in the rotomixer device by means of viscous heating, yet the mixing times was considered from the moment the sample achieved 160°C.

Asphalt Torsion bars (ATBs) production

In the case of bitumens, a bitumen sample was warmed up in an oven up to 160°C. Once heated the sample was poured in rubber molds of set dimensions (4.7 mm thickness, 11.8 mm width, and either 25.0 or 60.0 mm height). The bitumen excess was eliminated by means of a hot spatula, and subsequently the samples were placed in a freezer at - 10°C. After 5-10 min samples were ready to de-mold. In most of the cases edges trimming was needed, which was made with scissors. Then, samples were identified and placed in individual plastic bags and preserved in the freezer until their rheological characterization was carried out.

In the case of PMB, above procedure was carried out immediately after manufacturing (to avoid aging effects or phase separation).

To produce ATBs of different height, a 60 mm bar was cut at the desired height by using a hot cutter (T~ 140°C). Since the cut was done at the edges, then the medium part of the bars which is the one that is subjected to torsion was not affected.

Empirical characterization

Penetration test and ring and ball temperature tests were carried out as described in [26]. This was done as a quality control for reproducibility between batches.

Rheological characterization

All rheological characterization tests were done in a strain controlled rheometer of the advanced rheometric expansion system (ARES) rheometer kind, from TA instruments, equipped with a torsion rectangular bar set or a parallel plate 50 mm. The anvils used were the #1 for STB and #3 for asphalt samples. The parallel plate geometry was only used for the viscosity standard testing, and the gap used was 1.0 mm. Temperature regulation was not possible since the operating range of the oven (with air convection) fell out of the temperature range corresponding to asphalt service. Thus, the air conditioner of the lab was used to control the temperature. All measurements were carried out at temperatures between 19 – 21°C, a better temperature control being not possible.

Sample loading

The standard procedure for sample loading was based on the one suggested in the ARES manual. First, the sample was placed and centered in the lower geometry tool. Then the upper geometry was moved down at a proper distance just to ensure that the bar was also centered for the upper geometry. In which case, care was taken for the bar to be confined inside the geometry limits. After this, the lower anvil was adjusted to the proper clamping torque, given in Table 3-3. Then, the upper geometry was moved down till it touched the sample which was recorded in the software by an increase in 20-40 g in the normal force transducer. After this the upper anvil was adjusted, and then the upper geometry was moved upwards to ensure that there was enough grip between the bar and the geometry. The pulling was done till there was a residual normal force lower than 10 g, this figure was determined as part of the calibration procedure to obtain repeatable measurements.

Table 3-3 Clamping force used to lock the samples in the rectangular geometry

Sample	Clamping force [cN.m]
Steel	35.0
35/50	2.0
70/100	1.5
70/100EVA5	1.8
70/100HDPE5	1.8

Prior to loading the sample dimensions (thickness and width) were measured with a digital caliper (Schut 0-150 mm DQ⁺⁺ – resolution 0.01 mm). Both dimensions were measured at the extremes and at the middle of the asphalt TB, then an average was computed. These data were needed as an input in the rheometer software (Orchestrator) for computing strains and stresses from motor deflection and torque transducer readings.

Data acquisition for FFT analysis

For FT analysis raw data acquisition of motor and transducer signals was digitized using a 12-bit analog to digital converter (ADC) operating at sampling rates up to 100 kHz [$t_{dw} = 1/(100\ 000)$ s]. The model was DAQPad-6020E NI serial number 11F2B50, from National Instruments. This ADC card was plugged into a stand-alone PC equipped with LabView software (National Instruments). For each strain value at least 18 cycles after the transient in strain were recorded and digitized. FT data analysis was done as described in detailed in the FT LR section using home-written Lab View programs. This program allowed to set during the acquisition the sampling rate and the fundamental frequency. The details about the sampling rate chosen for all binder samples are given on Table 3-4 for all the frequencies tested. The Nyquist frequency was calculated considering that data will be recorded up to the 40th (or 50th for 0.1 Hz) harmonic. This is based on the fact that for any of the measurements higher harmonics than 40th were buried in the signal noise. For the STB and the viscosity standard the Nyquist frequency was at least 20x ω_0 . For data analysis the software allowed windowing \therefore integer number of cycles were analyzed to minimize leakage.

Table 3-4 Data acquisition details for FFT computation

ω [Hz]	Sampling rate [1/s]	Nyquist ω [Hz]	Max harmonic
0.1	10	5	50
0.3	24	12	40
0.7	56	28	40
1	80	40	40
2	160	80	40
2.25	180	90	40
7	560	280	40

Dynamic tests

Standards

LAOS tests were done at different frequencies, and more details are given in section 5.1. For the viscosity standard, a 6 min time sweep test performed under SAOS was used before testing with LAOS, as to monitor the sample relaxation after loading and thus ensure that the sample was fully relaxed prior to LAOS testing.

Asphalt binders

The linear viscoelastic region was determined by means of a strain sweeps at 0.1 Hz frequency. From a strain interval between 0.1 to 20%, with at least 20 cycles per point.

SAOS tests were carried out at 0.1 % strain (inside the LVE region) for all the samples. The frequency interval studied was from 0.1 to 60 Hz. Three replicates per sample, with different ATB, were done to correctly identify the crossover point and the mechanical spectra.

LAOS tests were done in three different modes. In the first mode, samples were studied at the same value of δ , i.e. samples mechanically equivalent. In the second mode, samples were studied at the same De number, i.e. at the same relaxation state. In the third mode, samples were studied over one frequency interval from 0.1 to 2.0 Hz. The strain amplitude was varied from 0.47% to 25%.

LAOS tests in time sweep mode were done at the condition of same δ . The strain levels were set for the samples to have the same level of I_3/I_1 %. Therefore the samples were mechanically equivalent and at the same level of nonlinearity. The details are given in Table 8-1 on the fatigue test section. The time sweep measurement time was restricted to no more than 15 min per test.

Data manipulation in LabView (external software)

To support the validity of the data analysis done in the LabView software, I_3/I_1 % LabView data from the transducer response were compared with the non-linear parameter (I_3/I_1) from the Orchestrator software (rheometer software), shown in Figure 3-1.

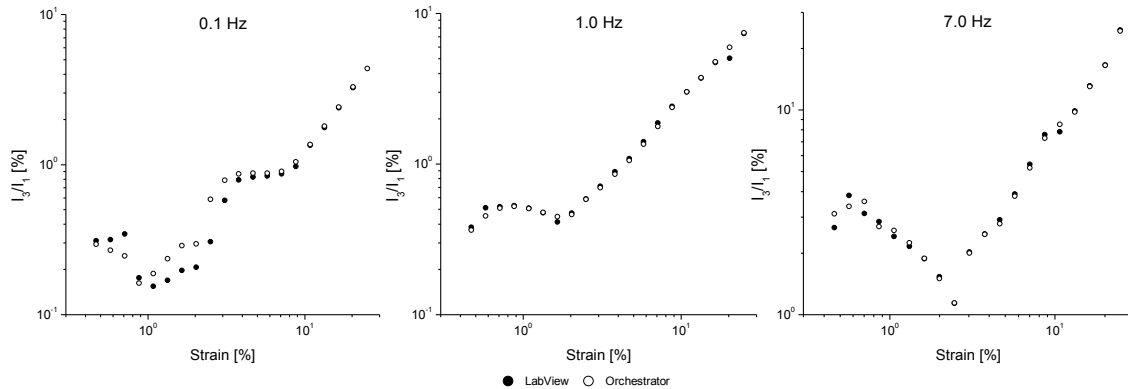


Figure 3-1 Comparison of data analysis between Orchestrator (rheometer) and LabView (external) software.

There was a good agreement in between both analysis. Therefore, the option of incorrect data analysis was excluded.

Stress relaxation

Stress relaxation tests² were measured following 0.05%, 0.1%, 1%, 3%, 5%, 10%, and 20% step strains, that specifically spanned the transition between LVE region and NLVE in LAOS tests for each sample. This protocol was used with the aim to directly compare both non-linear tests. Data acquisition was done for a total time of 1000 s. The data point collection was logarithmic, the total experimental time was split in 4 time zones (2, 10, 100, 1000 s), and 50 points were acquired per time zone. However the maximum sampling rate of the rheometer was 0.01 s. The shearing direction was clockwise. For each test a different ATB was used, but for the first 2 step strains which correspond to the linear regime with no damage for ATB samples. Due to motor inertia an instantaneous strain step was not possible, therefore only data acquired after 98% of the target strain was settled were considered. For all the samples and testing conditions, this target was obtained either at 0.07 or 0.08 s, which means that maximum the first 7 points were eliminated, as shown in Figure 3-2a and b. Due to transducer sensitivity, only torque data higher than 0.02 g.cm (as per rheometer's specification) can be considered reliable, therefore all data below that limit were eliminated, as shown in Figure 3-2 c and d. Due to electronic limitations, there was a saturation in the acquired torque signal at the beginning of the time zones, in such a way that the data acquired were scattered around the mean value, as presented in Figure 3-2 e and f. For that reason, any data that belonged to any of the above described experimental pitfalls were discarded

² A brief introduction to stress relaxation tests is given in Appendix B.1

prior to data analysis, i.e. only experimentally “clean” data were considered for analysis, as shown in Figure 3-2f.

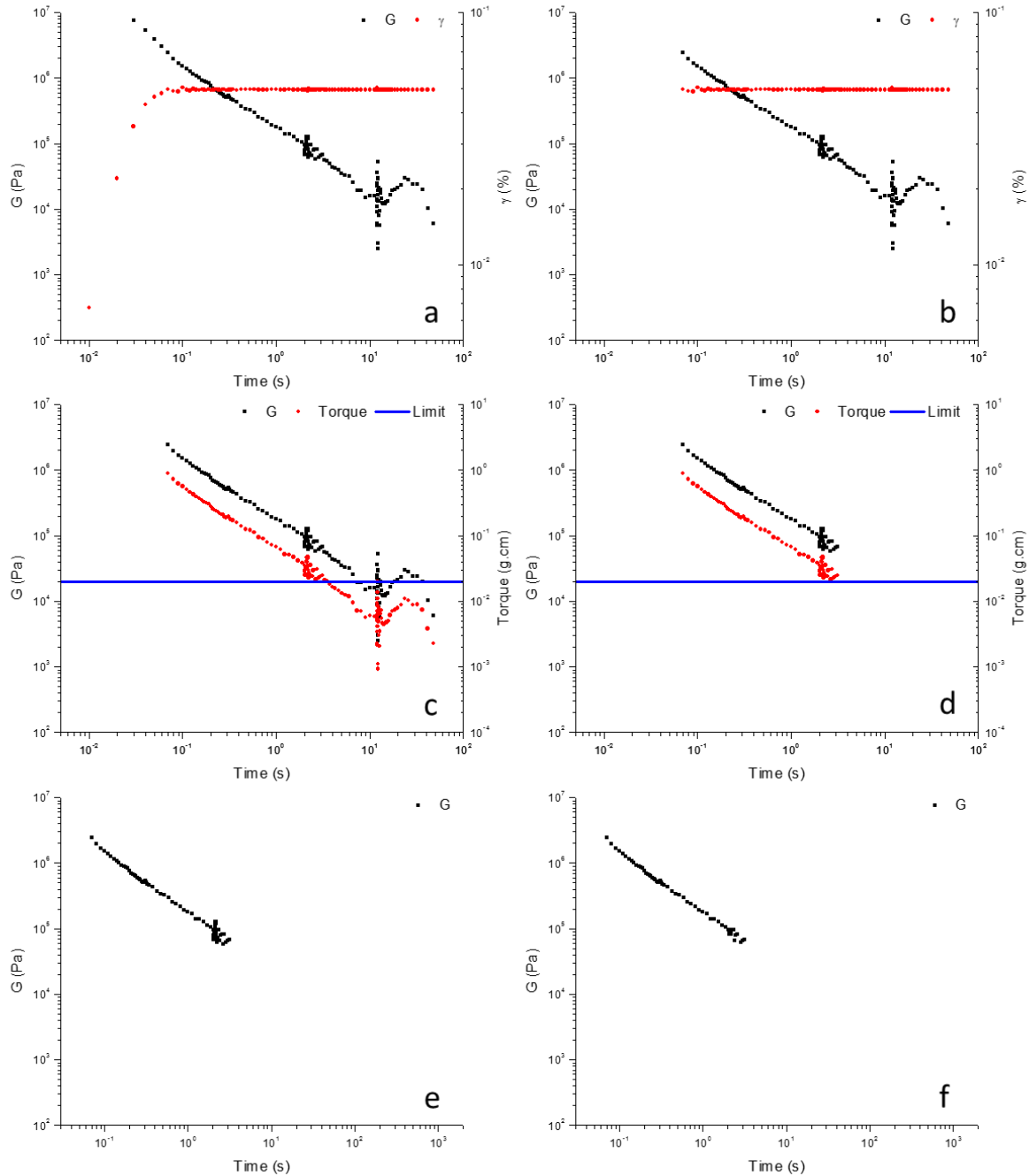


Figure 3-2 Stress relaxation data analysis: a) raw data acquired from rheometer, b) data obtained at 98% of target strain, c) raw torque and modulus data acquired at 98% of target strain, d) data acquired above the transducer sensitivity limit, e) same as d) showing saturation of data acquisition at ~ 2 s, f) data clean of experimental pitfalls and used for analysis.

Data analysis of the stress relaxation data in the non-linear regime was done by means of the damping function $h(\gamma)$. For the damping function computation the $G(t)$ was taken as the one at $\gamma=0.05\%$. Then at a fixed strain, a value of $h(\gamma)$ was computed for each time, and all the values of $h(\gamma)$ were averaged and a standard deviation associated to this variation was also computed. This approach was possible because the data acquisition was the same for all the samples. Therefore for all the samples, data points at the same times were available.

Fluorescent optical microscopy.

Samples preparation consisted in dipping a clean glass slide in the PMB sample immediately after its manufacturing. Followed by placing the glass slide in horizontal to let the sample spread homogeneously. Then the glass slides were carefully covered with aluminum foil, for it to protect them from impurities without being adhered to the surface. Finally, samples were placed in the freezer at -10°C up to the moment of its analysis. By means of this method no mechanical manipulation was induced in the samples, yet the surface was kept visibly smooth only for 70/100EVA5 sample. The bottom part of the glass slide was cleaned from binder remnants to be able to also acquire micrographs from the bottom of the sample as well.

Micrographs were acquired in an Olympus BH2 – RFCA mounted with a UV lamp HBO 100W/2 in reflection and bright field. The magnification used was 10x in objective lens and 2.5x in eyepiece lens for a total magnification of 25x, BH2-ANF. Micrographs were acquired with a digital camera (Leica DFC280) linked to the Leica software for imaging analysis.

4. Linear viscoelasticity of asphalt binders and morphological characterization

In this chapter a brief study of the rheological behavior of asphalt binders in the LVE region along with the PMBs morphological analysis done with fluorescence optical microscopy will be presented. First, it will be presented the SAOS test and the mechanical spectra of the different binders. Second, stress relaxation tests in the linear regime will be given. Finally the FOM results will be presented.

4.1. SAOS test

The outputs of the SAOS test were the viscoelastic behavior of the binders in terms of G' , G'' , and δ as well as the crossover frequency, ω_c , between G' and G'' .

In terms of $G'(\omega)$ and $G''(\omega)$, shown in Figure 4-1, it was possible to identify the differences between the unmodified binder (70/100) and the PMBs (70/100EVA5 and 70/100HDPE5). For this purpose, the elastic modulus was more sensitive to the modification rather than the viscous one, this based on the differences between the samples error bars.

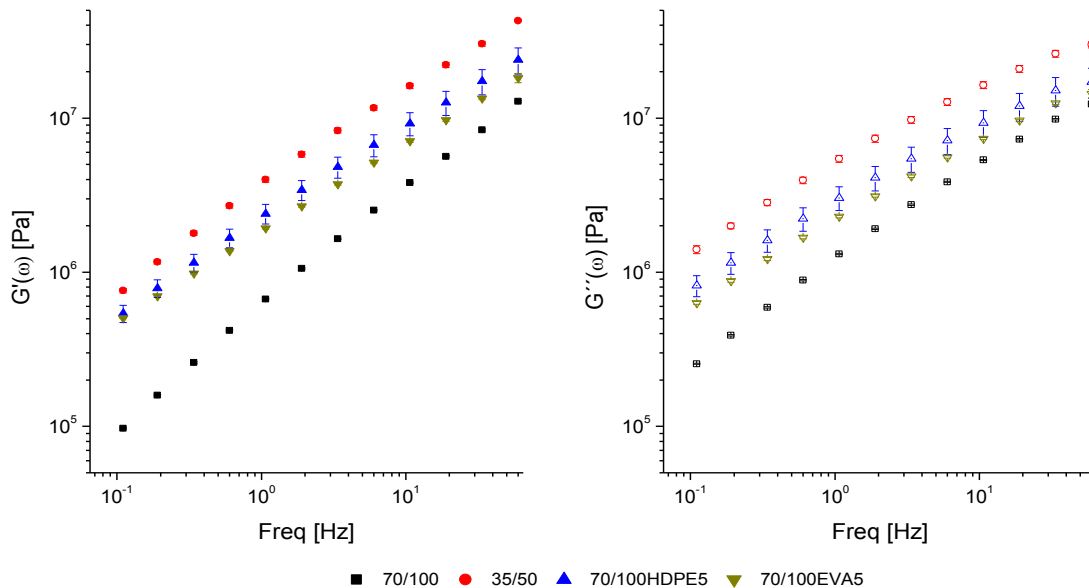


Figure 4-1 Mechanical spectra of bitumen binders at $T \sim 20^\circ\text{C}$: G' filled symbols and G'' unfilled symbols.

However, it was not possible to clearly discriminate between PMBs, which is congruent with other results reported [24], as illustrated in Figure 2-24. Besides, in both PMBs the moduli were increased in such a way that their mechanical spectra were approaching the 35/50 binder ones, thus departing from the initial 70/100 ones. Still the viscoelastic characteristics of 35/50 binder were not reproduced by any of the PMBs. Between the PMBs, 70/100HDPE5 binder had slightly higher moduli values (and significantly different at some frequencies) than the ones of 70/100EVA5 binder at all frequencies: 70/100HDPE5 was stiffer than 70/100EVA5.

The phase angle $\delta(\omega)$ relates G' and G'' moduli, refer to equation (2.1.4-16), and therefore can give an alternative representation of above data, as shown in Figure 4-2.

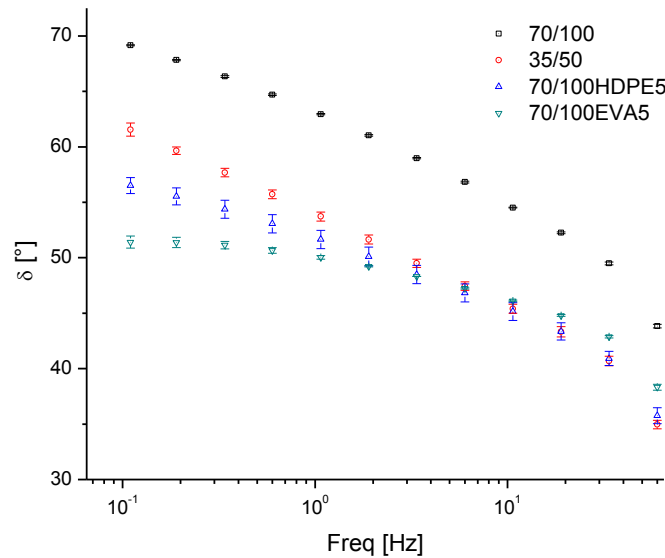


Figure 4-2 Phase angle of binders as a function of ω at $T=20^\circ\text{C}$.

In terms of the phase angle, the effect of the modification was visible at any frequency. By comparing the PMBs with the 35/50 binder, the 70/100HDPE5 trend was more alike to the 35/50 one, yet at low frequencies all samples were significantly different. In terms of the two bitumen grades, they both had a similar δ tendency as a function of ω , but 70/100 had consistently higher values of δ . It is also worth to mention that at low frequencies the value of δ leveled off for 70/100EVA5 sample $\omega < 1 \text{ Hz}$, and in the case of 70/100HDPE5 binder a tendency to level off was also detected. This can be either the beginning of a plateau region or a local maximum of delta; to figure it out measurements at lower frequencies would be needed. Based on $\delta(\omega)$, Figure 4-2, at low

frequencies the samples can be ranked in terms of elasticity as 70/100EVA5 > 70/100HDPE5 > 35/50 > 70/100.

Considering the $\delta(\omega)$ response, 70/100EVA5 phase angle did not vary a lot in the frequency range studied. Therefore in terms of design, the viscoelastic nature of 70/100EVA5 binder was more balanced over the whole frequency range studied as compared with any of the other binders. This means that 70/100EVA5 will show more or less the same viscoelastic behavior either at low or high frequencies: it will be less sensitive to frequency (or temperature) changes.

The other parameter that was possible to analyze between the samples was the frequency at crossover, ω_c , between $G'(\omega)$ and $G''(\omega)$. The crossover frequency (given in Table 4-1) was related to the characteristic relaxation time of the system, i.e. $\lambda = 1/\omega_c$. The ω_c for the PMBs was smaller than that of the parent 70/100 bitumen, i.e. the relaxation time was increased. This supported previous findings: the polymer modification made the binders more solid-like [21, 24]. The ω_c of the 35/50 binder was the same as the 70/100HDPE5 one. As expected ω_c of 35/50 binder was lower than that of 70/100 binder.

Table 4-1 Crossover frequency of the different binders at $T \sim 20^\circ\text{C}$.

Sample	ω_c
35/50	11.7 ± 1.3
70/100	53.3 ± 0.9
70/100EVA5	15.8 ± 0.5
70/100HDPE5	11.0 ± 2.6

4.2. Stress relaxation in linear regime

Stress relaxation tests were done at strains of 0.05% and 0.1%. Since both measurements were identical ($h(\gamma)=1$ at $\gamma=0.1\%$, as shown in Figure 7-2), the modulus obtained was the linear stress relaxation modulus $G(t)$, shown in Figure 4-3.

By means of stress relaxation modulus it was possible to detect the effect of the polymer modification in the 70/100 bitumen: higher PMBs modulus is visible at long times. At short times, 70/100EVA5 had the same modulus than 70/100, but at long times it was higher, which means that its decaying rate was slower. The 70/100HDPE5 binder had also a decay rate smaller than the 70/100 sample. Therefore the modification not only increased the modulus but also affected its decaying rate.

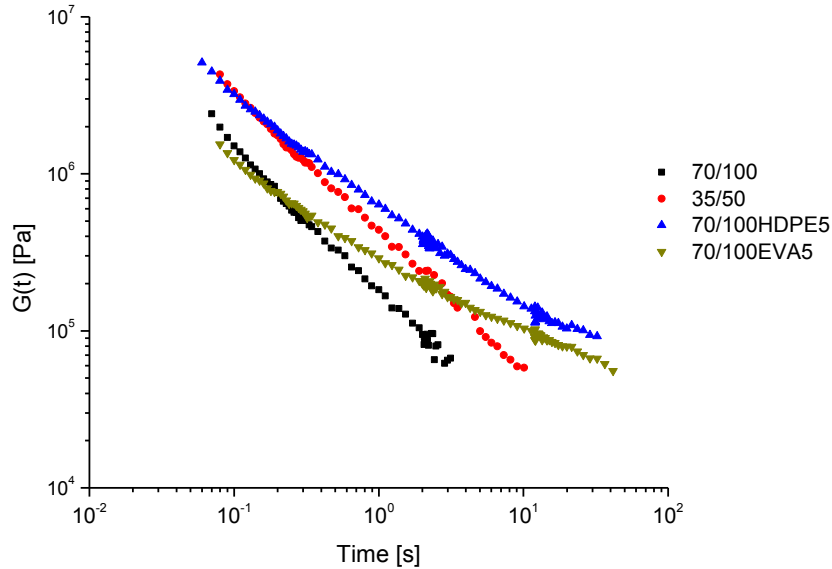


Figure 4-3 Linear stress relaxation modulus of binders at $T \sim 20^\circ\text{C}$.

PMBs can be differentiated at all times, and 70/100HDPE5 had a higher modulus. Further comparison of PMBs with 35/50 binder led to the conclusion that 70/100HDPE5 was more similar to 35/50 sample, cfr. with 70/100EVA5.

Regarding bitumen grades, the curves of both bitumens were similar in shape (same memory function), with the main difference that the 35/50 bitumen was stiffer than the 70/100 one.

4.3. PMBs morphology (FOM)

Micrographs acquisition was done in 70/100 and PMBs binders. In the 70/100 parent bitumen no contrast was observed, as expected [41]. In the case of PMBs representative micrographs of each sample are shown in Figure 4-4. In the PMBs the physical distillation phenomenon was observable since the PRP shown contrast in UV light. Between the PMBs, 70/100EVA5 binder shown higher swelling and better compatibility than the 70/100HDPE5 one, shown in Figure 4-4a and d, as per the larger distribution of droplet size and higher amount of droplets. This is in agreement with the expected higher compatibility of 70/100EVA5 binder which would lead to a higher swelling degree. This fact was confirmed by the higher covered area of 70/100EVA5 binder as compared to the 70/100HDPE5 one.

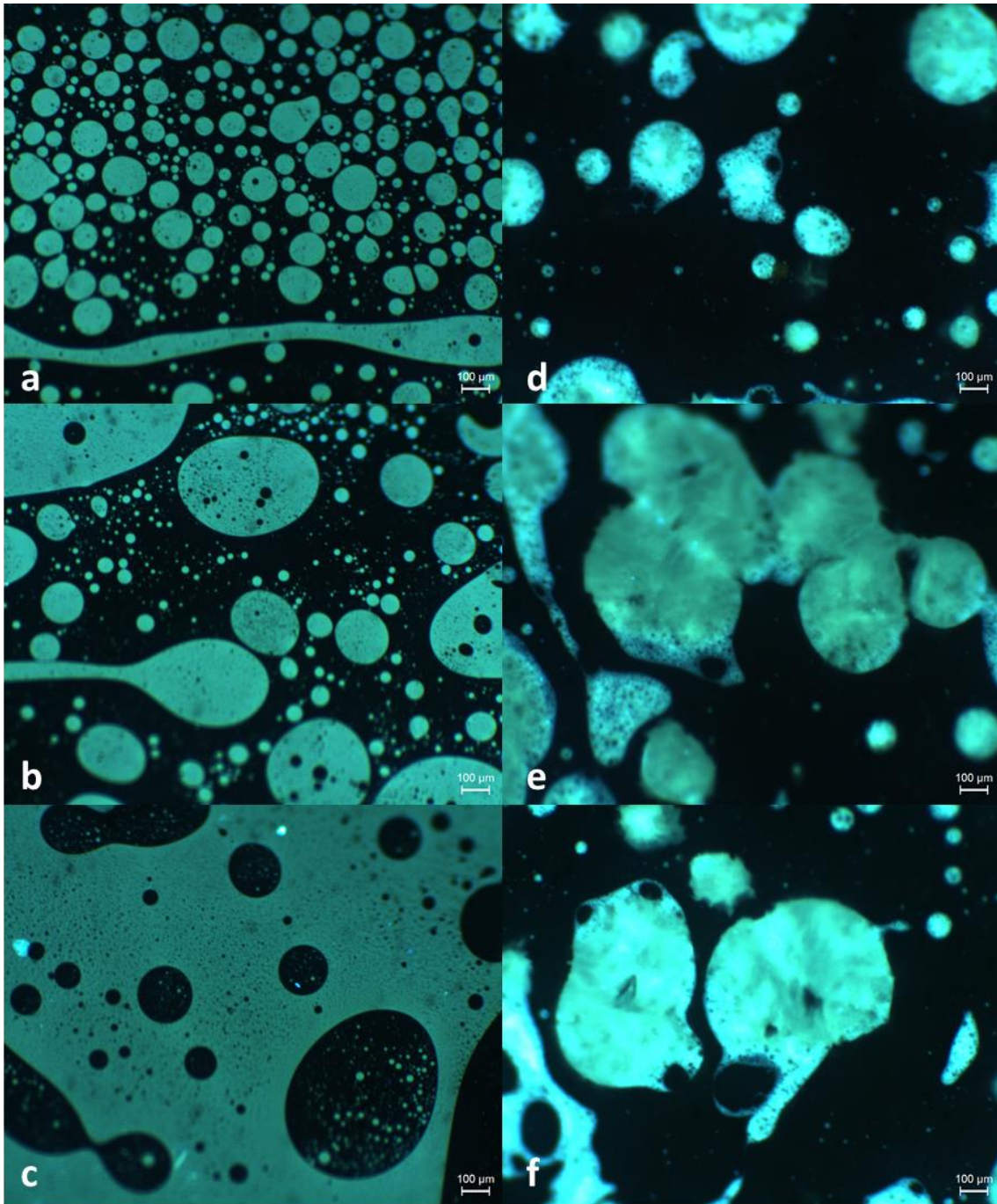


Figure 4-4 FOM micrograph of 70/100EVA5 binder (a,b,c) and 70/100HDPE5 (d,e,f), acquired from the top part of the glass slide..

The 70/100EVA5 binder seemed to be borderline to a co-continuous or phase inversion state, since inside of some of the PRP droplets ARP spots were present, shown in Figure 4-4b. This is reminiscent of the w/o/w emulsions which are systems that are formed at conditions between o/w and w/o emulsions [45]: in this case the presence of such ARP spot in PRP was an indication of

being close to a phase inversion. Indeed, a co-continuous morphology is pictured in Figure 4-4c which was a singularity (one out of twenty micrographs taken) in all the sample tested. There were also elongated droplets which could be either a signal of the coalescence and break-up process which was happening at high temperature but once in the RT was not able to relax to a spherical shape, or to the coalescence of several droplets. However, also the slide preparation (immersion and emersion) could have induced such droplet shapes.

Regarding 70/100HDPE5 very big droplets, shown in Figure 4-4e and f, were found which in the frame of PMBs corresponds to a phase separation process [46]. In some cases, it was even evident that the droplets were interconnected, in which could lead to coalescence and formation of only one big aggregate.

Based on this also micrographs from the bottom part of the glass slide were taken, shown in Figure 4-5. A very different morphology was observed for both binders \therefore confirming that creaming was present in the samples. This was not surprising since it is well documented that phase separation is a big issue in thermoplastic PMBs [22]. However this suggested that the methodology used to prepare the glass slide samples needs to be improved.

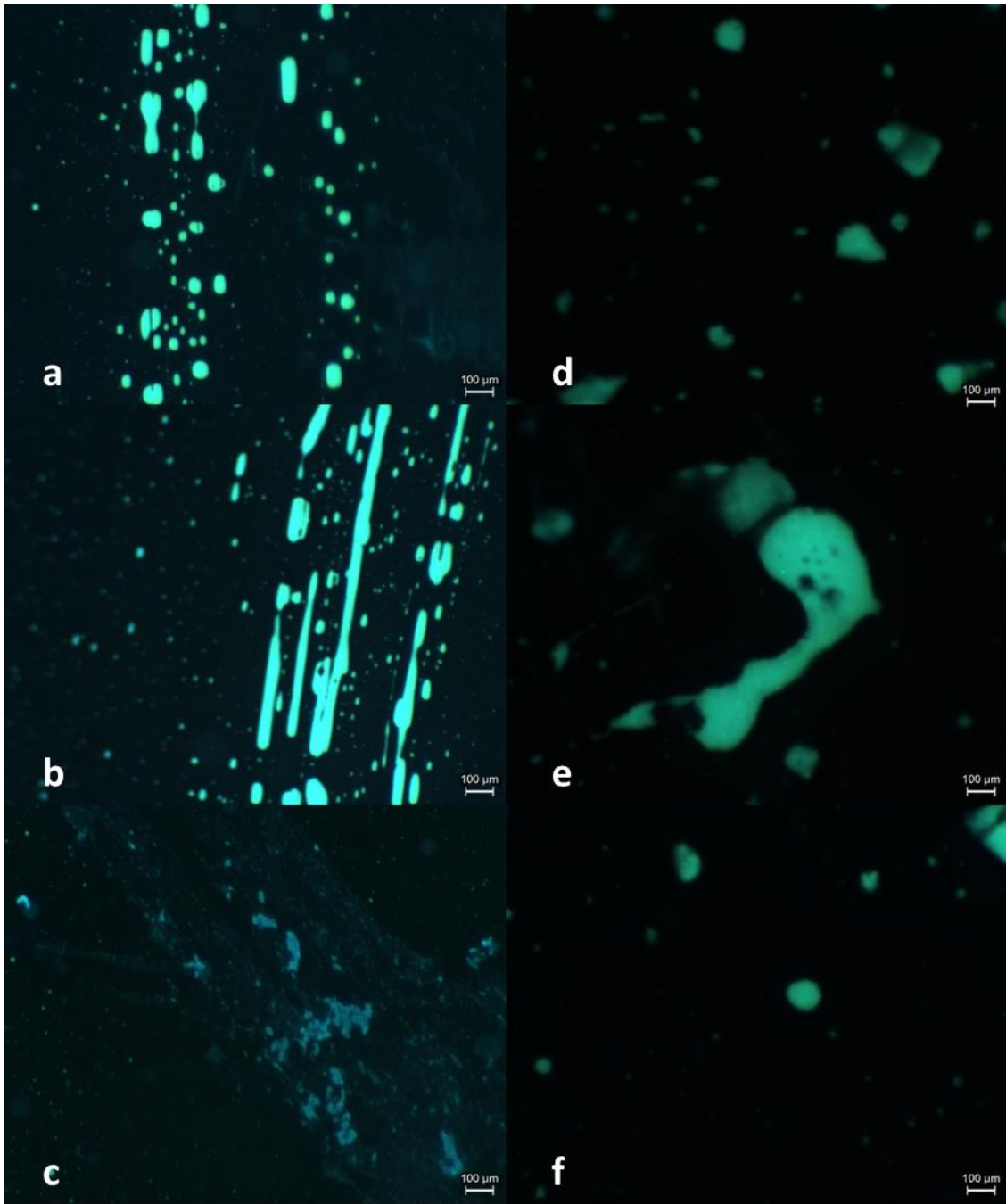


Figure 4-5 FOM micrograph of 70/100EVA5 binder (a,b,c) and 70/100HDPE5 (d,e,f), acquired from the bottom part of the glass slide.

5. Experimental method validation of LAOS-FTR test for binders at room temperature.

The purpose of this chapter was to establish the basic experimental procedure for the correct study of asphalt binders nonlinear rheology at service temperature. This was done with a special focus towards LAOS test, but the procedure for samples production was equally valid for the rest of the tests.

Specifically for LAOS characterization, it was needed to control that the nonlinearity observed in the stress signal only came from the sample and not from the rheometer nonlinearity. Based on this requisite, the range of conditions under which the ARES rheometer behaved linearly needed to be identified. This is independent of the type of samples to be tested, since it is a rheometer characteristic. In respect to the binder samples, it was needed to establish a reliable procedure for samples production and LAOS testing, to ensure experimental repeatability with lowest associated errors.

Considering above statements this chapter was subdivided in the study of linearity range of ARES rheometer in dynamic tests and in the experimental repeatability under LAOS testing of asphalt torsion bars.

5.1. Linearity range of ARES rheometer

In order to define the operational interval for experimentation in LAOS test, the linearity range of the motor to produce a monochromatic strain on one hand, and the linearity of the torque transducer to transmit a monochromatic response on the other hand, were determined.

In this way a series of strain sweep tests were performed at different frequencies. Two different materials and geometries were used in order to be able to span a broad interval of strains and torque amplitudes. This is a common practice for LAOS test [6]. The materials used were a polydimethylsiloxane (PDMS) viscosity standard and a steel torsion bar (STB), which specifications were given in section 3.1. The geometries used were parallel plates (PP) for the viscosity standard and a torsion rectangular bar set (TB) for the STB.

To analyze the motor signal, the motor angular displacement was used instead of the strain, because a strain level in PP and in TB geometries is not equivalent in terms of motor displacement. This can lead to inconsistencies, i.e. for the same strain level, in one geometry the motor signal could be non-linear and in another it could be linear, just because the motor displacement is different on each geometry. Such problem is overcome by analyzing all the geometries in terms of motor angular displacement, which is geometry independent.

The studied intervals for frequency (ω), strain (γ), motor angular displacement (θ), and torque are given in Table 5-1.

Table 5-1 Experimental conditions studied to determine the linearity range of the ARES rheometer.

Variable	Range
Frequency	0.1 – 70 Hz
Strain	0.001 – 100 %
Motor angular displacement	4×10^{-5} – 4×10^{-1} rad
Torque	0.02 – 1970 g.cm

The intervals covered with each geometry are shown in Figure 5-1.

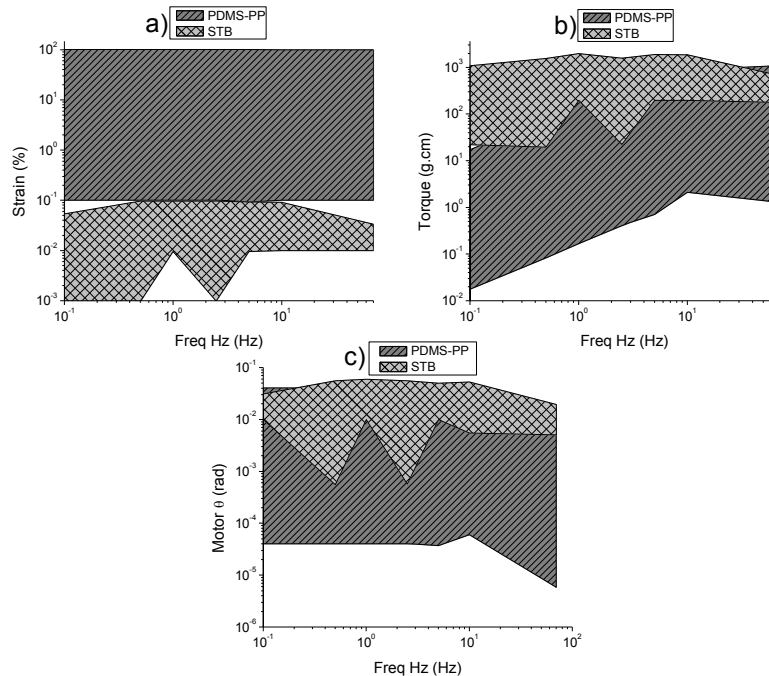


Figure 5-1 Intervals tested to determine the rheometer linearity range: a) strain, b) torque, and c) motor θ .

As can be seen in the figures, with the PDMS and PP geometry high strains and wide interval of motor angular displacement were attained, but the torque response was low at low frequencies. On the other hand, with STB and TB geometry high torques can be produced even at low frequencies. However, due to the high stiffness (shear modulus) of the steel, the torque limit of the transducer was reached before high strains (or motor angular displacements) were produced. Thus lower and higher limits in both motor displacement and torque sensitivity were tested and the inherent nonlinearities of the rheometer could be mapped.

The criteria used as a linearity limit for linear response was $I_3/I_1 \leq 1.0\%$, for both motor and transducer.

In all the tested conditions, at frequencies higher than 10 Hz the motor signal was found to be nonlinear. Hence, the following discussion will be restricted to $\omega \leq 7\text{Hz}$. The I_3/I_1 for the motor signal is shown in Figure 5-2.

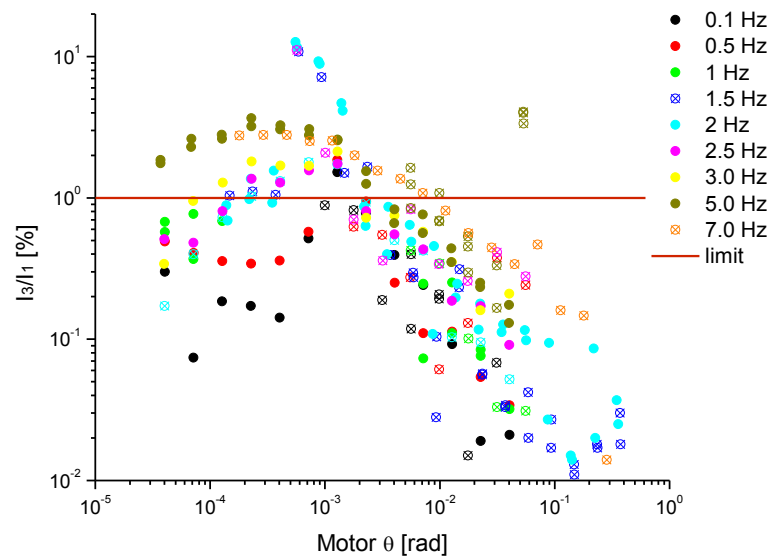


Figure 5-2 Leading nonlinear signal (I_3/I_1) of the ARES motor at different frequencies measured with PP (filled symbols) and TB (crossed symbols).

At small angular motor displacements, the excitation is highly non-linear for frequencies higher than 1 Hz.

To analyze the transducer signal all the data acquired with a motor nonlinear input (i.e. $I_3/I_{1\text{motor}} > 1\%$) were not considered. The transducer was non-linear at low torques (sensitivity limit) and at high torques (saturation limit), as shown in Figure 5-3.

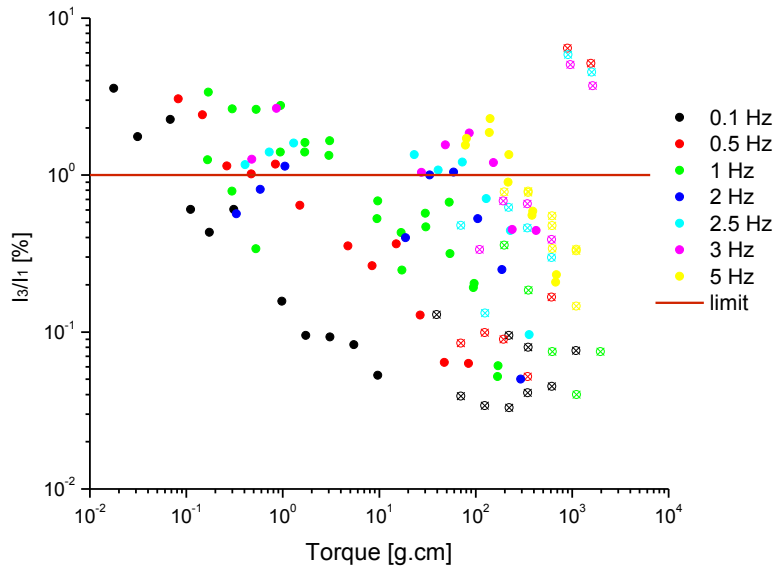


Figure 5-3 Leading nonlinear signal (I_3/I_1) of the ARES transducer at different frequencies measured with PP (filled symbols) and TB (crossed symbols).

Considering that the transducer is fixed, provided that compliance effects can be neglected, the transducer linear region should be fixed on a torque range independent of the excitation frequency, cfr. with motor linear range which is dependent on the excitation frequency. Nevertheless, as shown in Figure 5-3 a tendency to be non-linear as the frequency increased was found. This can be regarded more to a borderline linearity (i.e. $I_3/I_1 \sim 1\%$) coming from the motor, rather than an intrinsic transducer non-linearity, as shown in Figure 5-4.

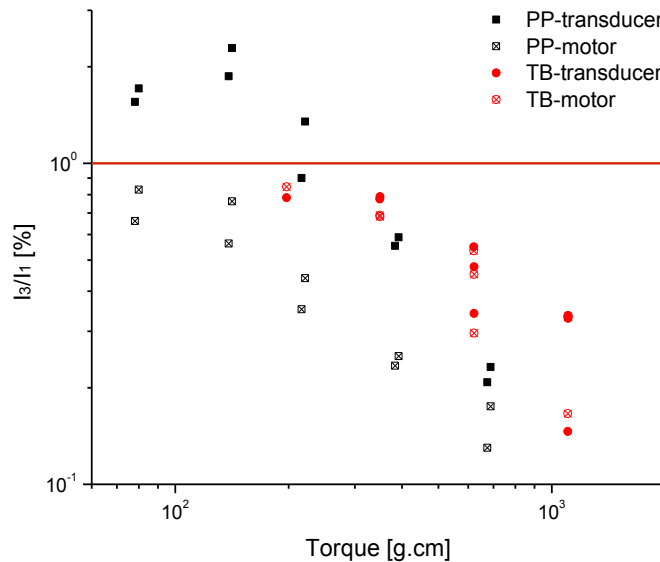


Figure 5-4 I_3/I_1 asaf of torque at 5 Hz. For both geometries used it is depicted the transducer I_3/I_1 % and the motor I_3/I_1 % that corresponded to the given torque: PP (filled symbols) and TB (crossed symbols).

At low frequencies (0.1 Hz and 0.5 Hz), the transducer $I_3/I_1\%$ signal had a constant decrease up to $I_3/I_1 \sim 0.1\%$. The $I_3/I_1\%$ at those frequencies was free from motor noise, because $I_3/I_1 < 1\%$ for all data acquired. Considering that

$$I_1 \sim G^* \cap G^* \sim \sigma (\text{torque}) \quad (2.4.2-1)$$

In the case that I_3 would be a constant a linear decrease of $I_3/I_1\%$ should be found

$$I_3/I_1 \sim 1/\text{torque} \quad (2.4.2-2)$$

However the decrease of $I_3/I_1\%$ had a slope of 0.8 and 0.5 for 0.1 Hz and 0.05 Hz respectively, which means that the $I_3/I_1\%$ signal from transducer was increasing as a function of torque.

The ARES rheometer linearity range is given in Figure 5-5, where the contour of $I_3/I_1 < 1\%$ delimits the linearity range. In all the subsequent measurements, it was monitored that both the motor angular displacement as well as the torque registered were inside this linear regime.

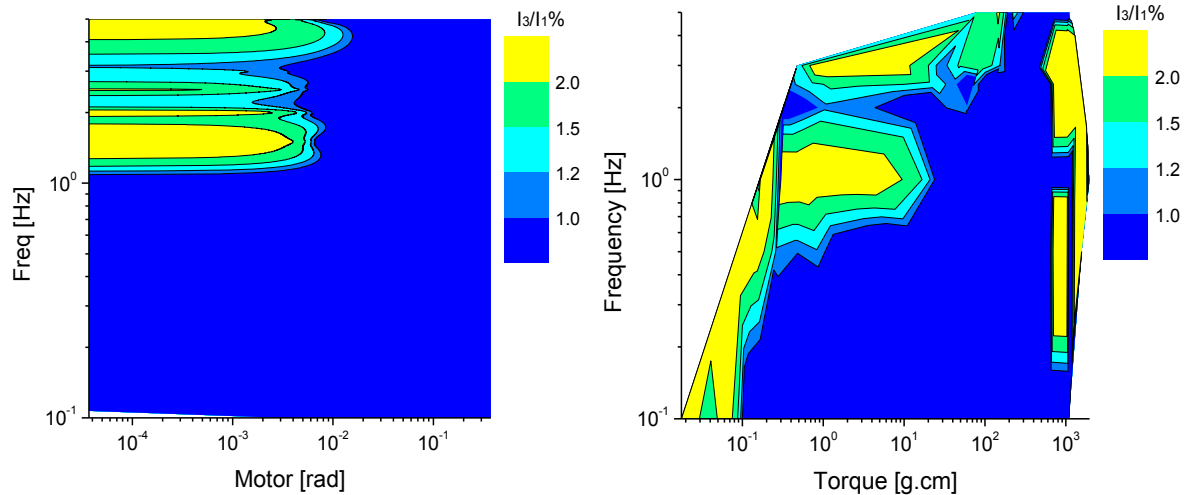


Figure 5-5 Linearity range of ARES rheometer: (left) motor and (right) transducer signal.

5.2. Experimental conditions for repeatability of LAOS test of binders at room temperature.

In order to achieve experimental repeatability, a set of experimental conditions that could potentially affect the repeatability were identified, namely the manufacture of PMB, the production of ATB, the sample loading, the storage period of ATB in the freezer, and ATB height. The first

three factors were not studied but they were controlled, and they are the delivery of the experimental details given in section 3.2. The other two factors (days in the freezer and ATB height) were considered as key aspects to get repeatability between LAOS runs, and therefore were further studied. The repeatability study was done in terms of LAOS tests and not in terms of SAOS tests, considering that repeatability in the linear regime would not guarantee repeatability in nonlinear conditions.

5.2.1. Storage duration

After their production, the ATBs were stored in a freezer at -10°C up to the time of their rheological characterization. Since the store temperature was higher than the bitumen T_g ($T_g \sim -20^{\circ}\text{C}$) some aging was expected to occur in the samples. On this regard a validation of the maximum days in the freezer was done. The parameters used were G' and δ in the linear regime, critical strain γ_c , and I_3/I_1 at γ_c . The critical strain was defined as the ultimate strain before the increasing of I_3/I_1 started. Statistical analysis was done based on ANOVA at 95% confidence interval for the experimental data, shown in Table 5-2. The sample coded as 4.5 was a sample that was erroneously left outside the freezer for 12 h, as can be seen this affects the critical strain, yet the linear properties remained unchanged. Considering that no differences were found up to 4 days in the freezer, neither in the linear nor in the non-linear regime, was this value taken as the maximum days that samples could be stored in the freezer before testing them. In this case only the critical strain and the delta value were more sensitive towards changes in the samples due to storage in the freezer, as per the lower p-values.

Table 5-2 Statistical analysis of linear and nonlinear parameters asaf of the days in the freezer

Days in freezer	#data	γ_c [%]	group*	#data	I_3/I_1 [%] @ γ_c	group*	#data	G' [Pa]	group*	#data	δ [°]	group*
1	2	0.78 ± 0.31	a	2	0.22 ± 0.24	a	2	324131 ± 4447	a	2	48.8 ± 0.3	a
2	2	1.00 ± 0.00	a	2	0.14 ± 0.04	a	2	441737 ± 2811	a	2	49.1 ± 0.2	a, b
3	1	1.77 *	a, b	1	0.58 *	a	3	408519 ± 52829	a	3	50.7 ± 0.9	b
4	1	0.56 *	a	1	0.27 *	a	2	434891 ± 140857	a	2	50.4 ± 0.4	a, b
4.5	1	3.16 *	b	1	0.45 *	a	2	479630 ± 1037	a	2	49.1 ± 0.1	a, b
p-value:	0.037		0.462		0.290		0.032					

* days in the freezer that do not share a letter are significantly different.

5.2.2. Torsion bar height

Variation of the torsion bar height was considered in order to eliminate any geometrical dependence of the rheological properties, i.e. artifacts, and also to optimize the maximum strain limit possible to apply to the sample. Torsion bar height was tested at 2.2, 2.5, and 2.8 cm for all the samples. Two bars at each height were tested for all the binders. The following results presented are related to those two measurements per height. The frequencies at which the samples were tested are given in Table 5-3.

Table 5-3 Frequencies used in the LAOS tests for bar height determination

Sample	ω [Hz]
70/100	9
35/50	2
70/100HDPE5	1
70/100EVA5	7

The results are shown in Figure 5-6.

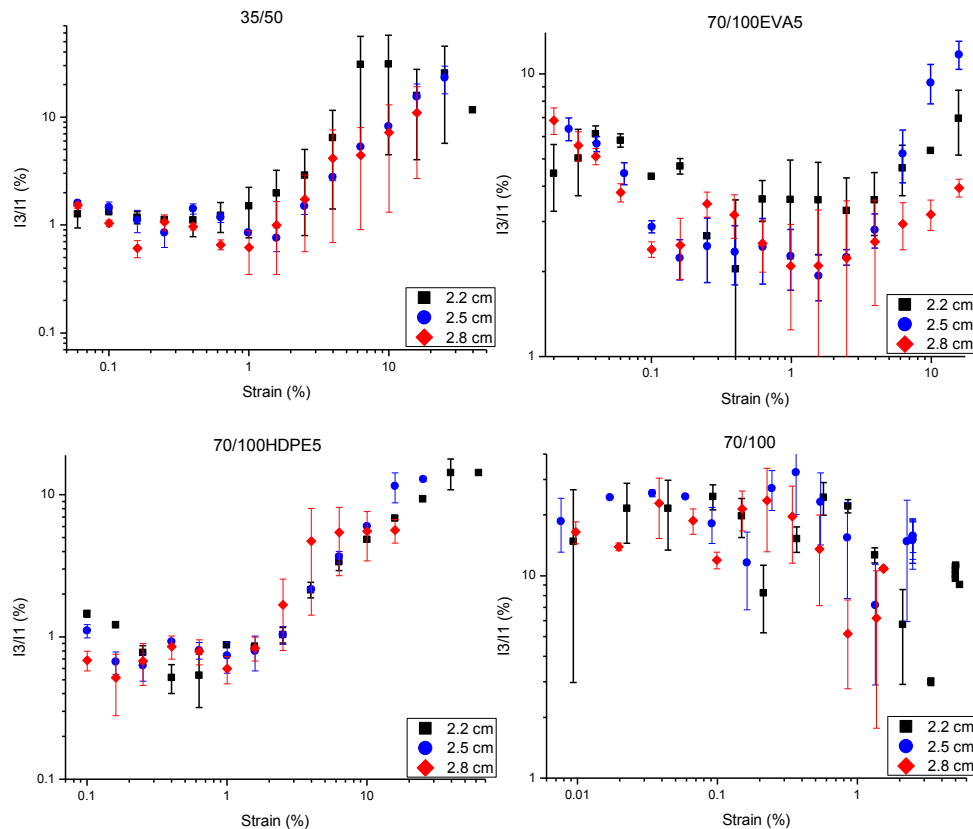


Figure 5-6 Nonlinear response at different bar heights for all the binders.

The error bars shown in Figure 5-6 were computed with standard procedures for standard deviation calculation. For instance the ones provided in Minitab, OriginPro, and excel. In this case, since only two measurements were available, the standard deviation is simply the difference between the two values of each bar. The best repeatability, as per the smaller error bars, was obtained at 2.5 cm height, as shown in Figure 5-6, for all the samples.

Hence, 2.5 cm height was taken as a standard for further measurements. The lack of reproducibility at 2.8 cm was thought to be due to artifacts associated to the grips. Because the longer the bar the higher the angular deflection needed to create the same level of strain, and \therefore the higher the possibilities to have gripping issues involving slip and sample fracture at the fixture. On the other hand the lack of reproducibility at 2.2 cm was related to the possibility of having a residual normal stress (buckling), which in such case would affect more the smallest sample size. On this regard, for further measurements³ the residual normal force was set to be $< 10 \text{ g}_{fc}$, based on the instrument control panel.

A statistical analysis for the I_3/I_1 repeatability at 2.5 cm height was done at the conditions given in Table 5-3. For all samples, there were available two experimental points at each strain (one for each bar used). Then for every pair of points (I_3/I_1 and strain), the average, and the standard deviation were calculated along with the relative standard deviation ($\frac{std \ dev}{average} \times 100\%$) associated to each point. To detect whether this relative error was dependent either on the sample or on the strain level, a balanced ANOVA was done respect to the sample type with the strain as a covariant. The result was that the relative standard deviation was neither sample dependent nor was affected by the strain level (p-values were for strain level 0.279 and for sample type 0.489). Hence this relative error was inherent of the experiment. To have a figure associated to this error the mean and standard deviation of the error were calculated and they are reported in Table 5-4

Table 5-4 Relative standard deviation associated to the experimental repeatability

Variable	Mean	StDev	Minimum	Maximum
Relative standard deviation	13.33	11.03	0.28	34.70

³ These measurements were the first measurements done, even before the SAOS ones. Therefore, after these results were obtained, the ATB height and the residual normal force were standardized for all the other measurements.

In the interval studied, as shown in Figure 5-6, the I_3/I_1 signal held a power law tendency respect to the strain

$$I_3/I_1 = a\gamma^b \quad (5.2.2-1)$$

A repeatability test with respect to the fitting was done for each sample at 2.5 cm height. The two dataset one for each bar were considered. They were analyzed in OriginPro8 in a weighted (variance $\sim y_{\text{fit}}^2$) non-linear fitting. Outliers were identified according to 95% confidence interval. The results are shown in Table 5-5.

Table 5-5 Repeatability results for power law fitting of ATBs at 2.5 cm height

Sample	bar	pre-exponent [%]	exponent [-]	R²
70/100HDPE5	1	0.48 ± 0.04	1.05 ± 0.04	0.99
	2	0.44 ± 0.12	1.10 ± 0.13	0.90
35/50	1	0.51 ± 0.05	1.28 ± 0.05	0.98
	2	0.46 ± 0.10	1.18 ± 0.10	0.91
70/100EVA5	1	1.06 ± 0.16	0.83 ± 0.08	0.95
	2	0.75 ± 0.24	1.05 ± 0.17	0.85

It was possible to find repeatability for the fitting parameters for each sample, besides the high values of R^2 confirm that the trend is well fitted by a power law equation.

After the conditions for experimental repeatability in LAOS-FTR tests were established, the next step was to determine whether this technique was useful for asphalt binders' characterization. This is studied in the following chapter.

6. LAOS characterization of asphalt binders

In this chapter, large amplitude oscillatory shear (LAOS) tests were performed at different experimental conditions to analyze the nonlinear viscoelastic response of asphalt binders. All the LAOS data were acquired in the viscous regime, i.e. below the crossover point where $G' < G''$. The samples were compared either at the same experimental conditions or at the same material rheological state. In case of the same experimental conditions, a series of strain sweeps in LAOS were run at different frequencies for all the samples. In the case of the same rheological state, two conditions were tested in separate experiments: same δ and same De .

6.1. LAOS asaf of frequency

In this section, the nonlinear response of all the binders is presented as a function of the input parameters of the LAOS tests (ω and γ). The frequencies tested spanned one order of magnitude, from 0.1 to 2 Hz. Extra measurements for 35/50 at 2.25 Hz and for 70/100EVA5 at 7 Hz were available, and when pertinent the results will be shown as well. The details about the experimental conditions are given on Table 6-1.

Table 6-1 Experimental conditions for LAOS tests at different frequencies

Sample	ω [Hz]	strain [%]
70/100	0.1, 0.3, 0.7, 1.0, 2.0	0.5 - 25
35/50	0.1, 0.3, 0.7, 1.0, 2.0, 2.25	0.5 - 25
70/100HDPE5	0.1, 0.3, 0.7, 1.0, 2.0	0.5 - 25
70/100EVA5	0.1, 0.3, 0.7, 1.0, 2.0, 7.0	0.5 - 25

The results analysis of the LAOS tests were done in the time domain and in the frequency domain: Lissajous curves and FTR respectively.

The Lissajous curves for the different binders are shown in Figure 6-1, Figure 6-2, Figure 6-3, and Figure 6-4, on a Pipkin representation, on which the elastic vs viscous response is represented by means of changes on strain vs frequency. For the Lissajous curves presented only the distortion of the curve shapes was analyzed (qualitative analysis). However, it is worth to mention that quantitative analysis of Lissajous curves is also possible by means of area integration per cycle (related to the dissipated energy per cycle) [47].

Based on the Lissajous curves, for all the samples an increase in frequency at constant strain increased the nonlinear response of the binders. This is evidenced by the deformation of the characteristic ellipsoidal shape of viscoelastic materials, Figure 2-5. The shift from linear to nonlinear response as the strain was increased at a constant frequency is also visible in the diagrams. In this regard, the sensitivity limit to detect nonlinearities by means of shape distortion of Lissajous curves was 3.1% strain, i.e. at this strain, even at high frequencies, all samples were detected as linear: undeformed ellipsoidal shape. Besides, it can be observed how this nonlinearity onset (similar to a critical strain) decreased as frequency was increased. This evidences the viscoelastic nature of binders. Because in a viscoelastic material, the LVE limit, as well as the nonlinear response, are a function of both frequency and strain, i.e. their rheological response depends on $\dot{\gamma} = \gamma\omega$ (liquid-Newton) as well as on γ (solid-Hooke). In all the diagrams, an increase in strain had a higher impact in the nonlinear response than a frequency increase. Therefore, the elastic nature of the binders was the one that triggered the nonlinear response.

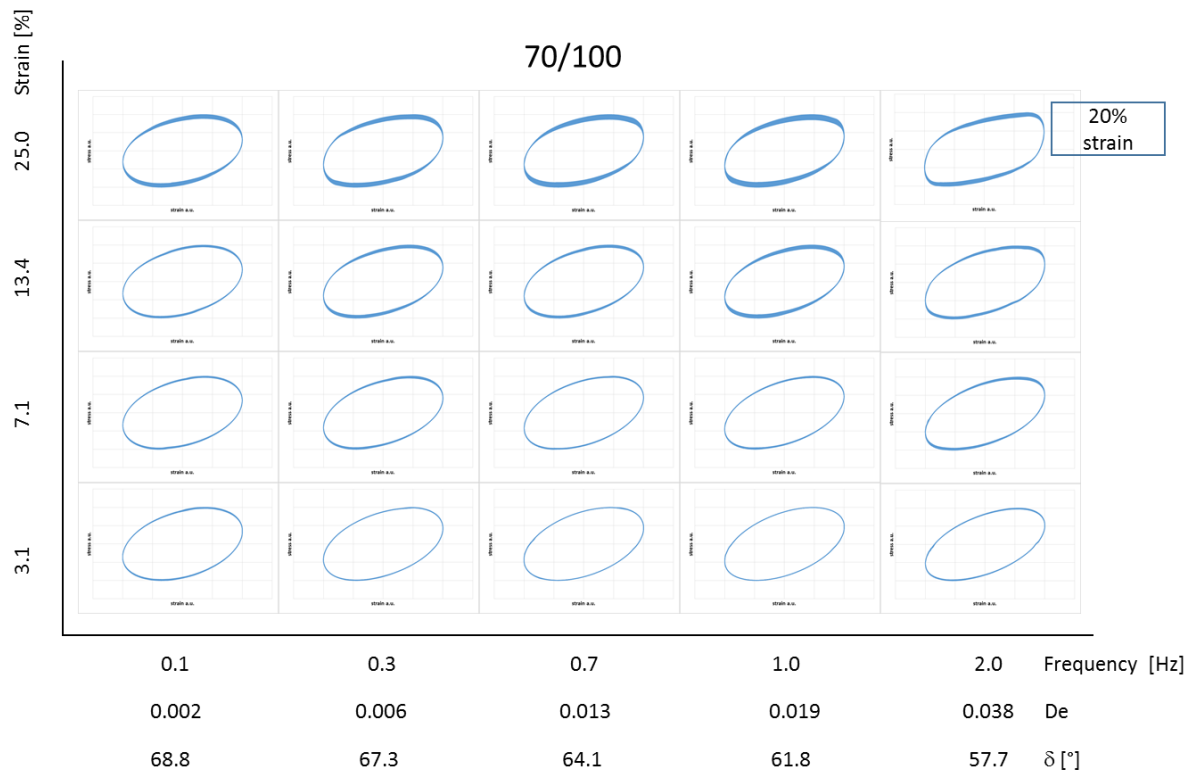


Figure 6-1 Pipkin diagram of γ vs ω for Lissajous curves of 70/100 binder. Additionally in the horizontal axis the corresponding De and δ values are given.

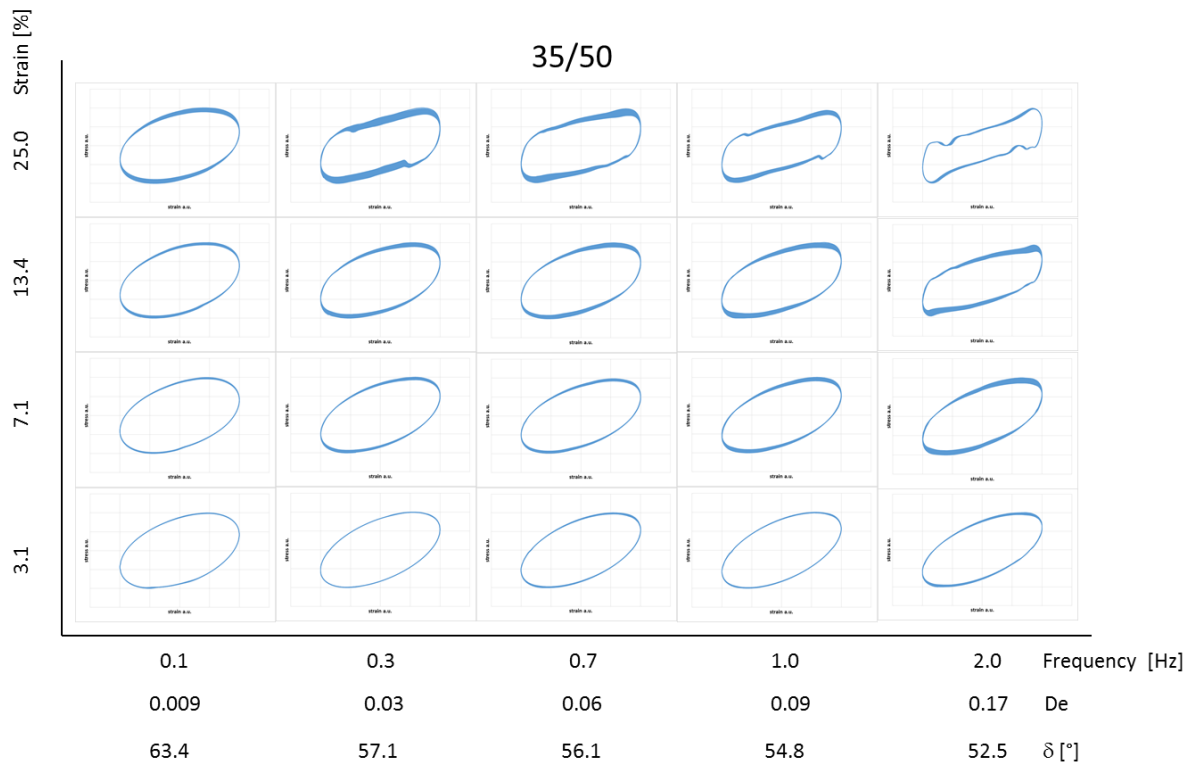


Figure 6-2 Pipkin diagram of γ vs ω for Lissajous curves of 35/50 binder. Additionally in the horizontal axis the corresponding De and δ values are given.

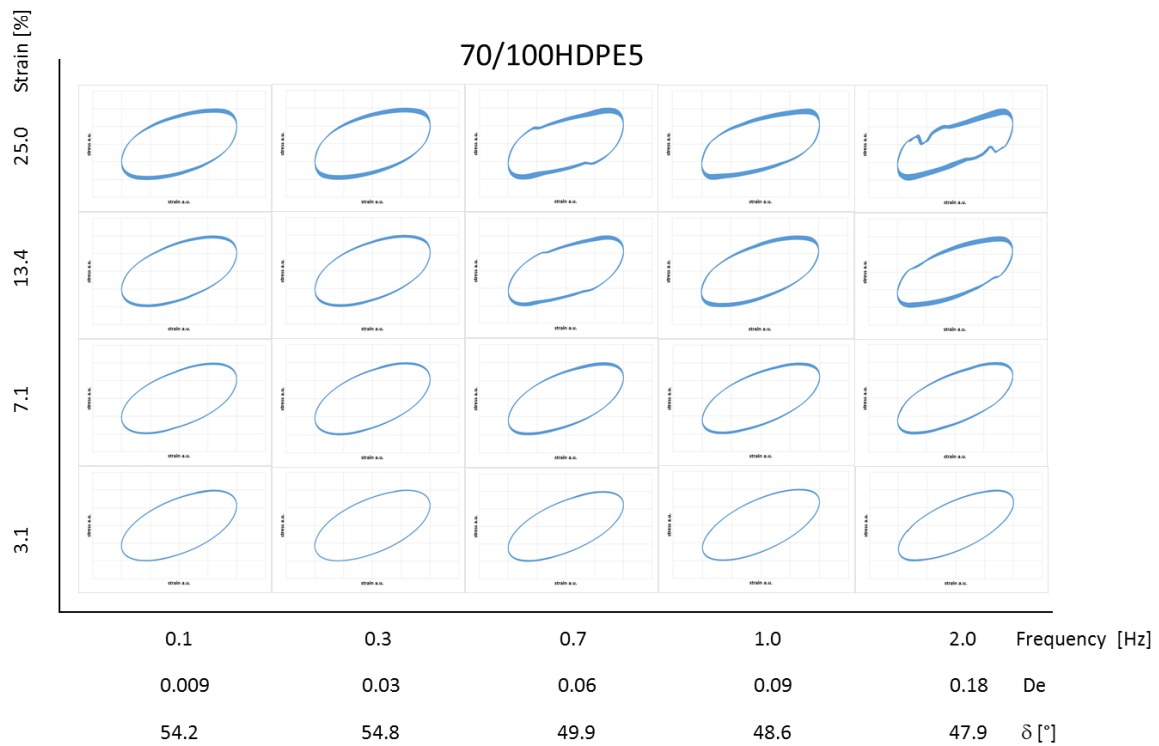


Figure 6-3 Pipkin diagram of γ vs ω for Lissajous curves of 70/100HDPE5 binder. Additionally in the horizontal axis the corresponding De and δ values are given.

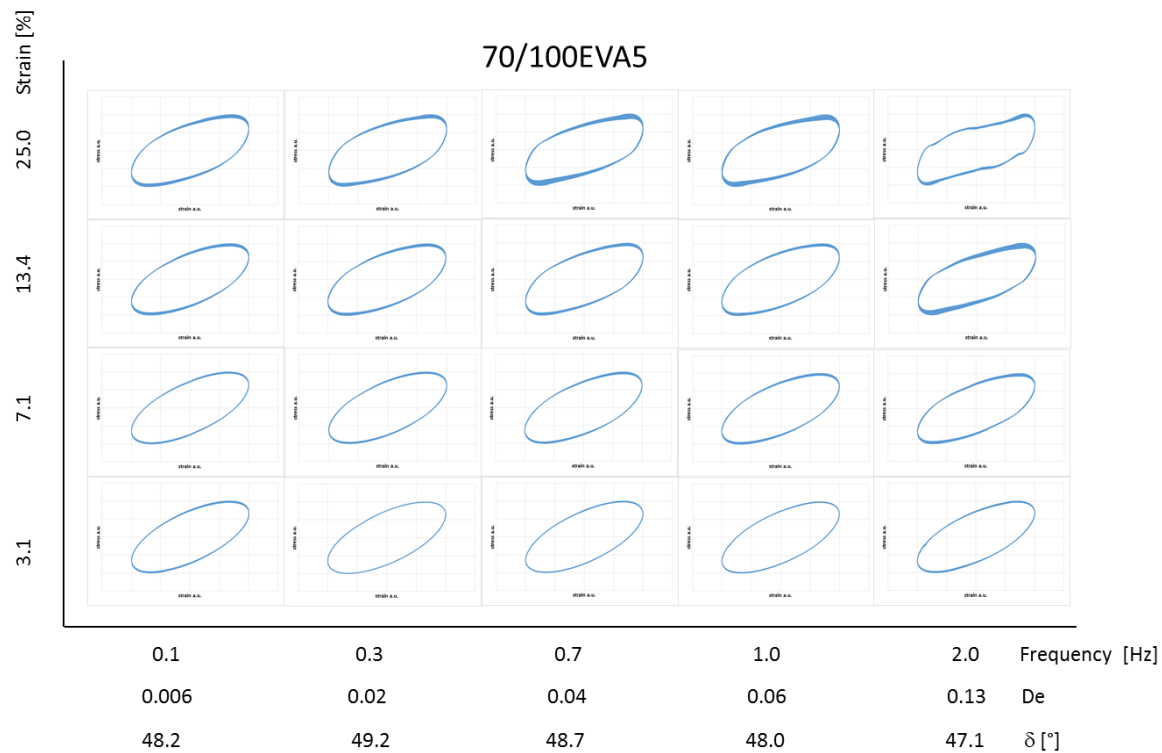


Figure 6-4 Pipkin diagram of γ vs ω for Lissajous curves of 70/100EVA5 binder. Additionally in the horizontal axis the corresponding De and δ values are given.

Only by comparing the Lissajous curves deformation profile of the different binders, it was evident that the 70/100 bitumen showed the lowest nonlinearity followed by 70/100EVA5 and then 70/100HDPE5, being the 35/50 bitumen the most nonlinear binder at the tested frequencies. Based in the shape distortion, it may be concluded that the distortion pattern was canonical of the binders samples, i.e. all samples started from an ellipsoidal shape at low strains and low frequencies, then distorted towards a more parallelogram shape as the nonlinearity increased, and peaks at the right upper and left bottom parts were formed for some samples.

Another common characteristic of binders Lissajous curves was the presence of a halo in the curves, which became more evident as the strain was increased. This change was an indication that the stress amplitude was decaying on time, and it was associated to an initial transient behavior in the stress response of the binder followed by a steady response. This is shown in Figure 6-5 where the Lissajous curves at different cycles and the corresponding stress waveforms in the time domain are shown. At long times the stress amplitude was constant so was the shape of the Lissajous curves.

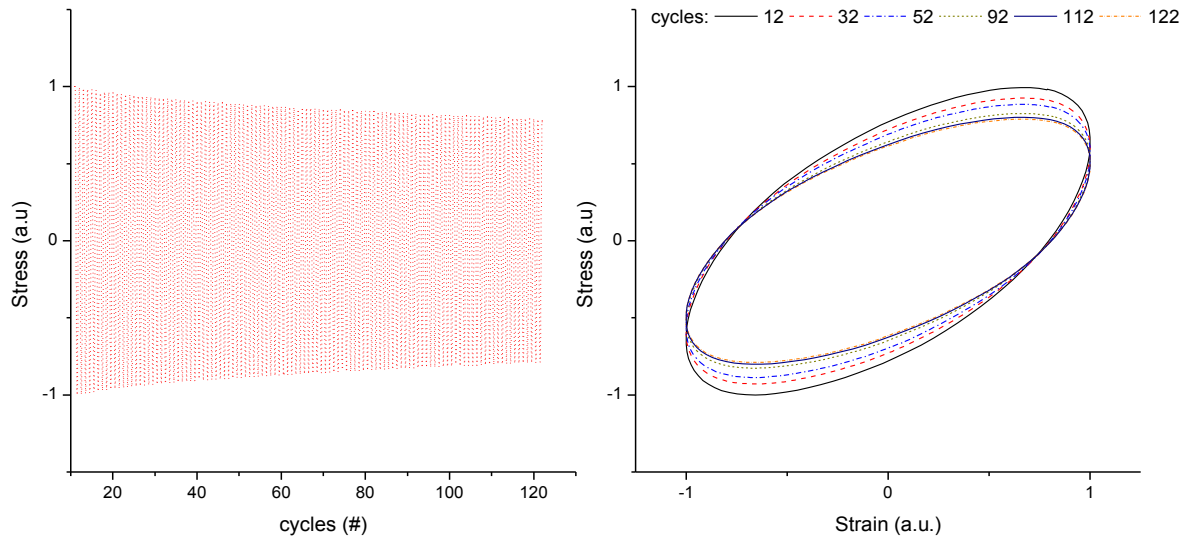


Figure 6-5 Example of the nonlinear transient response: (left) stress signal decayed over time and tended to leveled off, and (right) the transient was reflected in a halo in the Lissajous curves. Sample 70/100EVA5 at $I_3/I_1=2\%$

This transient in stress response was reflected in the Fourier transform spectra not only in a broadening of the harmonic peaks, but also in a change in the I_3/I_1 value. However to reduce the experimental time, the computation of the FTR data was done only with 18-20 cycles at each strain, which indeed fell inside the transient zone. Nonetheless, even with the inaccuracy associated to this value it was possible to differentiate between the samples, as will be shown in the following analysis.

In the frequency domain the analysis was done quantitatively by means of FTR. For all the binders the Fourier transform of the stress signal gave rise to a high number of odd harmonics, which was detected as a rising of the I_n/I_1 signal as a function of strain, as shown in Figure 6-6 (left). However, the relative intensities of the even harmonics were not relevant for any sample since its signal neither rose above noise level nor showed a specific trend, as shown in the example of Figure 6-6. Therefore the analysis was restricted to only the odd harmonics.

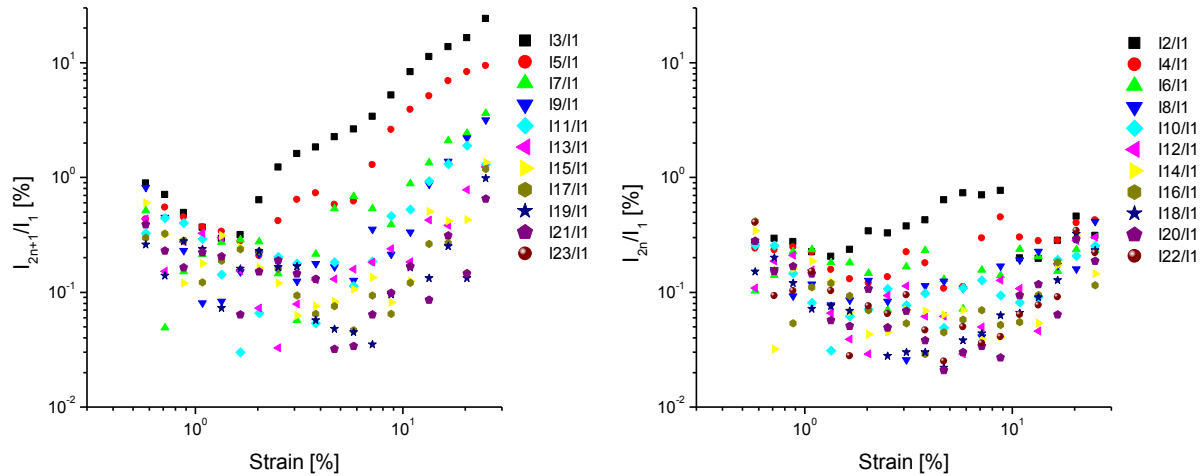


Figure 6-6 Comparison of odd (left) and even (right) harmonic signals for 35/50 binder at 2Hz.

To quantify this high number of significant odd harmonics the concept of harmonicity degree will be introduced. The harmonicity degree could be simply considered as the maximum harmonic on which a rising of the signal was detected. However, the number of harmonics detected depends not only on the instrument sensitivity but also on the strain at which the harmonic signal is measured. For instance, considering the data shown in Figure 6-7, if the harmonicity degree would be measured at the strain for onset of I_3/I_1 rising (signaled by an arrow in Figure 6-7) then the harmonicity degree would be 3. However, if the strain would be measured at 8.8% strain (signaled by a vertical line), then the harmonicity degree would be 5; because, the 7th and 9th signals started to rise at 10.8% and 13.4% strain respectively.

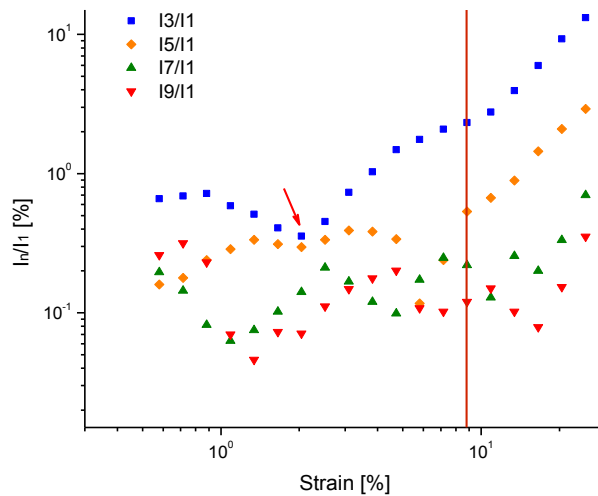


Figure 6-7 First odd harmonics asaf of strain for 35/50 binder at 0.7 Hz.

In view of this and to determine the harmonicity degree, for all the samples the strain for onset of I_3/I_1 rising was determined, shown in Figure 6-8. This strain was clearly dependent on the equipment sensitivity, because for $\omega > 0.7$ Hz all the binders had more or less the same strain value.

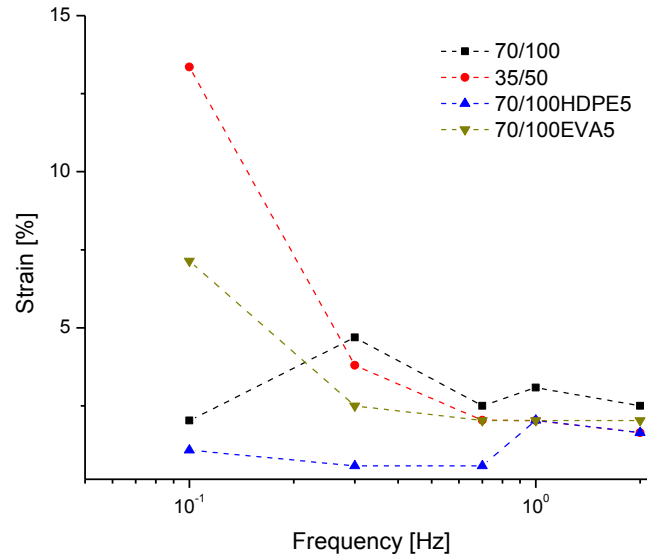


Figure 6-8 Strain for onset of rising of I_3/I_1 signal, for all binders at all the frequencies tested.

Based on this, the harmonicity degree was considered as the maximum harmonic on which a rising of the signal was detected, at a strain given by an arbitrary constant delta of 6.6% strain units from the strain for onset of I_3/I_1 rising. Therefore a similar analysis than the one shown in Figure 6-7 was done for all the samples at all the frequencies, out of which the harmonicity degree was determined and it is given in Figure 6-9.

As can be seen, the harmonicity degree was higher than 3 for almost all the samples at the frequencies tested. For 70/100 binder the harmonicity degree was lower than 7 and more or less constant, and for the rest of the binders a rising was detected at high frequencies. The samples with the higher harmonicity degrees were 35/50 and 70/100EVA5 binders.

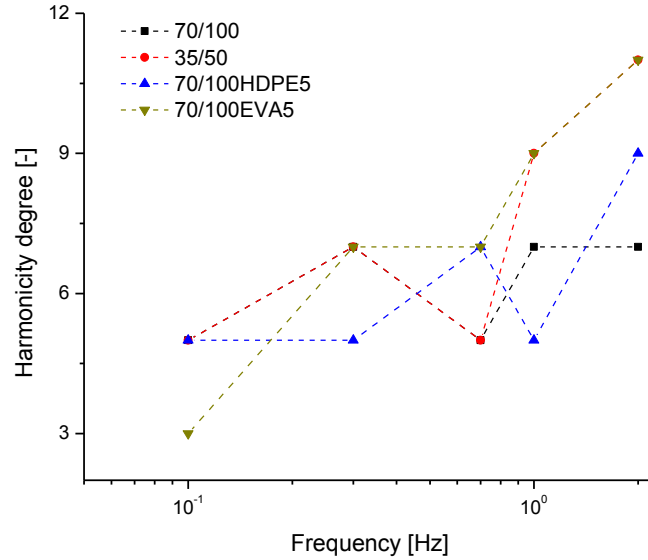


Figure 6-9 Harmonicity degree for all samples tested asaf of frequency.

The high harmonicity degree was an indication that the nonlinear analysis cannot be restricted to the 3rd harmonic, in doing so a big piece of information would be missing. Therefore, the FTR analysis was done not only respect to the third harmonic signal (I_3/I_1 and $\phi_3-3\phi_1$) but also respect to the total harmonicity one. The latter was defined as

$$Total\ harmonicity = \sum_{n_{odd}}^{19} \frac{I_n}{I_1} \quad (6.1)$$

and it will be also referred as odd sum.

Above quantifiers (I_3/I_1 and total harmonicity) were chosen because data were available at all the frequencies, and thus allowing for a comparative analysis.

Though all the measurements were acquired inside the linearity range of the motor (given in Figure 5-5), it was consistently monitored that the nonlinearity in stress signal was not a consequence of motor nonlinearities: for all measurements the I_3/I_1 signal (as well as for higher odd harmonics) was extrapolated up to the motor signal, shown in Figure 6-10. Then only data above this crossover point were considered for data analysis, i.e. free from motor noise. For the sake of brevity this

process was not shown for all the data, but it was done for all the samples and for all the harmonics signals analyzed.

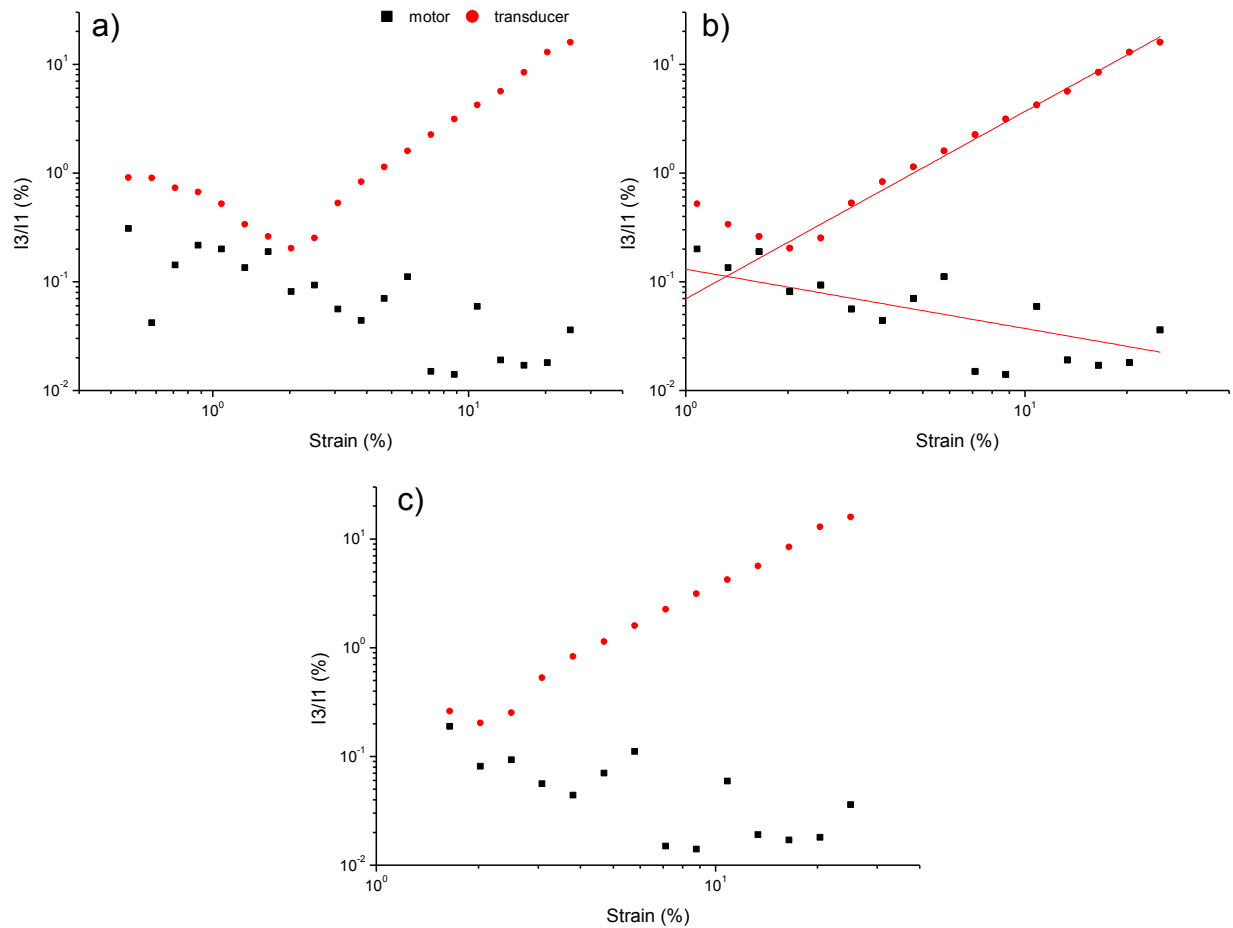


Figure 6-10 Example of criteria for valid data in LAOS test: a) raw data, b) fitting of transducer and motor signal, the crossover signaled the valid data without motor noise, which are given in c).

Data of I_3/I_1 for each sample are given in Figure 6-11, whereas I_3/I_1 data sorted by frequencies are shown in Figure 6-12.

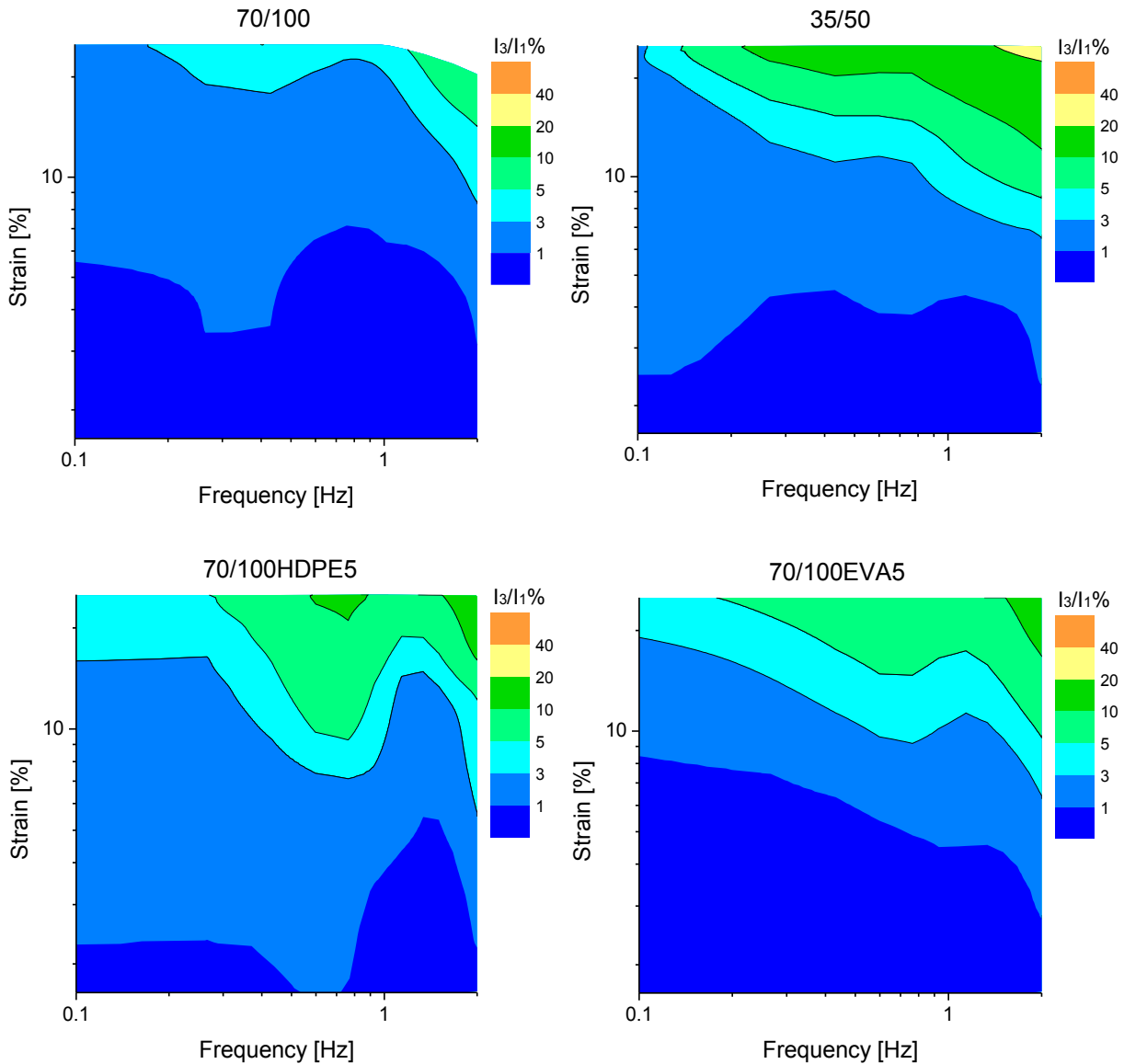


Figure 6-11 Pipkin diagrams for $I_3/I_1\%$ signal for all binders

The contour plots of Figure 6-11 are Pipkin diagrams for the I_3/I_1 signal of each binder. The general aspects detected by the Lissajous representation are confirmed by these diagrams. The I_3/I_1 signal depends on both ω and γ , evidencing the viscoelastic nature of the binders, and it is more affected by changes in strain rather than in frequency. For all the samples I_3/I_1 increased by increasing the strain. Only sample 35/50 had a linear increase of the I_3/I_1 signal respect to frequency. The rest of the samples had specific frequencies at which a steep increase in the nonlinear response was detected: 0.3 Hz for 70/100, and 0.7 Hz for both 70/100HDPE5 and 70/100EVA5. This dependence led to a nonlinear trend asaf of the frequency at specific strains.

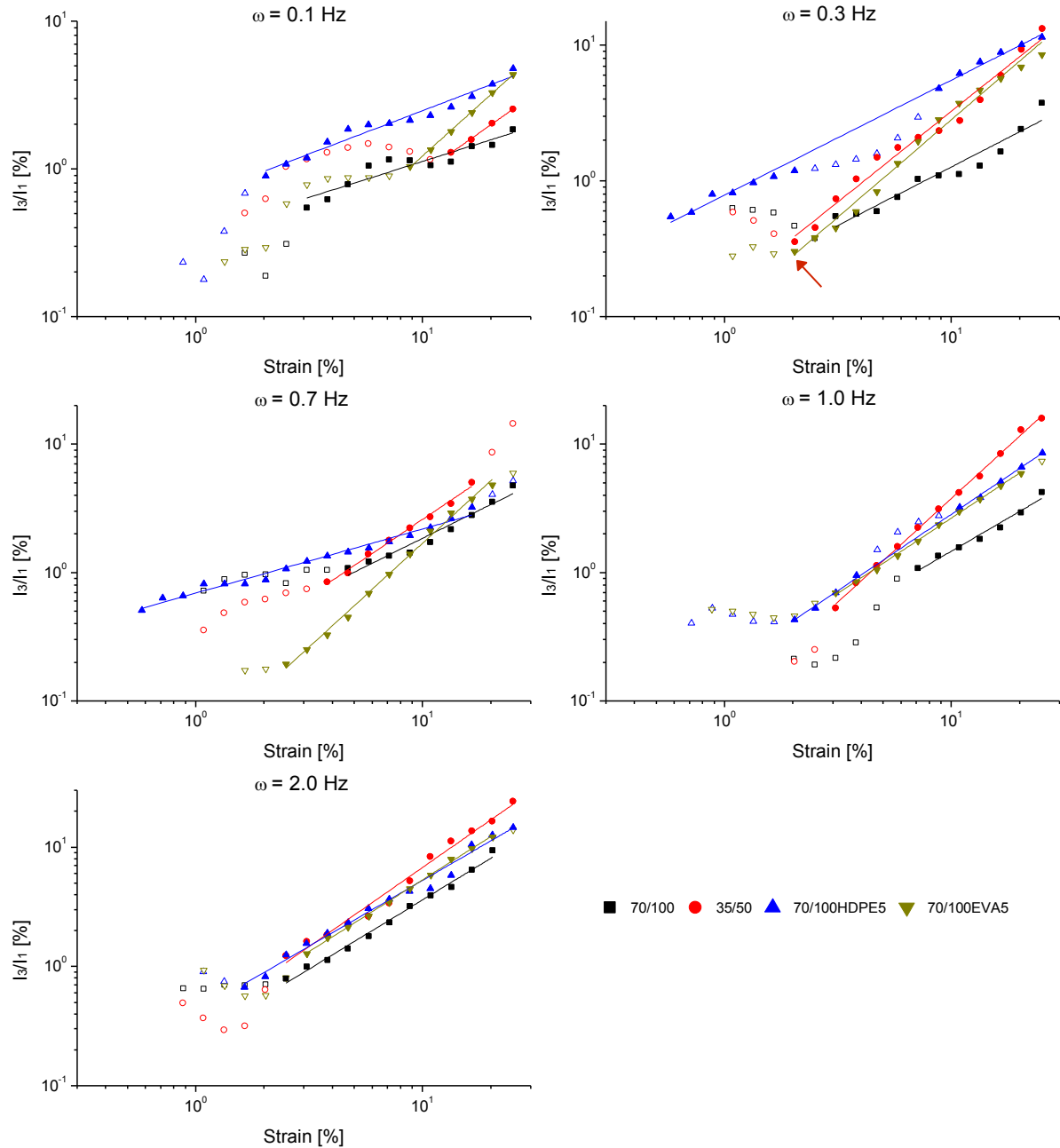


Figure 6-12 I_3/I_1 % data for all samples at all frequencies tested: (unfilled symbols) data free of motor noise, (filled data) data considered for power law, and (solid lines) power law fitting.

As can be seen in Figure 6-12, the onset of nonlinearity respect to I_3/I_1 was detected from strains lower than 3.1%, confirming the better sensitivity of FTR analysis, when compared with the qualitative study of Lissajous curves. However, to really confirm this better sensitivity of FTR vs Lissajous curves a quantitative treatment of the Lissajous curves, in terms of the curve area, should be performed.

In terms of the 3rd harmonic relative intensity, the polymer modification of bitumen can be detected, as well as differences between PMBs and between binder grades, as shown in Figure 6-12. The modification increased the intensity of the third harmonic of PMBs, i.e. the PMBs microstructure deformed more compared to the parent 70/100 binder. This trend is valid at all the frequencies tested for 70/100HDPE5 binder and only at $\omega > 0.7$ Hz for 70/100EVA5.

All binders showed a power law dependence of I_3/I_1 and total harmonicity (as well as higher odd harmonics, see further) on the strain, and this indicated that the samples were studied in the so-called MAOS regime [9]. Therefore all data inside this power law were fitted according to

$$\frac{I_n}{I_1} = a_n \gamma^{b_n} \quad n = \text{odd}$$

or

$$\sum_{n_{\text{odd}}}^{19} \frac{I_n}{I_1} = a \gamma^b \quad (6.1-2)$$

and the fittings were done using OriginPro 8.0: R^2 , pre-exponents a and a_n and exponents b and b_n were computed as well as the standard deviation associated to any of those fitting parameters. The R^2 value was associated to the goodness of the fitting, i.e. the closer to 1 the better the values followed the given power law. The exponent value, b , reflected the strain sensitivity of the sample, i.e. how changes in strain affected the sample nonlinearity. The pre-exponent value, a , has been considered by other authors as a measurement of the linear to nonlinear transition [9]. However, the linear to nonlinear transition depends on the equipment sensitivity. Therefore, this value was not considered for analysis.

The results of the fitting for $I_3/I_1\%$ signal are given in Table 6-2.

Table 6-2 Power law fitting results of I_3/I_1 signal for all binders at different frequencies

Frequency →	0.1 Hz		0.3 Hz		0.7 Hz		1 Hz		2 Hz	
Sample	a3	b3	a3	b3	a3	b3	a3	b3	a3	b3
70/100	0.37 ± 0.05	0.49 ± 0.06	0.25 ± 0.04	0.87 ± 0.07	0.17 ± 0.03	0.86 ± 0.08	0.14 ± 0.03	1.03 ± 0.07	0.25 ± 0.02	1.16 ± 0.03
35/50	0.08 ± 0.01	1.09 ± 0.03	0.17 ± 0.01	1.19 ± 0.04	0.15 ± 0.02	1.33 ± 0.06	0.09 ± 0.00	1.61 ± 0.02	0.32 ± 0.04	1.33 ± 0.05
70/100HDPE5	0.64 ± 0.05	0.59 ± 0.03	0.69 ± 0.02	0.50 ± 0.02	0.79 ± 0.03	0.85 ± 0.02	0.18 ± 0.00	1.19 ± 0.01	0.42 ± 0.03	1.10 ± 0.04
70/100EVA5	0.05 ± 0.00	1.38 ± 0.02	0.04 ± 0.00	1.62 ± 0.03	0.10 ± 0.01	1.44 ± 0.05	0.20 ± 0.01	1.13 ± 0.02	0.33 ± 0.01	1.20 ± 0.02

The exponent values are plotted in Figure 6-13 as a function of the input frequency. Aside sample specific trends, as a whole the exponent tended to increase as the frequency increased; at high frequencies (1 and 2 Hz) all the exponents were higher than one. Regarding the exponent at frequencies < 1 Hz, 70/100EVA5 had consistently a more or less constant value, but higher sensitivity to strain than 70/100 and 70/100HDPE5. At frequencies ≥ 1 Hz 70/100 and PMBs binders had roughly the same sensitivity to strain, i.e. they softened at a similar pace with respect to strain. The exponent in samples 70/100, 35/50, and 70/100HDPE5 increased asaf of the frequency, which meant that they became more sensitive to be deformed by the strain as the frequency was increased. In contrast, at the frequencies tested 70/100EVA5 strain sensitivity was constant respect to frequency. The difference between bitumen grades was on the higher exponent (strain sensitivity) of 35/50 binder with respect to 70/100 binder.

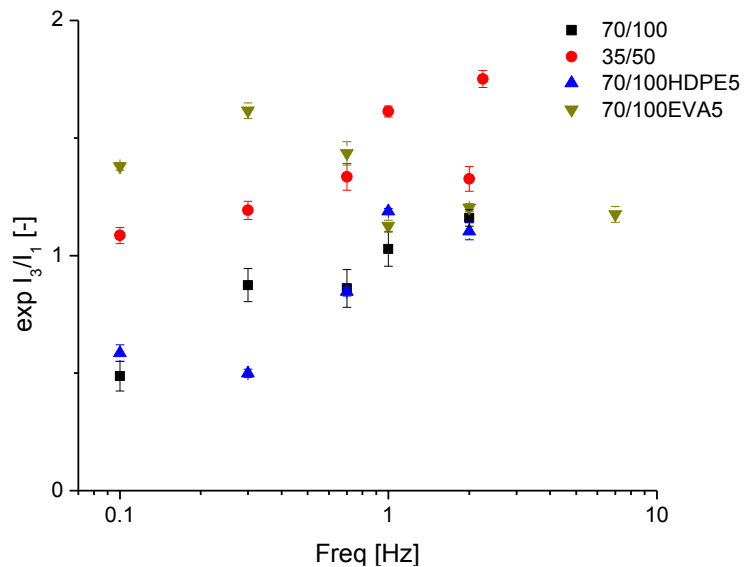


Figure 6-13 Exponent of the power law fitting asaf of frequency for all the binders.

In order to define a critical strain for the linear to nonlinear transition and to extract a more quantitative meaning to the value of the pre-exponent, a fixed value of $I_3/I_1 = 0.19\%$ was set and the value of the strain at which that I_3/I_1 value was achieved was considered as a measurement of the critical strain (γ_c) for onset of nonlinearities. This value of I_3/I_1 was chosen as representative since $I_3/I_1 = 0.19\%$ was the lowest I_3/I_1 signal detected on the power law zone; valid among all the samples at all frequencies (it is signaled by an arrow in Figure 6-12 at $\omega = 0.3$ Hz). An alternative option was to choose a fixed value of I_3/I_1 based on the noise level, but a dependence of the noise level on the frequency was found, which was expected since the transducer was reflecting the

nonlinearity of the motor, see Figure 5-4. Similarly, another critical strain definition could have been the strain before the I_3/I_1 signal started to increase, shown in Figure 6-8, but as pointed out previously at high frequencies this strain value was the same for all samples since it was restricted by the equipment sensitivity.

Therefore, for all samples a value of γ_c at $I_3/I_1=0.19\%$ was computed according to

$$\gamma_{c-n} = \left(\frac{I_n/I_{1limit}}{a_n} \right)^{\frac{1}{b_n}} \text{ with } n = 3 \quad (6.1-3)$$

and considering the fittings given in Table 6-2. The γ_{c-3} values are given in Figure 6-14. Briefly, samples 35/50 and 70/100EVA5 were able to withstand less strain as the frequency was increased. Meanwhile 70/100 withstood more strain as the frequency was increased, and sample 70/100HDPE5 critical strain were the lowest for all the frequencies tested. This respect to the 3rd harmonic.

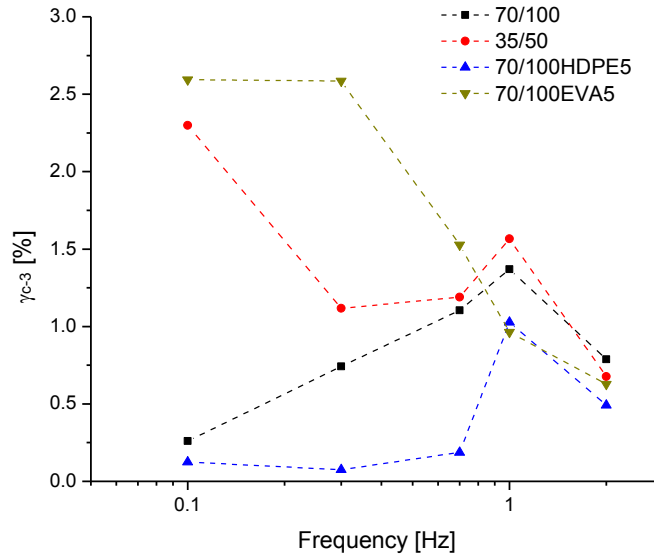


Figure 6-14 Calculated critical strain for onset of I_3/I_1 for all samples at different frequencies.

The total harmonicity data for each sample are given in Figure 6-15.

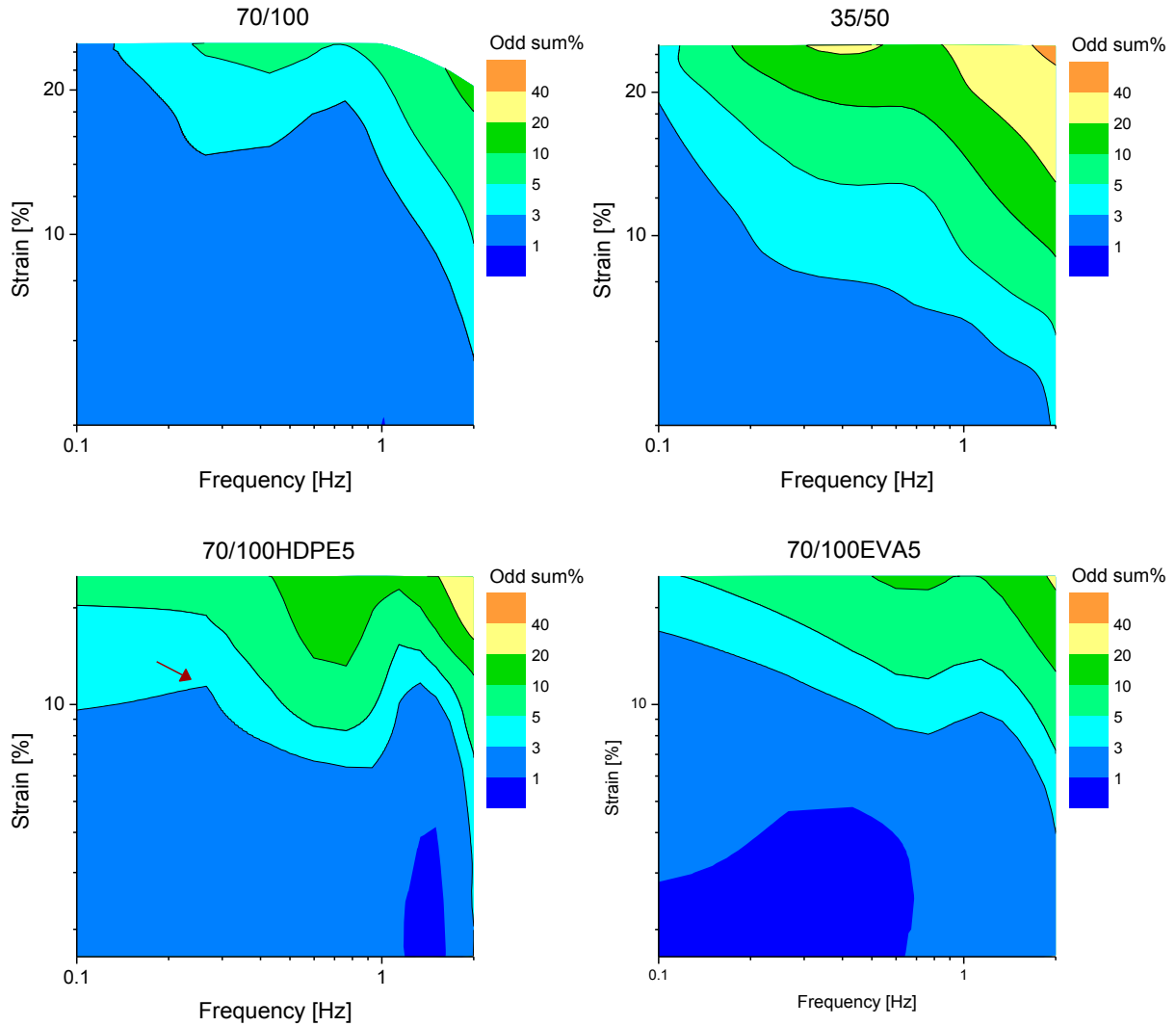


Figure 6-15 Pipkin diagrams for total harmonicity signal for all binders

In terms of the total harmonicity, the modification was detected, as well as differences between PMBs and between binder grades. As expected the total harmonicity signal was dependent on both strain and frequency. Even though some general features are the same between I_3/I_1 and total harmonicity (biggest nonlinearity at higher strains and higher frequency), some specific trends were found. In this case all samples had one frequency at which a step increase in nonlinearity occurred: close to 0.3 Hz for 70/100 and 35/50, and close to 0.7 Hz for 70/100HDPE5 and 70/100EVA5. Such behavior made possible a clear differentiation between bitumens and PMBs. Specifically for 70/100HDPE5 a decrease in the nonlinear signal was found around 0.3Hz and 10% strain (signaled by an arrow in Figure 6-15).

The total harmonicity trend as a function of strain and sorted by frequencies is given in Figure 6-16.

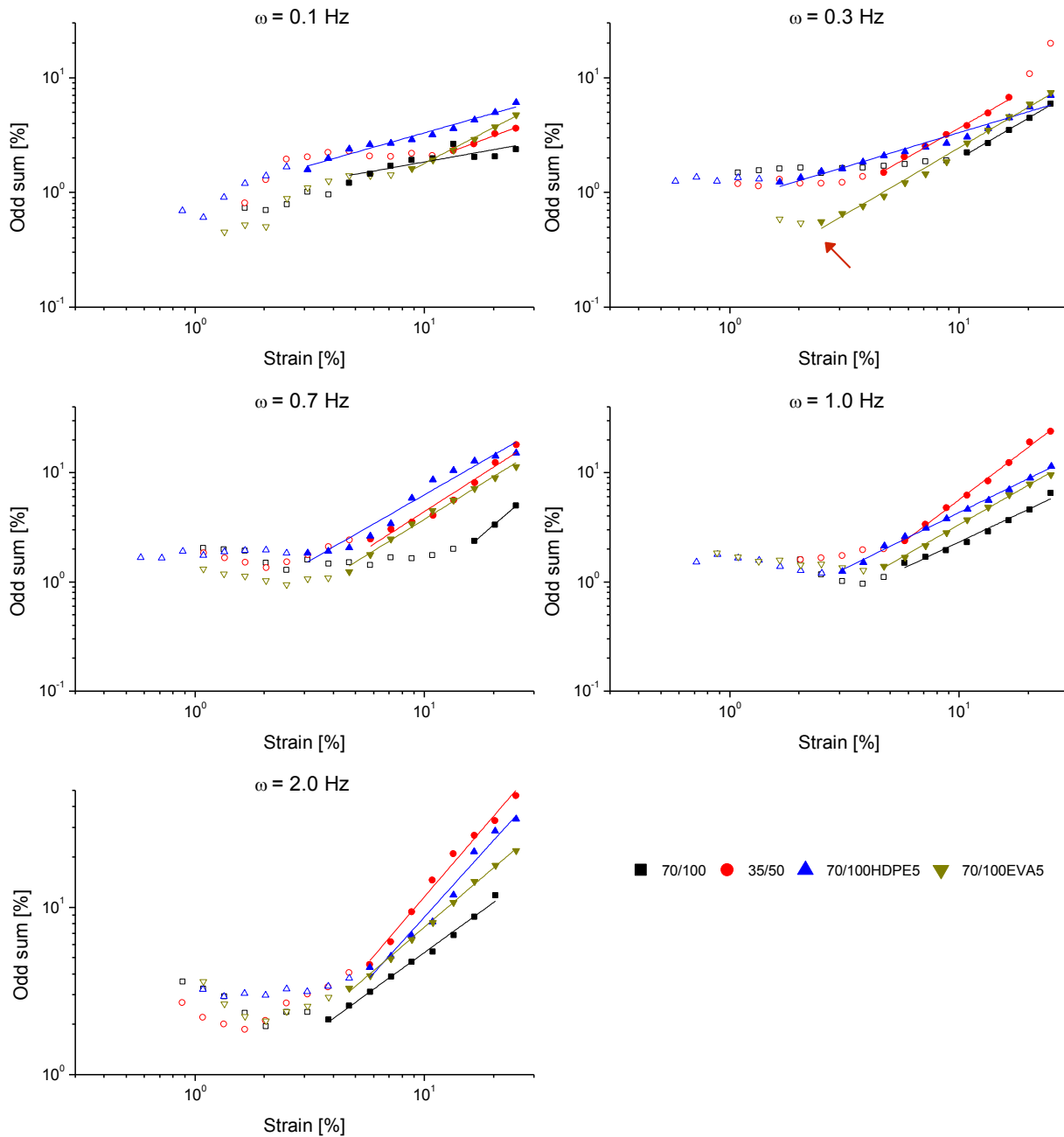


Figure 6-16 Total harmonicity data for all samples at all frequencies tested: (unfilled symbols) data free of motor noise, (filled data) data considered for power law, and (solid lines) power law fitting.

Based on Figure 6-16, sample 70/100HDPE5 had consistently higher nonlinearity levels than the rest of the samples for frequencies < 1 Hz. Meanwhile sample 35/50 was the one more affected by the frequency, i.e. at $\omega = 0.1$ Hz it had one of the lowest nonlinearities while at 2 Hz it had the highest level of nonlinearity, shown in Figure 6-16.

The results of the fitting are given in Table 6-3.

Table 6-3 Power law fitting results of odd sum signal for all binders at different frequencies

Frequency →	0.1 Hz		0.3 Hz		0.7 Hz		1 Hz		2 Hz	
Sample	a	b	a	b	a	b	a	b	a	b
70/100	0.81 ± 0.18	0.36 ± 0.09	0.13 ± 0.02	1.17 ± 0.05	0.02 ± 0.00	1.79 ± 0.09	0.24 ± 0.04	0.99 ± 0.06	0.55 ± 0.04	0.99 ± 0.03
35/50	0.33 ± 0.05	0.75 ± 0.05	0.30 ± 0.03	1.09 ± 0.04	0.20 ± 0.05	1.35 ± 0.11	0.14 ± 0.01	1.59 ± 0.04	0.29 ± 0.05	1.60 ± 0.07
70/100HDPE5	0.90 ± 0.07	0.57 ± 0.03	0.83 ± 0.05	0.60 ± 0.03	0.39 ± 0.07	1.21 ± 0.08	0.40 ± 0.02	1.03 ± 0.02	0.27 ± 0.07	1.52 ± 0.10
70/100EVA5	0.17 ± 0.02	1.03 ± 0.03	0.17 ± 0.01	1.17 ± 0.03	0.19 ± 0.02	1.30 ± 0.04	0.21 ± 0.01	1.20 ± 0.02	0.51 ± 0.03	1.18 ± 0.02

Regarding the exponent trend, shown in Figure 6-17, samples 70/100, 35/50, and 70/100HDPE5 had an increase in the exponent respect the applied frequency, which was consistent with the I_3/I_1 signal. In this case it was really evident that the susceptibility to strain of 70/100EVA5 sample was unaffected by frequency, as per its constant value of exponent. The main difference between the binder grades was the higher exponent value of 35/50 binder with respect to that of 70/100 at almost all frequencies, consistent with the I_3/I_1 signal.

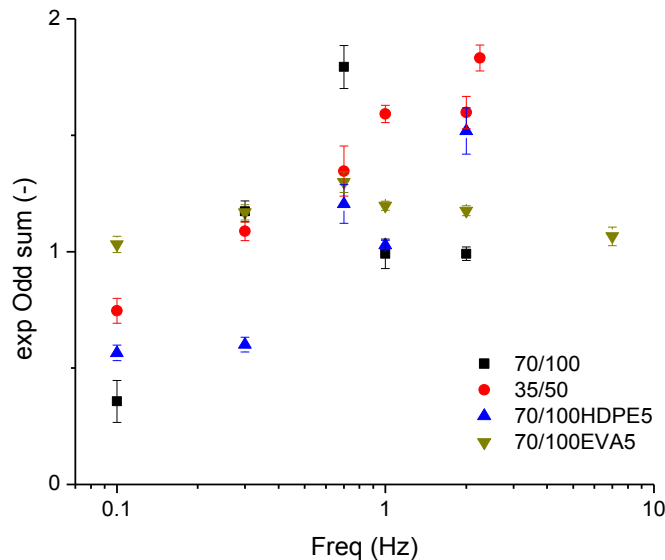


Figure 6-17 Exponent values of the odd sum power law fitting asaf of frequency for all the binders.

In this case the concept of the critical strain was also applied, and following the same rationale a limiting value of $\sum_n^{19} I_n/I_1\% = 0.55\%$ was established, which was identified as the minimum value of total harmonicity detected in the power law region for all the samples at all the frequencies, and it is signaled by an arrow in Figure 6-16 at $\omega = 0.3$ Hz. The values of critical

strain for onset of total harmonicity signal, γ_c , are reported in Figure 6-18. Only sample 70/100EVA5 shown a consistent decrease in γ_c value as frequency was increased. On the contrary, 70/100HDPE5 binder had an increase of the critical strain as the frequency increased. Sample 35/50 had a more or less constant critical strain value. For the 70/100 binder no clear trend can be drawn. This was sort of expected since in the sum of the odd the onset of all the harmonics gets mixed, meaning that even though all harmonics follow a power law trend with respect to strain its onset had no correlation from one to another.

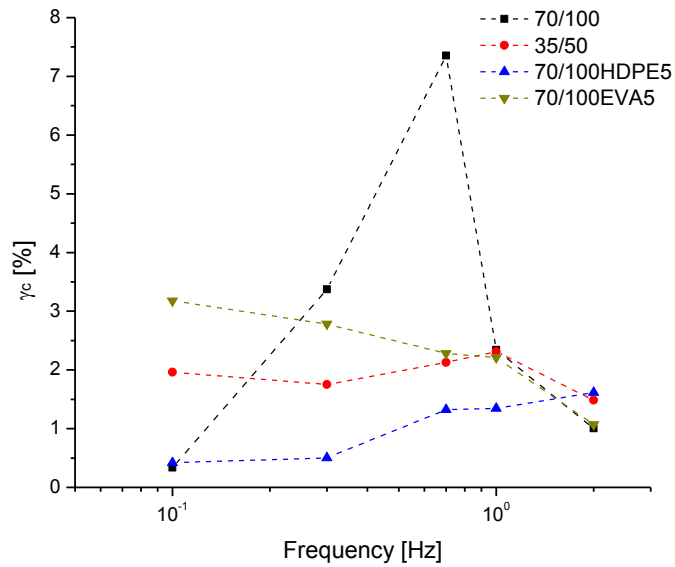


Figure 6-18 Calculated critical strain for onset of odd sum for all samples at different frequencies

It is worth to mention that sample 70/100HDPE5 seemed to have a change in tendency around 0.7 to 1.0 Hz, i.e. the pre-exponent values decreased and the exponent values increased, this was consistent in both I_3/I_1 and odd sum trend.

The last FTR quantifier analyzed was the relative phase angle of the third harmonic $\phi_3-3\phi_1$, which values are shown on Figure 6-19. The $\phi_3-3\phi_1$ values were only reported for valid points of the I_3/I_1 signal: free of motor noise and in the power law region.

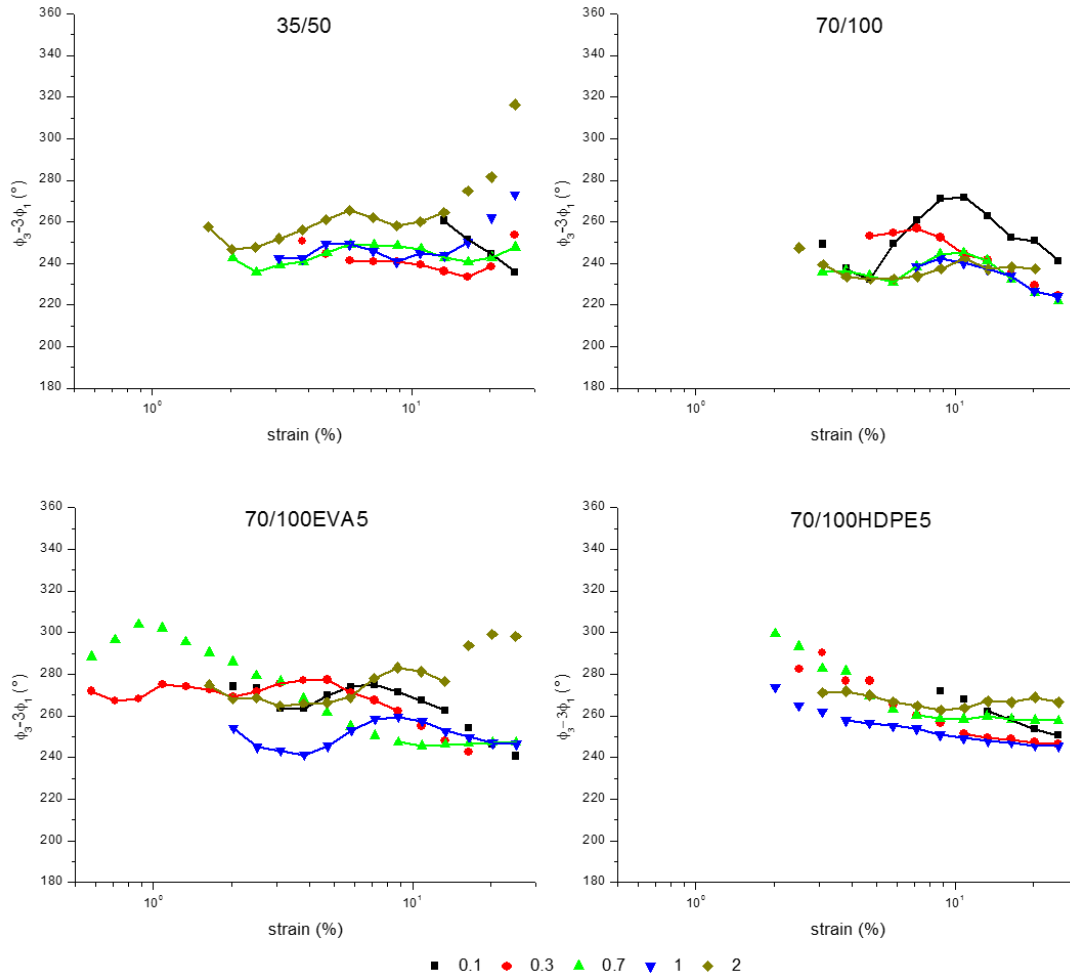


Figure 6-19 Relative phase angle at different frequencies asaf of strain for all samples.

In most of the cases a plateau of $\phi_3-3\phi_1$ was found for the strains where the power law of I_3/I_1 was valid. In such cases a characteristic relative phase angle was defined as the average value of $\phi_3-3\phi_1$ signal in the plateau region. In Figure 6-19, only the data joined by lines were considered to compute the characteristic relative phase angle, given in Table 6-4.

Table 6-4 Characteristic relative phase angle of the 3rd harmonic for all the samples at different frequencies.

Frequency →	0.1 Hz	0.3 Hz	0.7 Hz	1 Hz	2 Hz
Sample	$\phi_3-3\phi_1$ [°]	$\phi_3-3\phi_1$ [°]	$\phi_3-3\phi_1$ [°]	$\phi_3-3\phi_1$ [°]	$\phi_3-3\phi_1$ [°]
70/100	253.0± 13.6	250.6± 6.1	237.7± 5.1	234.7± 6.9	236.4± 3.2
35/50	248.1± 10.6	238.6± 2.9	243.9± 4.1	245.4± 3.5	257.5± 6.3
70/100HDPE5	268.4± 4.9	271.5± 4.3	246.8± 0.7	250.3± 6.1	272.4± 6.6
70/100EVA5	256.1± 5.1	248.6± 2.0	258.8± 1.0	251.0± 4.6	267.2± 3.0

All the characteristic $\phi_3-3\phi_1$ values were $180^\circ < \phi_3-3\phi_1 < 270^\circ$, which was in agreement with the stress curves that were tilted to the right (an example is shown in Figure 6-20) and the continuous decay of G' and G'' (an example is shown in Figure 6-21) in the nonlinear region for all the samples. Though the trend found for G' and G'' has been related to strain thinning behavior (highlighted by Hyun et al. [1], who categorized this response as type I, shown Figure 2-2), the graphs of the 1st harmonic (G' and G'') asaf of γ were no further considered in the data analysis, as they give only partial information on the nonlinear behavior in LAOS.

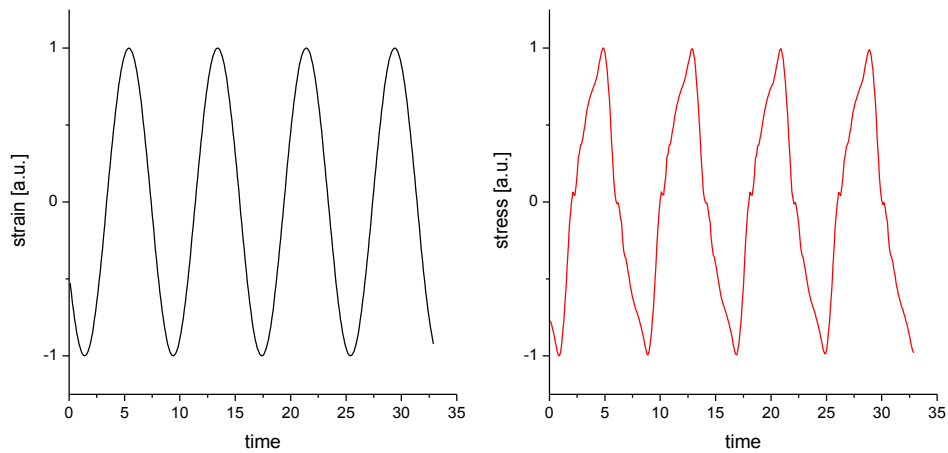


Figure 6-20 Strain (left) and stress (right) signals to exemplify the general trend of the stress signal to be tilted to the right. Sample 35/50 at 2 Hz and 25% strain.

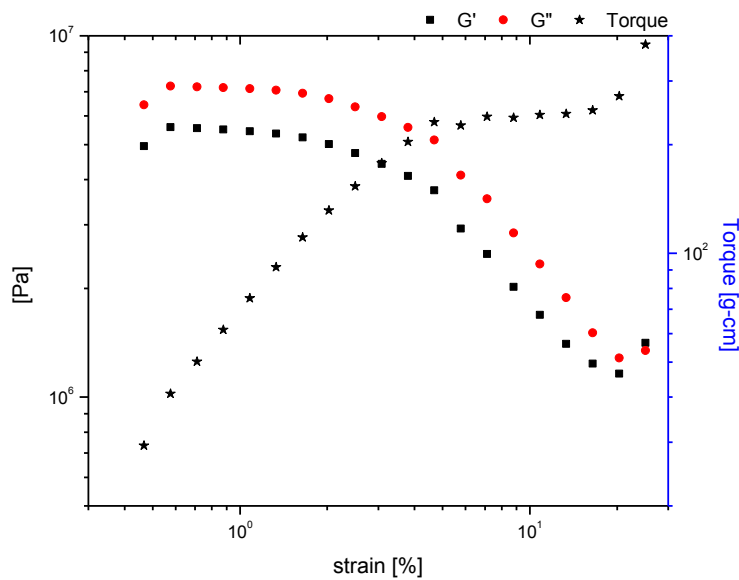


Figure 6-21 Example of the 1st harmonic trend asaf of strain.

Regarding the characteristic relative phase angle, it was possible to find differences with respect to the frequency for all the samples but for 70/100 binder. For the latter the trend was sort of constant (according not only on the means, but also on the error bars), and there was only a significant difference between 0.3 Hz and 2 Hz, which cannot properly be considered as a trend. It was possible to compute a characteristic value of $\phi_3-3\phi_1 = 242.4^\circ \pm 11.0^\circ$. For samples 70/100EVA5 and 35/50, the $\phi_3-3\phi_1$ was more or less flat between 0.1 and 1 Hz, and there seemed to be a slight tendency to increase as a function of the frequency at $\omega \geq 2$ Hz, which was confirmed by the relative phase angle value at 7 Hz ($\phi_3-3\phi_1 = 277.2 \pm 2.7$) for 70/100EVA5 and at 2.25 Hz ($\phi_3-3\phi_1 = 259.4 \pm 5.7$) for 35/50, shown on Figure 6-22. In the case of 70/100HDPE5 no specific trend can be drawn.

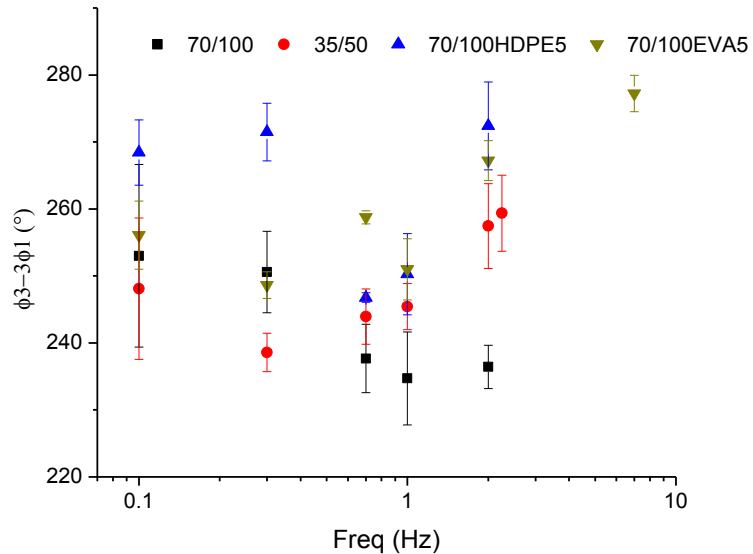


Figure 6-22 Characteristic relative phase angle as a function of frequency for all the binders.

In general the PMBs had either the same or higher phase angles than the 70/100 sample, meaning that the modification changed the strain softening to strain hardening balance [19]. The parent 70/100 bitumen had a more strain softening behavior than the modified bitumens, and this was more obvious at high frequencies, i.e. higher nonlinearities. Between binder grades, in general, 35/50 had a tendency towards a less strain softening behavior than 70/100. However the 35/50 strain thinning nature was the same or higher than the one of the PMBs. Sample 70/100HDPE5 had the highest $\phi_3-3\phi_1$ values, meaning that it had a less strain softening behavior when stretched than the rest of the samples.

By changing the frequency also the rheological parameters δ and De were modified. Therefore, some of the above data were replotted as a function of these parameters, and only the ones where a specific trend was found will be discussed further.

The relative phase angle of the 3rd harmonic as a function of De is shown in Figure 6-23. In this case both bitumens and 70/100EVA5 had a minimum in $\phi_3-3\phi_1$ at $De \sim 0.02$. Meanwhile 70/100HDPE5 had also a minimum in $\phi_3-3\phi_1$ but at $De \sim 0.08$.

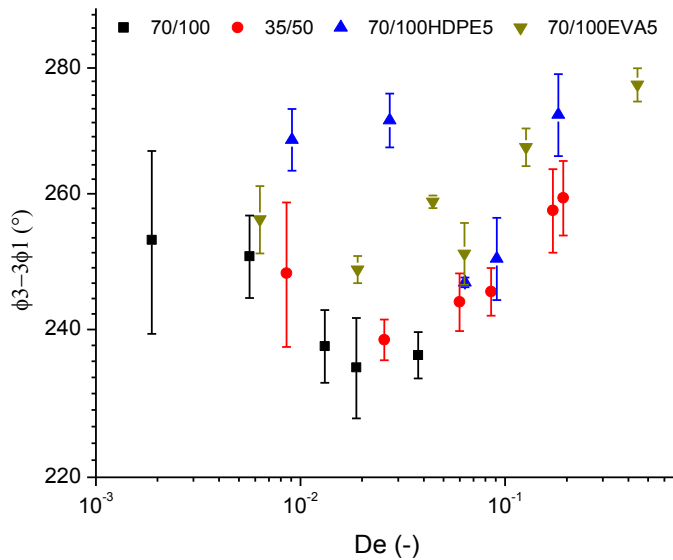


Figure 6-23 Relative 3rd phase angle as a function of De number for all the binders.

In respect to δ , PMBs reached a plateau at low frequencies, which was more noticeable for 70/100EVA5, refer to Figure 4-2. The value of the plateaus were close to $\delta \sim 49-51^\circ$ for 70/100EVA5 and $\delta \sim 55-56^\circ$ for 70/100HDPE5. Regarding the total harmonicity, shown in Figure 6-24-a,b, inside the plateau, both PMBs had constant values of pre-exponent and exponent. Outside that plateau, 70/100EVA5 had changes in the pre-exponent value, while for 70/100HDPE5 abrupt changes in both pre-exponent and exponent were detected. A similar behavior was also observed for $\phi_3-3\phi_1$, see Figure 6-24, inside the plateau the value of $\phi_3-3\phi_1$ remained more or less constant, while outside the plateau changes respect to δ were more evident. In the case of the bitumen grades, a minimum in $\phi_3-3\phi_1$ around $\delta \sim 60^\circ$ was found, shown in Figure 6-24.

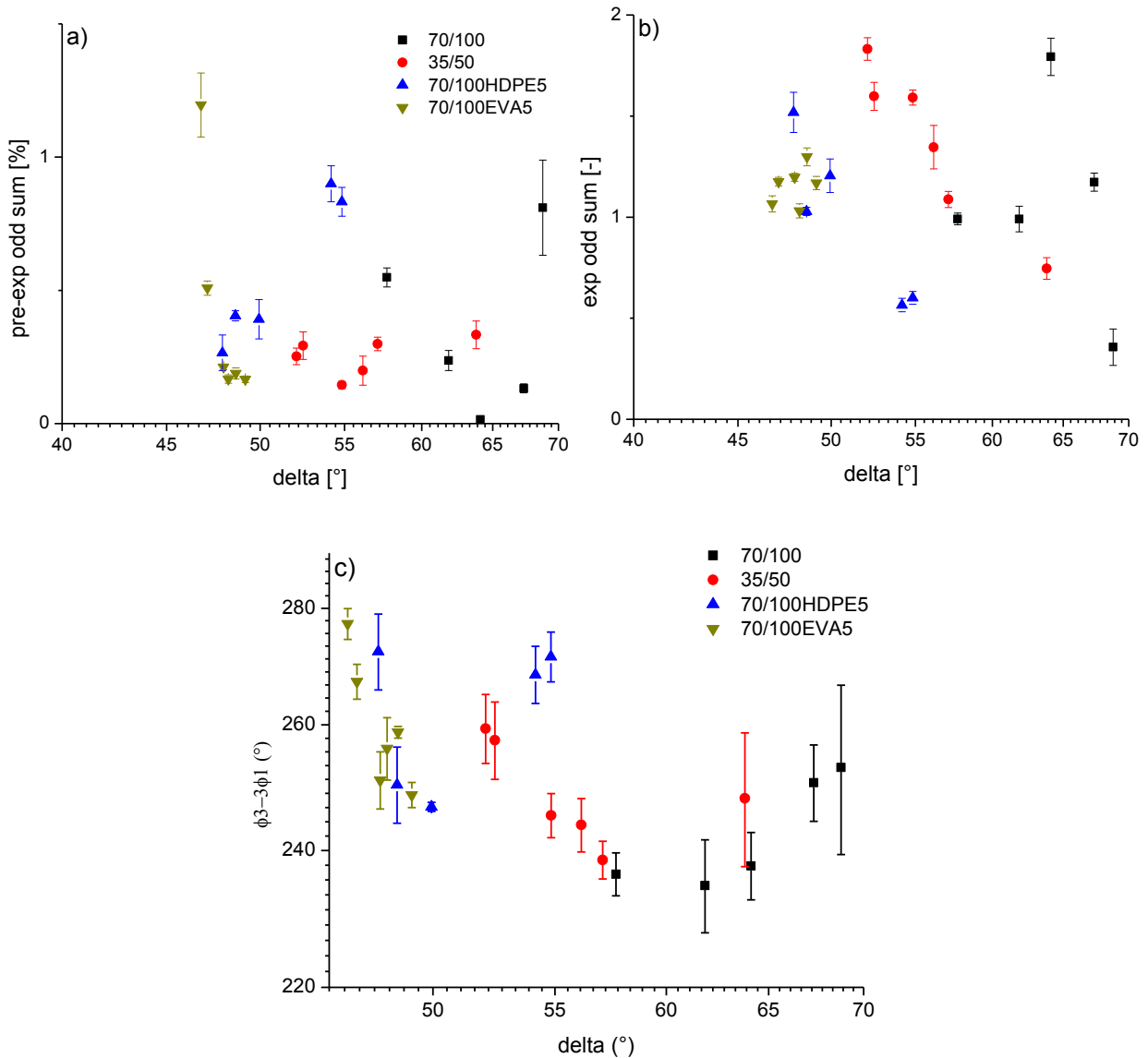


Figure 6-24 Odd sum fitting parameters re-plotted as a function of delta value (a) pre-exponent and (b) exponent. Characteristic 3rd harmonic phase angle (c) re-plotted as a function of delta.

In order to confirm if there is a correlation between δ and the nonlinear response of PMBs, LAOS test could be carried out at higher delta values far from the plateau.

6.2. LAOS at same delta (δ)

In this section the samples analysis was done at a similar delta value, i.e. at same viscoelasticity level. The frequency values to give the desired delta were obtained from SAOS experiments, refer to Figure 4-2. One analysis was done between binder grades at $\delta \sim 57^\circ$, and another analysis was

done among 35/50 and PMB samples at $\delta \sim 50^\circ$, because it was not possible to pick up a single common phase shift value for all materials (see Figure 4-2).

6.2.1. Bitumen grades at $\delta \sim 57^\circ$

Details about the experimental conditions are given on Table 6-5.

Table 6-5 Experimental conditions for $\delta \sim 57^\circ$

Sample	δ [°]	ω [Hz]	strain [%]
70/100	57.7	2.0	0.5 - 25
35/50	57.1	0.3	0.5 - 25

Lissajous curves of selected strain levels for the studied samples are given in Figure C-1 of Appendix C. In this case no big differences between the two binder grades could be noticed only by visual inspection of the Lissajous curves. Therefore, the binder grades shown a similar degree of nonlinearity as per the Lissajous curves shapes.

The harmonicity degree found in the bitumens at $\delta \sim 57^\circ$ is given in Table 6-6. The harmonicity degree in both samples was the same, so no further conclusions can be drawn from it.

Table 6-6 Harmonicity degree found in both bitumen grades at $\delta \sim 57^\circ$.

Sample	Harmonicity degree
35/50	7
70/100	7

In view of the high harmonicity degree, the relative intensity of the 3rd, 5th, and 7th harmonics and total harmonicity asaf of strain were analyzed, and the results are presented in Figure 6-25 shown in next page.

The results of the power law fitting are shown on Table 6-7.

Table 6-7 Power law fitting results of nonlinear signals for binder grades at $\delta \sim 57^\circ$.

Sample	a_3 [%]	b_3 [-]	R^2	a_5 [%]	b_5 [-]	R^2	a_7 [%]	b_7 [-]	R^2	a [%]	b [-]	R^2
70/100	0.18 ± 0.03	1.30 ± 0.06	0.988	0.05 ± 0.01	1.19 ± 0.06	0.971	0.03 ± 0.009	0.77 ± 0.14	0.833	0.55 ± 0.04	0.99 ± 0.03	0.990
35/50	0.14 ± 0.02	1.25 ± 0.06	0.987	0.02 ± 0.004	1.41 ± 0.09	0.925	0.01 ± 0.006	1.37 ± 0.25	0.761	0.30 ± 0.03	1.09 ± 0.04	0.987

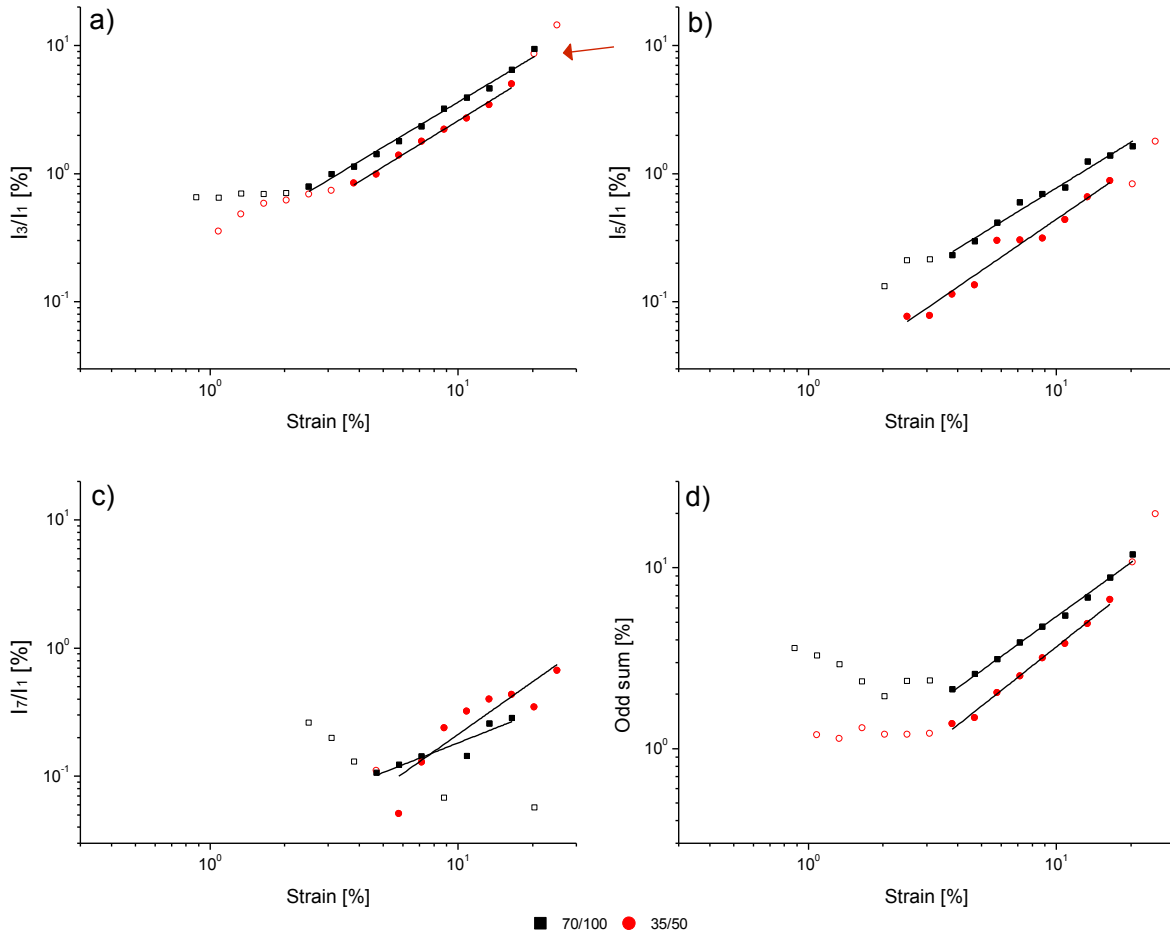


Figure 6-25 Relative intensity signals for bitumen grades at $\delta \sim 57^\circ$: (unfilled symbols) data free of motor noise, (filled data) data considered for power law, and (solid lines) power law fitting.

In terms of the I_3/I_1 signal, both binders had the same dependence respect to strain (exponent value). In respect to the I_5/I_1 signal, different values of exponent were found for both binders \therefore I_5/I_1 was more sensitive to differentiate between these samples. In this regard, 35/50 binder had the higher strain dependence. In terms of the I_7/I_1 signal the fitting was very poor, still the same trend as in the I_5/I_1 one could be drawn. Finally in the odd sum, both binders had more or less the same dependence with respect to strain, being 35/50 only slightly more affected by the strain level. This means that both bitumens softened (as per the general G' & G'' decaying tendency) at a similar pace respect to strain. In this case the binders softened linearly with the strain. Aside the similitudes, at higher strains outside of the initial power law region, 35/50 binder shown a steeper increase in the strain dependence of I_3/I_1 signal, pointed out by an arrow in Figure 6-25.

The critical strain concept was also considered for analysis. The same rationale as for I_3/I_1 and total harmonicity was followed to establish the I_n/I_1 limit for the 5th and 7th harmonic signals. The limits established, given in Table 6-8, were used for the computation of γ_{c-n} and γ_c for all the samples according to equation (6.1-3).

Table 6-8 Limit condition for nonlinear signal used to compute the critical strains, as well as the sample from which the limiting value was obtained.

Signal	Limit	Sample
$I_3/I_1\%$	0.19%	70/100EVA5 @ 0.3 Hz
$I_5/I_1\%$	0.05%	70/100EVA5 @ 1 Hz
$I_7/I_1\%$	0.09%	70/100EVA5 @ 1 Hz
Odd sum	0.55%	70/100EVA5 @ 0.3 Hz

The values of critical strains for all the signals analyzed are given in Table 6-9.

Table 6-9 Critical strains for nonlinear signals at $\delta \sim 57^\circ$ condition

Sample	γ_{c-3} [%]	γ_{c-5} [%]	γ_{c-7} [%]	γ_c [%]
70/100	0.79	1.00	3.99	1.00
35/50	1.12	2.10	5.34	1.75

As expected for both samples the critical strain increased asaf of the harmonic number. In this case for all the harmonic signals the 70/100 binder started to be affected by strain before than the 35/50 one. This is reflected also in the critical strain for total harmonicity, according to which sample 35/50 is able to sustain 75% more strain than 70/100 binder.

This was a good example of the importance of analyzing higher harmonic signals than the 3rd harmonic one when analyzing bitumen samples.

The relative phase angle responses, $\phi_n-n\phi_1$, are shown in Figure 6-26. This signal is only given for the 3rd and 5th harmonic. In the case of the 7th harmonic the relative phase angle was very noisy, as expected, since it amplified the noise embedded in the ϕ_1 value. The plateau values were computed and the characteristic relative phase angle values are reported in Table 6-10. In terms of $\phi_3-3\phi_1$ the there was no significant difference between the values, then this value can be considered as specific

of bitumen binders at the given delta, and an average of this value was done and it is reported in Table 6-10.

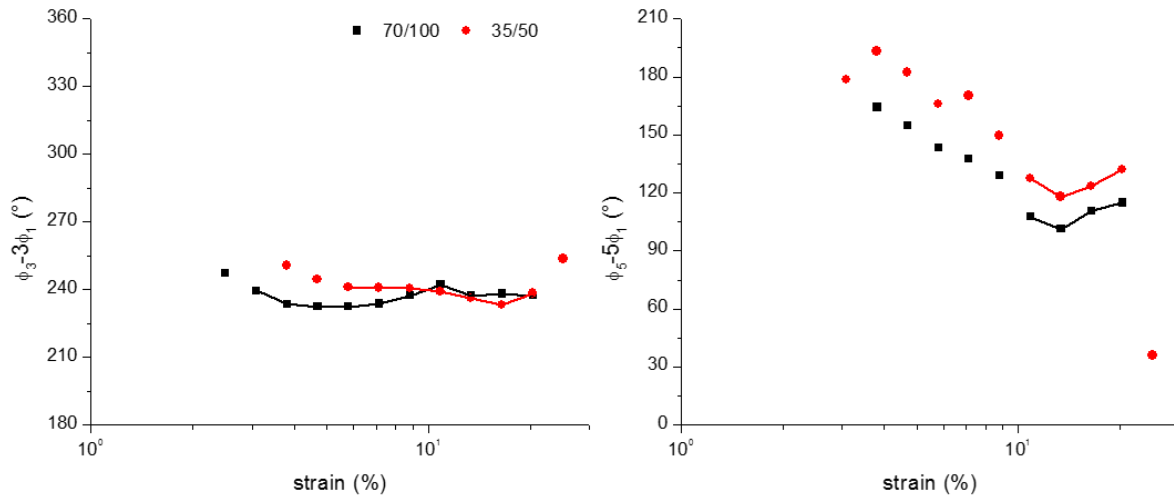


Figure 6-26 Phase angle signal asaf of train for binder grades at $\delta \sim 57^\circ$ condition

Regarding $\phi_5 - 5\phi_1$ differences between the bitumens were found. However in the literature consulted [1, 2, 13, 19], no physics were related to this relative phase angle. Nevertheless, for both bitumens $\phi_3 - 3\phi_1 > \phi_5 - 5\phi_1$.

Table 6-10 Characteristic relative phase angle data for different harmonics of bitumen grades at $\delta \sim 57^\circ$.

Sample	$\phi_3 - 3\phi_1$ [°]	$\phi_5 - 5\phi_1$ [°]
35/50	241 ± 6	125 ± 6
70/100	236 ± 3	109 ± 6
average	239 ± 5	-

6.2.2. PMBs and 35/50 at $\delta \sim 50^\circ$

Details about the experimental conditions used in this section are given in Table 6-11.

Table 6-11 Experimental conditions for $\delta \sim 50^\circ$

Sample	δ [°]	ω [Hz]	strain [%]
35/50	52.1	2.25	0.5 - 25
70/100HDPE5	48.7	1.0	0.5 - 25
70/100EVA5	48.2	0.1	0.5 - 25

Lissajous curves of selected strain levels for the studied samples are given in Figure C-2 of Appendix C. Based on the shape distortion, 35/50 was more nonlinear than 70/100HDPE and this in turn was more nonlinear than 70/100EVA5.

The harmonicity degree for samples at $\delta \sim 50^\circ$ is given in Table 6-12. As in the previous analysis the harmonicity degree was higher than 3rd harmonic for most of the samples, therefore justifying the analysis of higher harmonics as well as total harmonicity. In this case the harmonicity degree of sample 35/50 was higher than in the PMBs, which means that 35/50 binder had a much higher nonlinear response i.e. its microstructure was more deformed when compared to the one of PMBs.

Table 6-12 Harmonicity degree for binders at $\delta \sim 50^\circ$

Sample	Harmonicity degree
35/50	9
70/100HDPE5	5
70/100EVA5	3

The relative intensity of the 3rd, 5th, and 7th harmonics and total harmonicity asaf of strain are shown in Figure 6-27 given in the next page. All significant harmonics (above noise level) followed a power law trend. In the case of 70/100HDPE5 a bump in the data was found in the mid-section of the 3rd harmonic power law. In order to make a better power law fitting these points were taken as outliers and only the initial and final points of the power law region were considered. As can be seen, for all the harmonic signals sample 35/50 had always the higher nonlinearity, meaning that this sample was more susceptible to undergo microstructural changes induced by shear than any of the PMB samples, according to [1] . The results of the power law fitting are shown in Table 6-13.

Table 6-13 Power law fitting results of nonlinear signals for binder grades at $\delta \sim 50^\circ$.

Sample	a ₃ [%]	b ₃ [-]	R ²	a ₅ [%]	b ₅ [-]	R ²	a ₇ [%]	b ₇ [-]	R ²	a [%]	b [-]	R ²
35/50	0.17 ± 0.01	1.75 ± 0.04	0.989	0.03 ± 0.01	2.08 ± 0.17	0.949	0.001 ± 0.000	3.07 ± 0.31	0.984	0.25 ± 0.03	1.83 ± 0.06	0.991
70/100HDPE5	0.18 ± 0.00	1.19 ± 0.01	0.999	0.04 ± 0.01	1.20 ± 0.05	0.987				0.40 ± 0.02	1.03 ± 0.02	0.998
70/100EVA5	0.05 ± 0.00	1.38 ± 0.02	0.999							0.17 ± 0.02	1.03 ± 0.03	0.993

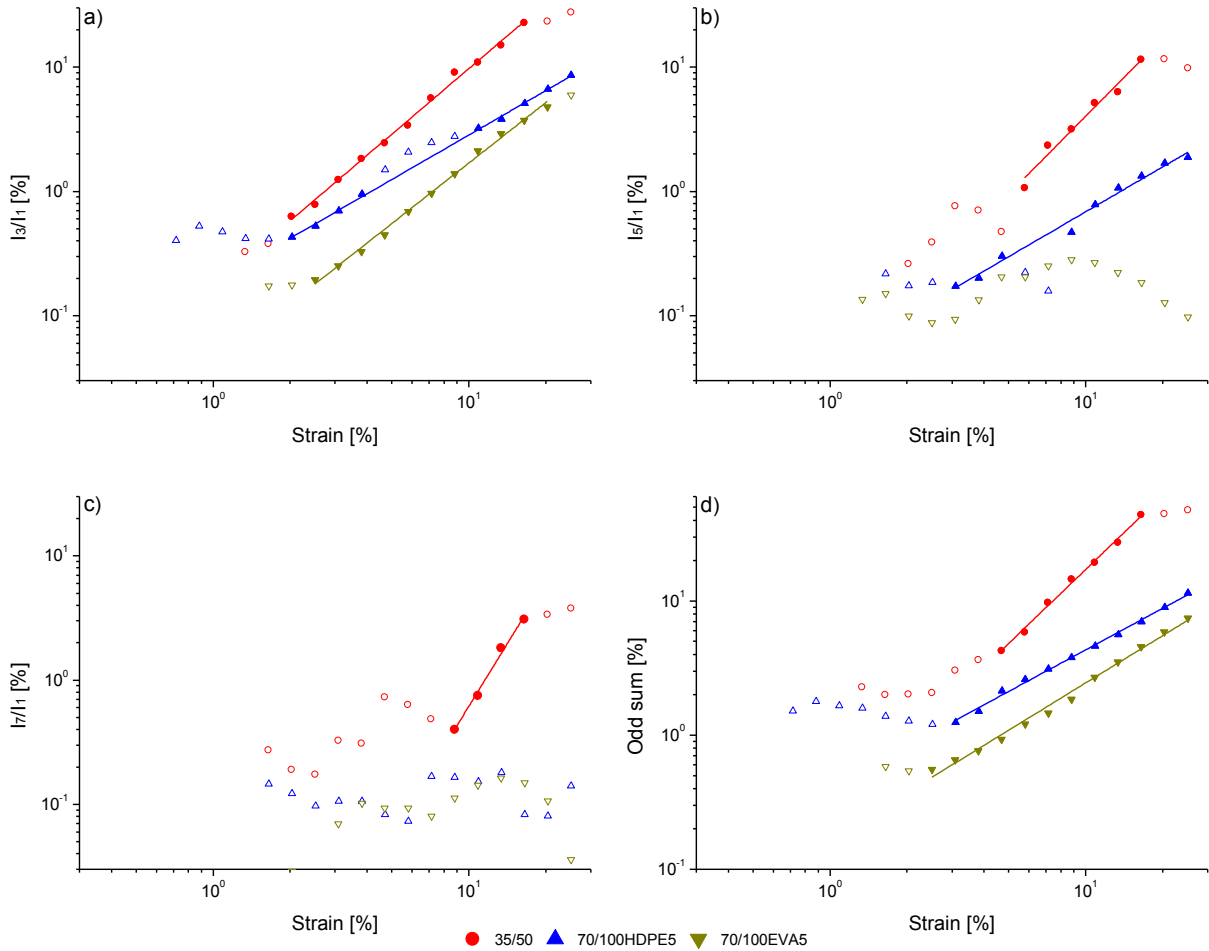


Figure 6-27 Relative intensity signals for bitumen grades at $\delta \sim 57^\circ$: (unfilled symbols) data free of motor noise, (filled data) data considered for power law, and (solid lines) power law fitting.

Regarding the I_3/I_1 signal, significant differences were found among the samples in the exponent value (different strain sensitivities). In this regard, 35/50 binder was more sensitive to strain changes than 70/100EVA5 binder and this was more sensitive than 70/100HDPE5 one. According to the I_3/I_1 response 70/100HDPE5 binder was more alike to 35/50 one. In the case of the I_5/I_1 signal, only 35/50 and 70/100HDPE5 had a power law trend. The 70/100EVA5 I_5/I_1 had a response free of motor noise, but it did not have a power law trend over the strain interval studied. The I_5/I_1 70/100EVA5 signal was around the same value where the I_5/I_1 non-linearity started for the other binders which supports the fact that 70/100EVA5 I_5/I_1 was not significant. The I_5/I_1 signal of 35/50 was more sensitive to strain than 70/100HDPE5 one, idem as in I_3/I_1 signal. In terms of the I_7/I_1 signal, only 35/50 I_7/I_1 had a rinsing, i.e. the PMBs signal remained constant in the strain interval

studied. In regard to the total harmonicity, the 35/50 binder softened faster respect to strain than the PMBs, which softened at the same rate. In this case the PMBs softened linearly with the strain. The critical strains were calculated according to the procedure described in section 6.1 and considering the limiting values given in Table 6-8 as well as the fitting values of Table 6-13. The critical strains for the FTR signals at $\delta \sim 50^\circ$ are given in Table 6-14.

Table 6-14 Critical strains for nonlinear signals at $\delta \sim 50^\circ$ condition

Sample	γ_{c-3} [%]	γ_{c-5} [%]	γ_{c-7} [%]	γ_c [%]
35/50	1.06	1.21	5.63	1.53
70/100HDPE5	1.03	1.13	>25%	1.35
70/100EVA5	2.59	>25%	>25%	3.18

In this case only sample 35/50 had significant signals for the 3rd, 5th, and 7th harmonics, for which the corresponding critical strain increased asaf of the harmonic number (as in the case of $\delta \sim 57^\circ$). At $\delta \sim 50^\circ$ sample 70/100EVA5 sustained higher strains before deformation than the other two binders in any of the harmonic signals. In fact 70/100EVA5 sustained at least twice more strain than any of the other samples. In respect to the 3rd and 5th harmonic, sample 70/100HDPE5 sustained only slightly less strain than 35/50 binder. However, in the total harmonicity that cumulative effect was the consequence of the lowest critical strain of 70/100HDPE5 binder.

The relative phase angle responses are shown in Figure 6-28.

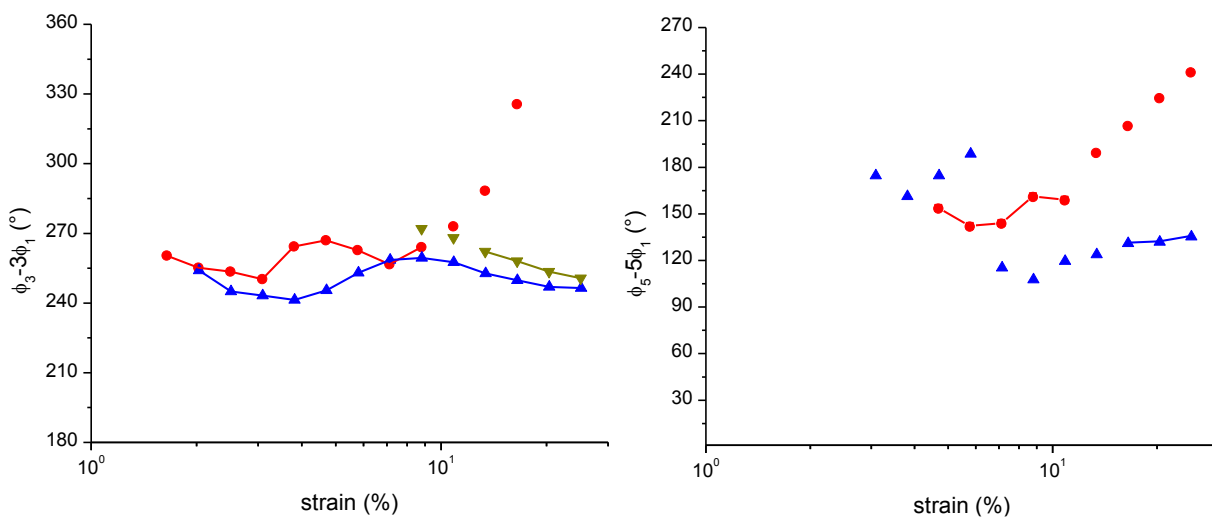


Figure 6-28 Relative phase angle signal asaf of strain for binders at $\delta \sim 50^\circ$.

As previously, this signal is only given for the 3rd and 5th harmonic. Only the data joined by lines were considered to compute the characteristic relative phase angle.

The average values are given in Table 6-15. In the case $\phi_3-3\phi_1$ signal, its value was the same for all the samples, higher than 180°, but closer to 180° than 360°. Therefore all samples presented the same softening to hardening balance, which was more biased towards softening. Besides the $\phi_3-3\phi_1$ value was consistent with the stress curves tilted to the right. Regarding the $\phi_5-5\phi_1$ signal, no value was available for 70/100EVA5, and the value of 35/50 was significantly higher than the one of 70/100HDPE5. However, as stated previously, in the literature consulted [1, 2, 13, 19], no physics were related to this relative phase angle. Nevertheless, in congruence with $\delta \sim 57^\circ$, the value of $\phi_3-3\phi_1$ is again higher than the one of $\phi_5-5\phi_1$.

Table 6-15 Characteristic relative phase angle data for different harmonics of bitumen grades at $\delta \sim 57^\circ$.

Sample	$\phi_3-3\phi_1$ [°]	$\phi_5-5\phi_1$ [°]
35/50	259 ± 6	150 ± 9
70/100HDPE5	250 ± 6	133 ± 2
70/100EVA5	256 ± 5	-
average	254 ± 7	-

6.3. LAOS at same Deborah number (De ~ 0.06)

In this section analysis of the samples was done at a similar Deborah number, i.e. at same relaxation stat. Based in the definition

$$De = \frac{\lambda_c}{\lambda} = \frac{\omega}{\omega_c} \quad (6.3-1)$$

the characteristic relaxation time λ_c was taken as the inverse of the crossover frequency ω_c between G' and G'' . Therefore to set the same De condition, the frequency values ω were obtained based on the crossover point ω_c which was previously determined in the frequency sweep in the SAOS regime, refer to Table 4-1. In this case it was possible to run comparisons among 35/50 bitumen and PMBs.

The De number for the samples studied is given in Table 6-16, along with the experimental conditions for data acquisition.

Table 6-16 Experimental conditions for $De \sim 0.06$

Sample	De [-]	ω [Hz]	strain [%]
35/50	0.060	0.7	0.5 - 25
70/100HDPE5	0.064	0.7	0.5 - 25
70/100EVA5	0.063	1	0.5 - 25

Lissajous curves of selected strain levels for the studied samples are given in Figure C-3 of Appendix C. Based on the shape distortion, the binders had different Lissajous patterns asaf of γ . However it is clear that 70/100EVA5 shown the lowest nonlinearity; meanwhile, 35/50 and 70/100HDPE5 had a higher nonlinear behavior.

The harmonicity degree for samples at $De=0.06$ was determined as previously and is given in Table 6-17. As in the previous analysis the harmonicity degree was higher than 3rd harmonic for most of the samples, therefore justifying the analysis of higher harmonics as well as total harmonicity. The harmonicity degree was higher for PMBs than 35/50 binder. In this regard, sample 70/100EVA5 had the higher harmonicity degree. In this case higher harmonicity degrees did not correspond to neither more deformed Lissajous curves nor to higher relative intensity signals (see further) as in the previous case of $\delta \sim 50^\circ$.

Table 6-17 Harmonicity degree for binders at $De \sim 0.06$

Sample	Harmonicity degree
35/50	5
70/100HDPE5	7
70/100EVA5	9

The relative intensity of the 3rd, 5th, and 7th harmonics and total harmonicity asaf of strain are shown in Figure 6-29. In this case a significant power law trend was found for all the samples in all the signals studied. Respect to the $De=0.06$ the curves of the samples were more similar as compared with the data at same delta $\delta \sim 50^\circ$. However, the results from the power law fits show that it was possible differentiate among the nonlinear behavior of the binders, see further. In general sample 70/100EVA5 had lower nonlinearity in all the signals. Meanwhile sample

70/100HDPE5 had the highest nonlinearity in I_3/I_1 and I_7/I_1 signal and \therefore in the total harmonicity as well.

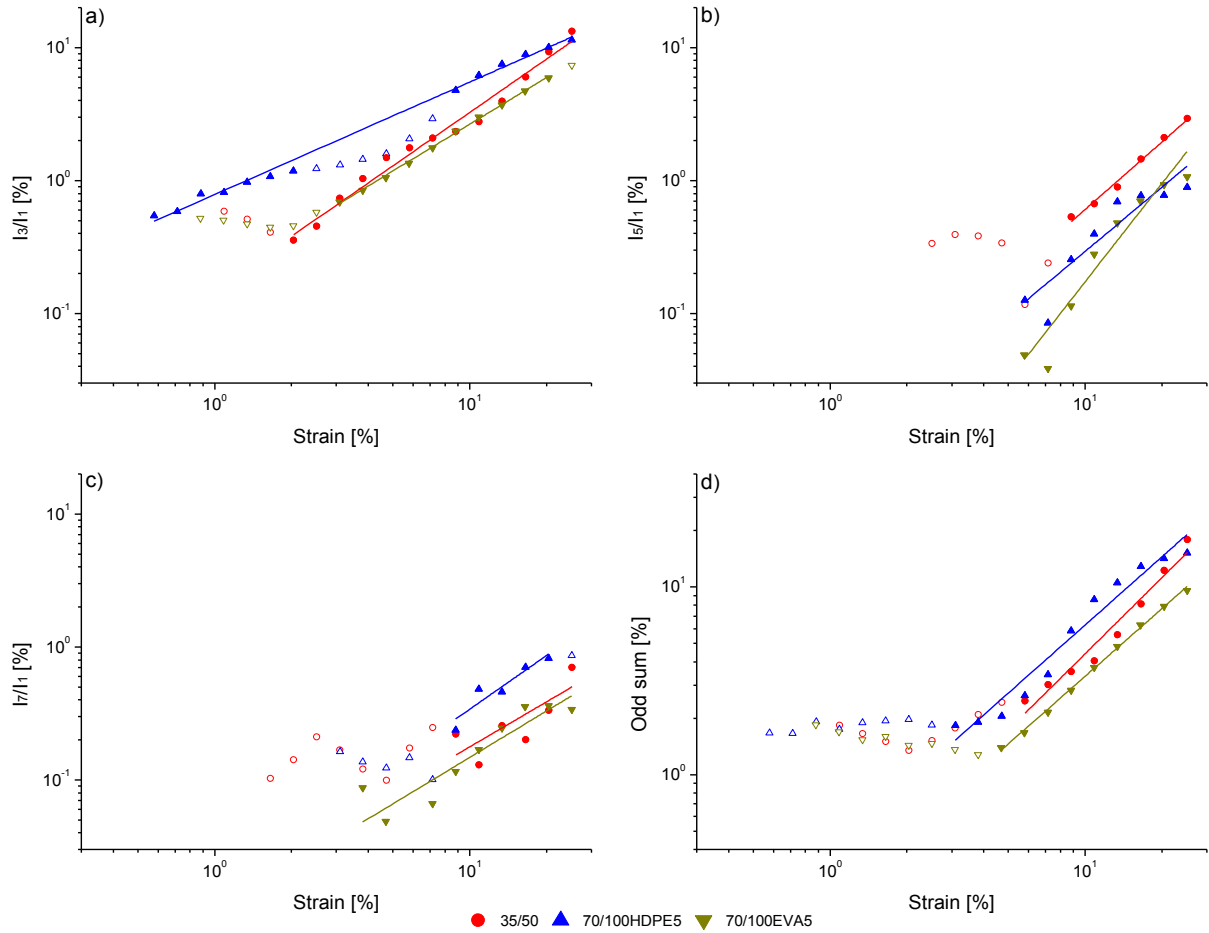


Figure 6-29 Relative intensity signals for bitumen grades at $De=0.0.6$ (unfilled symbols) data free of motor noise, (filled data) data considered for power law, and (solid lines) power law fitting.

The results of the power law fitting are shown on Table 6-18.

Table 6-18 Power law fitting results of nonlinear signals for binder grades at $De \sim 0.06$.

Sample	a_3 [%]	b_3 [-]	R^2	a_5 [%]	b_5 [-]	R^2	a_7 [%]	b_7 [-]	R^2	a [%]	b [-]	R^2
35/50	0.15 ± 0.02	1.33 ± 0.06	0.953	0.012 ± 0.003	1.69 ± 0.08	0.981	0.013 ± 0.02	1.12 ± 0.45	0.383	0.20 ± 0.05	1.35 ± 0.11	0.929
70/100HDPE5	0.79 ± 0.03	0.85 ± 0.02	0.983	0.007 ± 0.005	1.61 ± 0.25	0.791	0.016 ± 0.01	1.34 ± 0.30	0.809	0.39 ± 0.07	1.21 ± 0.08	0.921
70/100EVA5	0.20 ± 0.01	1.13 ± 0.01	0.996	0.003 ± 0.002	1.91 ± 0.19	0.966	0.002 ± 0.00	1.95 ± 0.10	0.985	0.21 ± 0.01	1.20 ± 0.02	0.997

In terms of I_3/I_1 signal, according to the exponent, sample 35/50 was more sensitive to strain than the PMBs, and between PMBs 70/100EVA5 was more sensitive to strain than 70/100HDPE5. Regarding I_5/I_1 signal, all samples had the same exponent, i.e. same sensitivity to strain. In the case of I_7/I_1 samples were differentiated, and it was clear that 70/100EVA5 had the highest strain dependence, though the fitting of 35/50 and 70/100HDPE5 binders was very poor. Finally according to the total harmonicity concept, the softening behavior was much higher for 35/50 than for the PMBs, which softened at the same rate according to the total harmonicity.

The critical strain concept was also applied to same De condition. The critical strains were calculated according to the procedure described in section 6.1 and considering the limiting values given in Table 6-8 as well as the fitting values of Table 6-18. The critical strains for the FTR signals at $De=0.06$ are given in Table 6-19.

Table 6-19 Critical strains for nonlinear signals at $De=0.06$ condition

Sample	γ_{c-3} [%]	γ_{c-5} [%]	γ_{c-7} [%]	γ_c [%]
35/50	1.19	2.28	5.47	2.13
70/100HDPE5	0.19	3.32	3.71	1.33
70/100EVA5	0.97	4.22	7.97	2.21

The binder 70/100HDPE5 was the sample that could withstand less strain prior to deformation in the 3rd, and 7th harmonic and as a consequence also in the total harmonicity. Though 70/100EVA5 had a lower critical strain than 35/50 in the 3rd harmonic, the opposite was true for the 5th and 7th harmonic. As a result both binders had a similar critical strain in the total harmonicity, which was 60% higher than the one of 70/100HDPE5.

The relative phase angle responses are shown in Figure 6-30. As previously, this signal is only given for the 3rd and 5th harmonic.

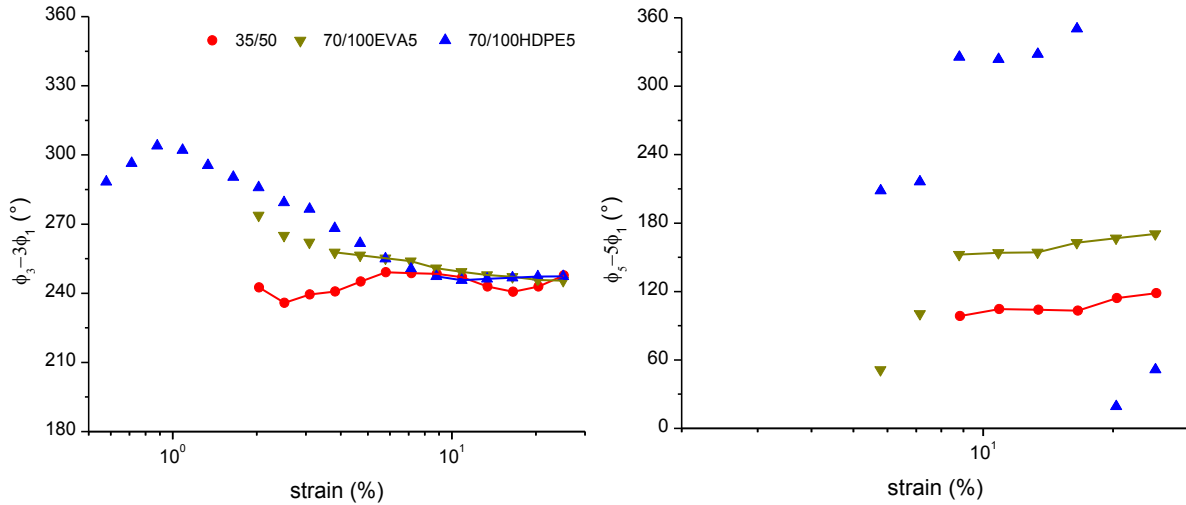


Figure 6-30 Relative phase angle for binders at $De \sim 0.06$

In terms of $\phi_3-3\phi_1$ there was no significant difference between the samples, then the values of $\phi_3-3\phi_1$ for all the samples were averaged, and the average of this value is given in Table 6-20. The averaged value was remained beyond 180° , which is consistent with the stress curves tilted to the right. Besides since the $\phi_3-3\phi_1$ average value was closer to 180° than to 360° the binders had a more softening than hardening behavior when submitted to shear deformation. Regarding $\phi_5-5\phi_1$ it was not possible to compute a value for 70/100HDPE5 and differences between the other two binders were found. Nevertheless, as in both same delta conditions previously studied, it was found that $\phi_3-3\phi_1 > \phi_5-5\phi_1$ for both bitumens.

Table 6-20 Relative phase angle for binders at $De \sim 0.06$

Sample	$\phi_3-3\phi_1$ [$^\circ$]	$\phi_5-5\phi_1$ [$^\circ$]
35/50	244 ± 4	107 ± 8
70/100HDPE5	251 ± 5	160 ± 8
70/100EVA5	247 ± 1	
average	247 ± 5	

7. Stress relaxation test of asphalt binders in NLVE region

In this section the nonlinear characterization of asphalt binders by means of stress relaxation will be given.

Stress relaxation in shear was performed for all the samples. Data are shown in Figure 7-1.

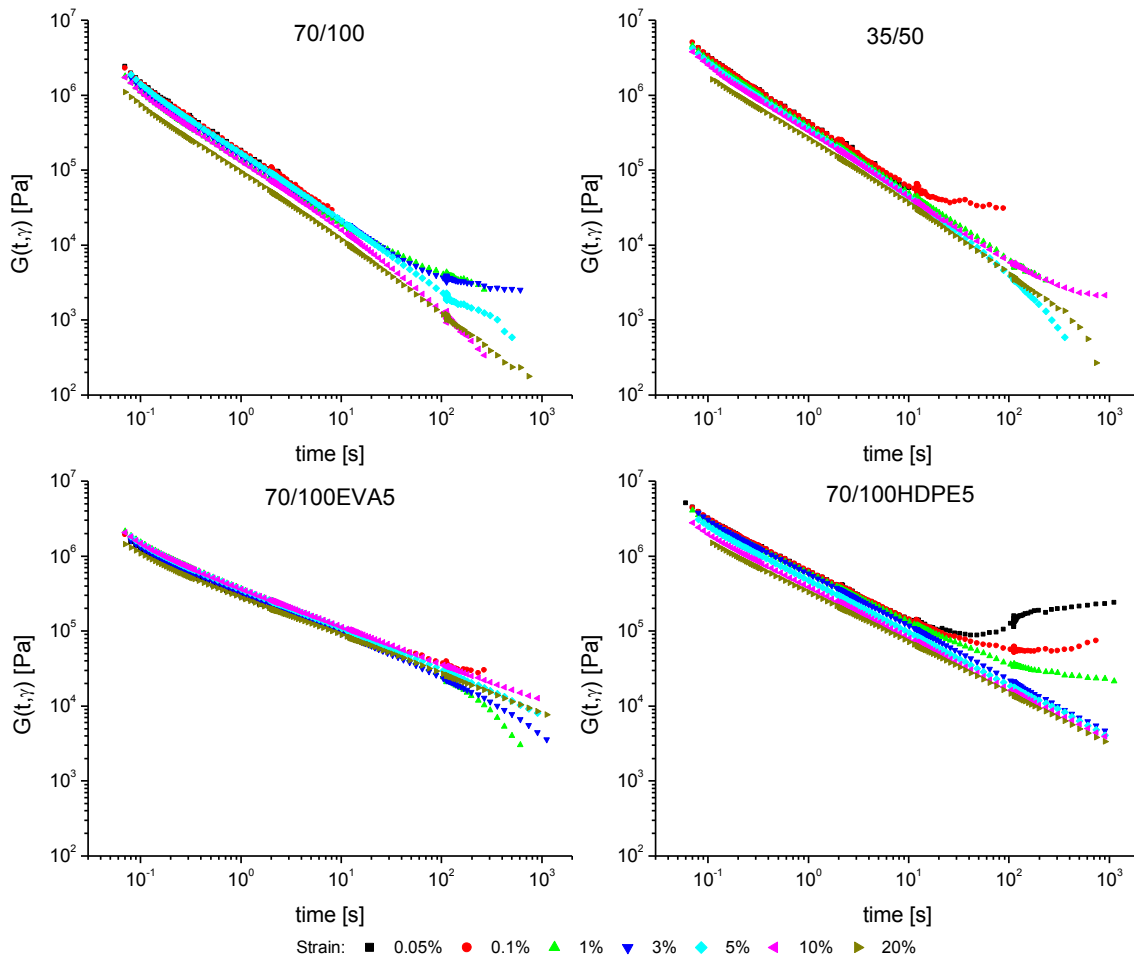


Figure 7-1 Stress relaxation test in nonlinear regime for all binders at $T=20^\circ\text{C}$.

At short times ($t < 10$ s), all samples shown a power law decay respect to time either in the linear or in the nonlinear regime. For all the samples, but for 70/100EVA5, it was possible to clearly span the linear and non-linear region. The nonlinear regime was characterized by a nonlinear relaxation modulus with a value significantly lower than the linear one. Considering that the shape of the

curve was unaffected by the strain, the damping function concept was applied at short times for all the samples. The damping function is the most commonly used rheological parameter to analyze stress relaxation data in the nonlinear regime, [48]. The damping function can be seen as the offset in a log-log plot between the linear relaxation modulus and the nonlinear shear relaxation modulus

$$\ln h(\gamma) = \ln G(t, \gamma) - \ln G(t) \quad (7-1)$$

The details about the $h(\gamma)$ computation were given in section 3.2. The damping function was valid over 3 decades on time for each sample, as shown in Figure 7-2 and in Table 7-1.

However, the time interval for the validity of $h(\gamma)$ was dependent on the sample. In this regard, the validity time was higher for 70/100 and 70/100EVA5 binders than for 35/50 and 70/100HDPE5, shown in Table 7-1.

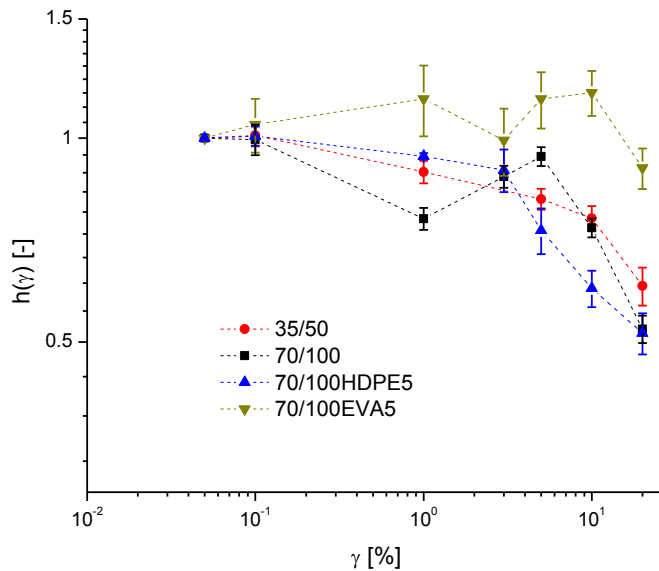


Figure 7-2 Damping function computed for all the binders at $T \sim 20^\circ\text{C}$, lines are only to guide the eye.

The damping functions for 35/50, 70/100, and 70/100HDPE5 binders decreased with respect to strain. The damping function was fitted according to a sigmoidal equation

$$h(\gamma) = \frac{1}{1 + a_{SR} \gamma^{b_{SR}}} \quad (7-2)$$

The parameters of the fitting are given on Table 7-1.

Table 7-1 Damping function sigmoidal fitting and time validity.

Sample	Time interval	a_{SR} [%⁻¹]	b_{SR} [-]	R²
35/50	0.07 - 12	0.08 ± 0.02	0.69 ± 0.12	0.9555
70/100	0.07 - 30	0.01 ± 0.01	1.38 ± 0.25	0.9352
70/100HDPE5	0.07 - 20	0.06 ± 0.02	0.95 ± 0.15	0.9325
70/100EVA5	0.07 - 40	n/a	n/a	n/a

The parameter a_{SR} is related to the onset of the nonlinear behavior. Small values of a_{SR} indicate a high critical strain, γ_c , i.e. the smaller the a_{SR} the more strain is able to sustain the material before deforming the microstructure. The parameter b_{SR} reflects the strain dependence of the deformed material, i.e. once it has started to deform the higher the b_{SR} the faster the deformation will happen respect to the strain.

Based on this, the 70/100HDPE5 damping function started to decrease (critical strain) similar to the 35/50 one, still its rate of decrease was faster than 35/50 binder and more similar to the 70/100 one. In the case of 70/100EVA5 sample it was not possible to fit the data since the non-linear region was not clearly defined. Hence, 70/100EVA5 binder had the lowest non-linearity as per the damping function computation. However the stress relaxation experiment at 0.05% strain for 70/100EVA5 binder was recorded at 3°C higher than the rest of the samples, which could have affected the stress relaxation modulus values, and therefore be the root of the apparent small increase of the damping function. In any case, none of the PMBs performed as the benchmark 35/50 binder, however 70/100HDPE5 binder had the closest similarity to 35/50 binder.

Data at long times ($t > 10$ s) were more difficult to analyze since not all the curves followed the same trend, shown in Figure 7-3. In fact, the behavior at long times was not only strain dependent but also sample dependent. However, for all samples at low strains $G(t)$ and $G(t,\gamma)$ tended to level off.

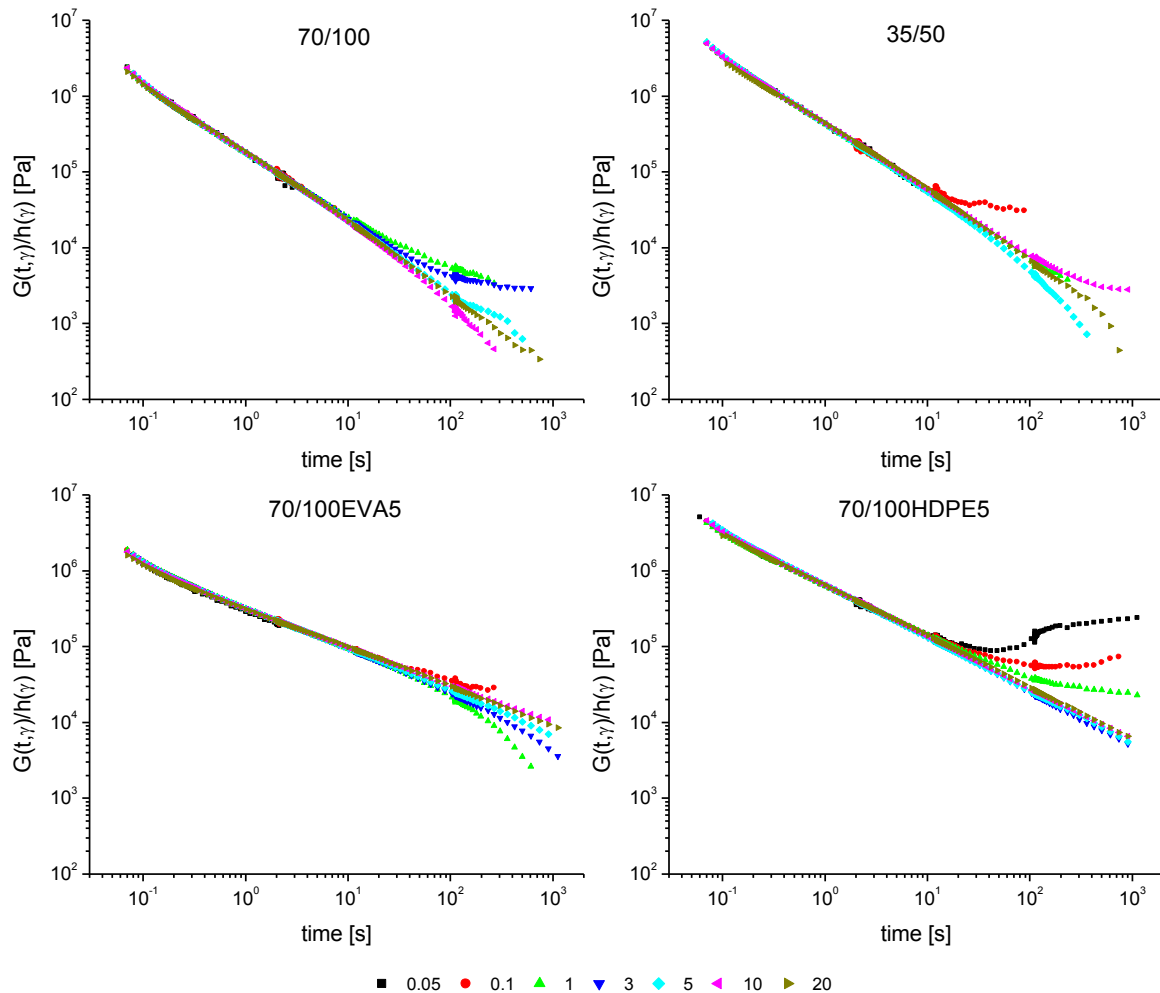


Figure 7-3 Stress relaxation modulus shifted according to the damping function value for all samples.

In the sample 35/50 the plateau at 0.1% strain can be regarded as an artifact, due to the proximity of the torque value to the sensitivity limit (torque in plateau was 0.023 g.cm and the sensitivity limit is 0.020 g.cm). For the rest of the curves that exhibited a level off in the relaxation modulus no experimental pitfall can be clearly associated to them. In the case of the sample 70/100HDPE5 at 0.05 % strain, where a level off and a subsequent increase in the relaxation modulus was shown, the measurement was repeated, but the same trend was found as shown in Figure 7-4 (left). Also the strain signal was monitored in order to see if a change in strain could be the root of this behavior. As can be seen in Figure 7-4 (right), in the original measurement the strain signal had a small decrease at the end of the experiment, but this was not enough as to be the root of the pronounced increase. In the repetition the strain was kept constant all over the measurement and

still an increase in the torque signal was observed. Nonetheless, this behavior was not a standard one, and it can be initially regarded as an experimental pitfall, but yet its origin was not clear.

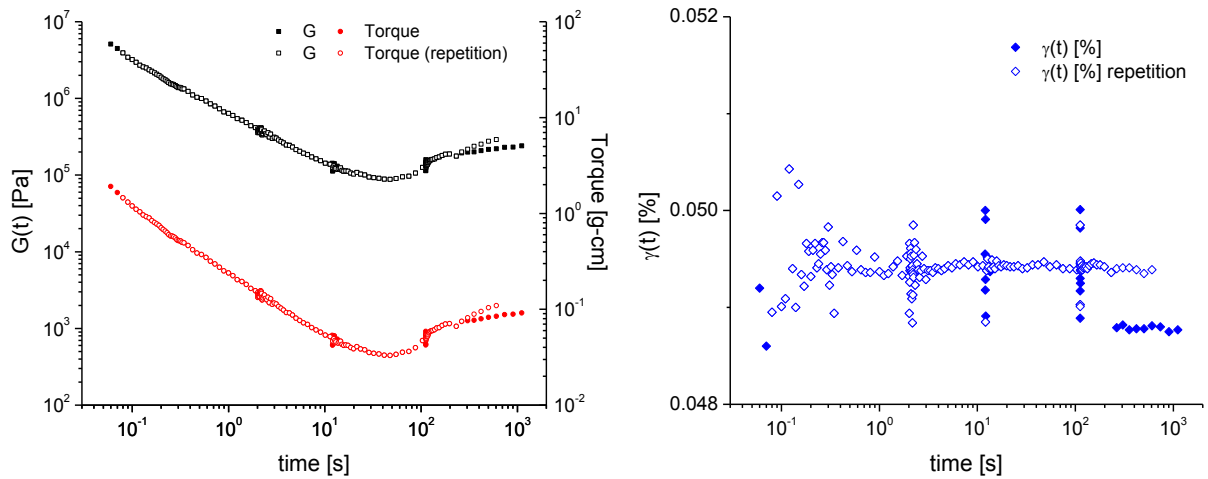


Figure 7-4 Repetition of the stress relaxation test at 0.05% strain for sample 70/100HDPE5 at $T \sim 20^\circ\text{C}$: (left) stress relaxation modulus and torque signals, (right) strain signal.

Nevertheless, in all samples at high strains the $G(t, \gamma)$ level off disappeared and the trend either followed a power law decrease or a strong decrease on time. For the samples where a power law trend was found longer experimental times would be needed to identify either a level off or a decrease on $G(t, \gamma)$.

8. LAOS-FTR test to predict fatigue behavior

In this chapter the results of time sweeps in NLVE region will be presented. The results were analyzed by means of FTR, and the output of these tests was intended to be related to the fatigue behavior of the binder.

Time sweeps with a constant strain amplitude in the NLVE region (LAOS) were performed to study the temporal stability of the samples. This was an exploratory study which objective was to detect whether a doable fatigue protocol could be set within 15 min. Based on this and due to time constraints, the scope of the test was narrowed to only some specific experimental conditions of frequency and strain. The frequency was specified for the samples to have the same delta value, $\delta \sim 50^\circ$, given in Table 6-11. Therefore sample 70/100 was not studied in this exploratory test. Furthermore, the strain amplitude was set for the samples to have the same level of nonlinearity quantified by I_3/I_1 . The I_3/I_1 tested levels were selected to be high enough as to detect changes in a small time frame (in view that for low nonlinearities the experiments will take long), and low enough to be contained for all the samples within the strain range previously explored (i.e. 0.5 to 25% strain). Based on the selected levels of I_3/I_1 , the equation (6.1-2) was used along with the fitting parameters reported in Table 6-13 to compute the strain levels at which the samples would be tested.

The specific tested conditions are given in Table 8-1.

Table 8-1 Experimental conditions for time sweep tests in NLVE regime.

Sample	Freq [Hz]	I_3/I_1 [%]	Strain [%]	I_3/I_1 [%]	Strain [%]	I_3/I_1 [%]	Strain [%]
35/50	2.25	2	4.1	3	5.1	-----	-----
70/100HDPE5	1	-----	-----	3	10.5	4	13.3
70/100EVA5	0.1	2	14.3	3	19.2	4	23.6

The results are given in Figure 8-1, Figure 8-2, and Figure 8-3 for all the samples. All the results are plotted respect to cycle numbers rather than time, because this was considered a better approach to compare data, and in order to adopt a results analysis similar to the one performed in the fatigue tests carried out in the scope of pavement engineering [29, 40] . In this case the total harmonicity was not considered for analysis since it led to the same conclusions than I_3/I_1 .

In the case of 35/50 and 70/100EVA5, both predicted and experimental values of I_3/I_1 matched, shown in Table 8-2. Reinforcing that the LAOS-FTR experimental conditions established on chapter 5 led to a very good level of repeatability, valid of course within the first 18-20 cycles on which the fitting data of Table 6-13 were applicable. However for 70/100HDPE5 the real values of I_3/I_1 were almost twice the ones predicted, shown in Table 8-2.

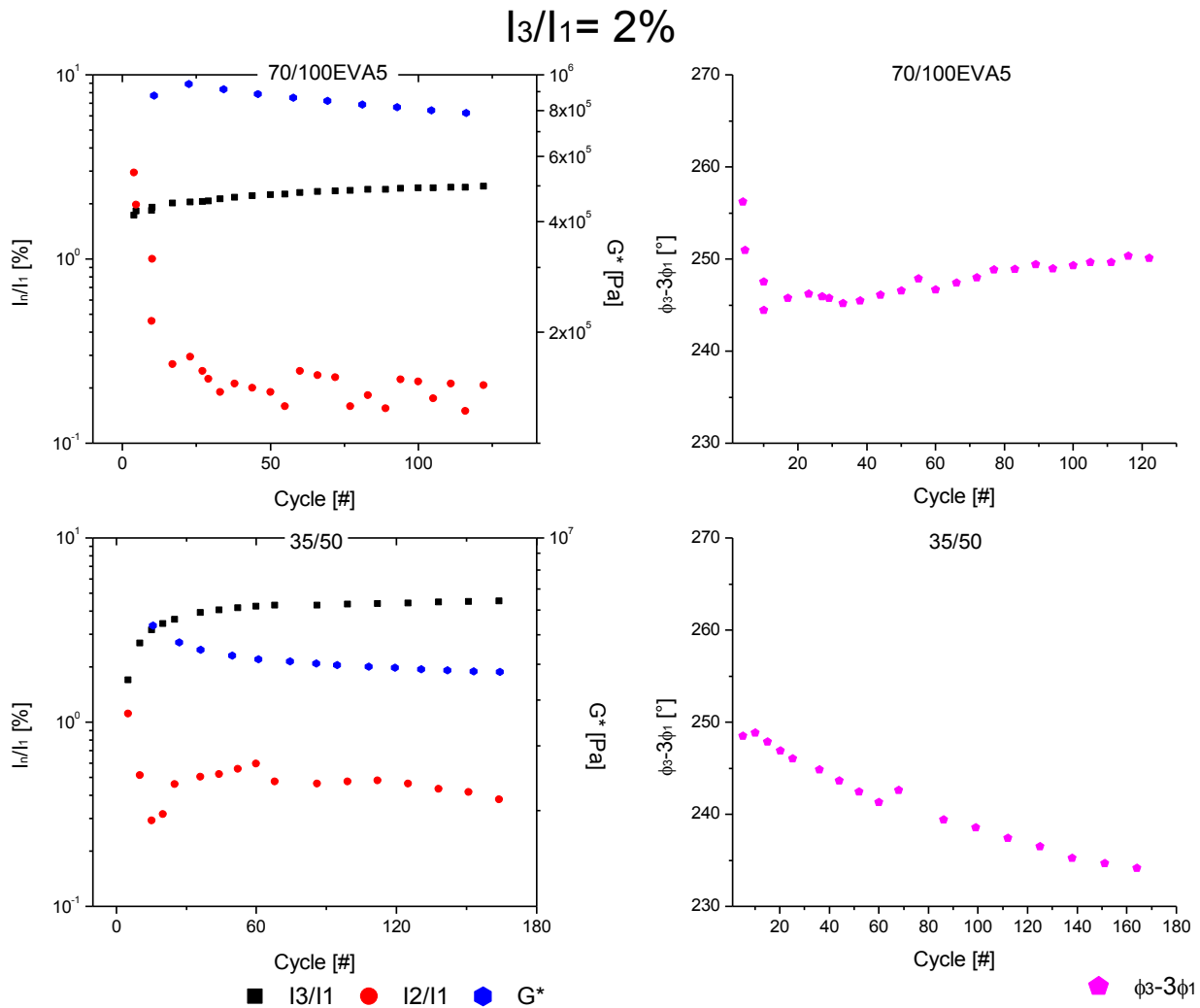


Figure 8-1 Time sweeps at same delta and $I_3/I_1=2\%$ for 35/50 and 70/100EVA5 binders.

All the samples had a decrease in G^* with shearing time that tended to level off at high cycles, concomitant to a decrease in the stress amplitude signal, similar to the one shown in Figure 6-5. This decrease was very pronounced at the beginning indicating that there was a transient phenomenon. This transient phenomenon involved not only a change in amplitude of the periodic stress but also in shape of the waveform since the I_3/I_1 and I_2/I_1 values changed as well.

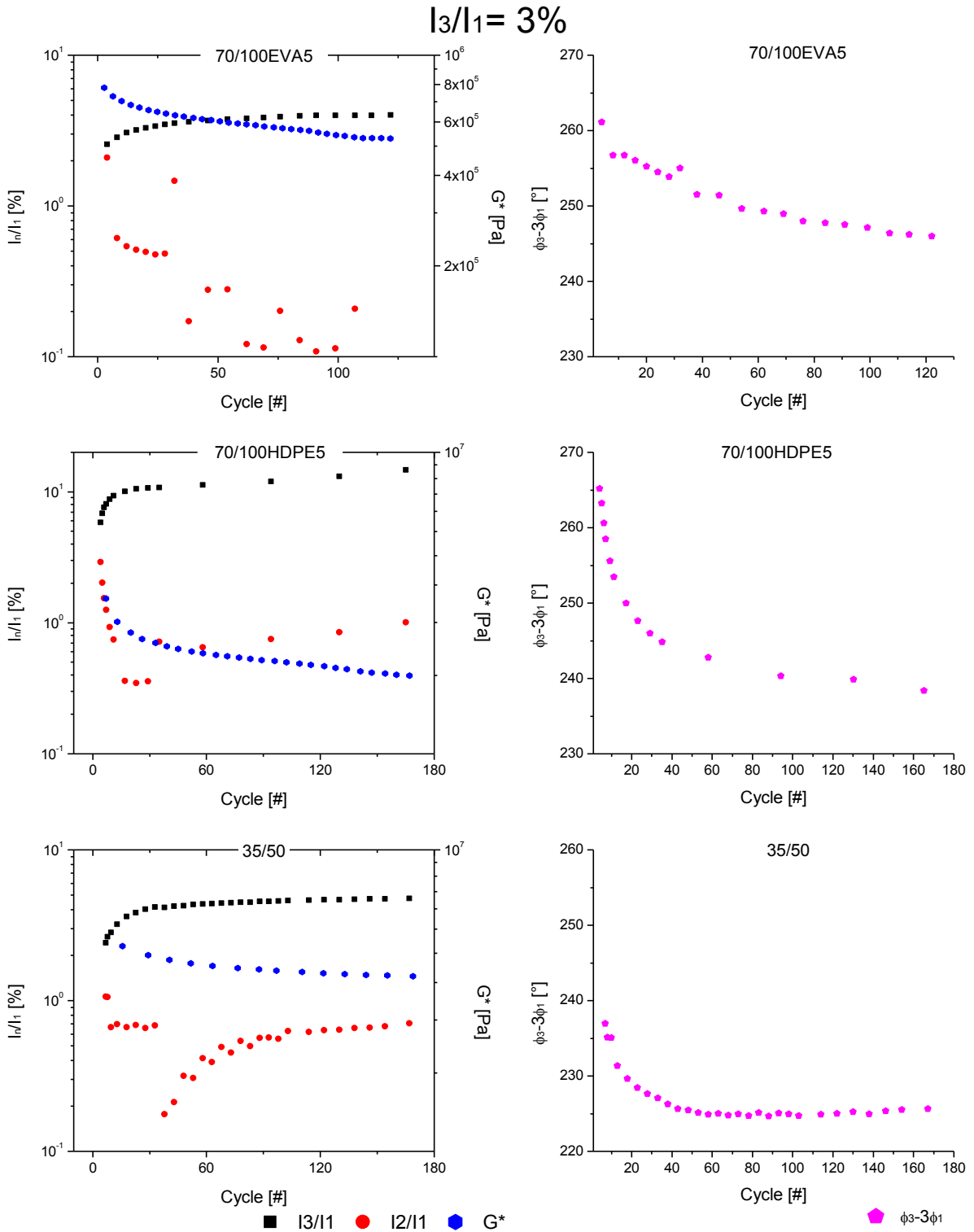


Figure 8-2 Time sweeps at same delta and $I_3/I_1=3\%$ for 35/50 binder and PMBs.

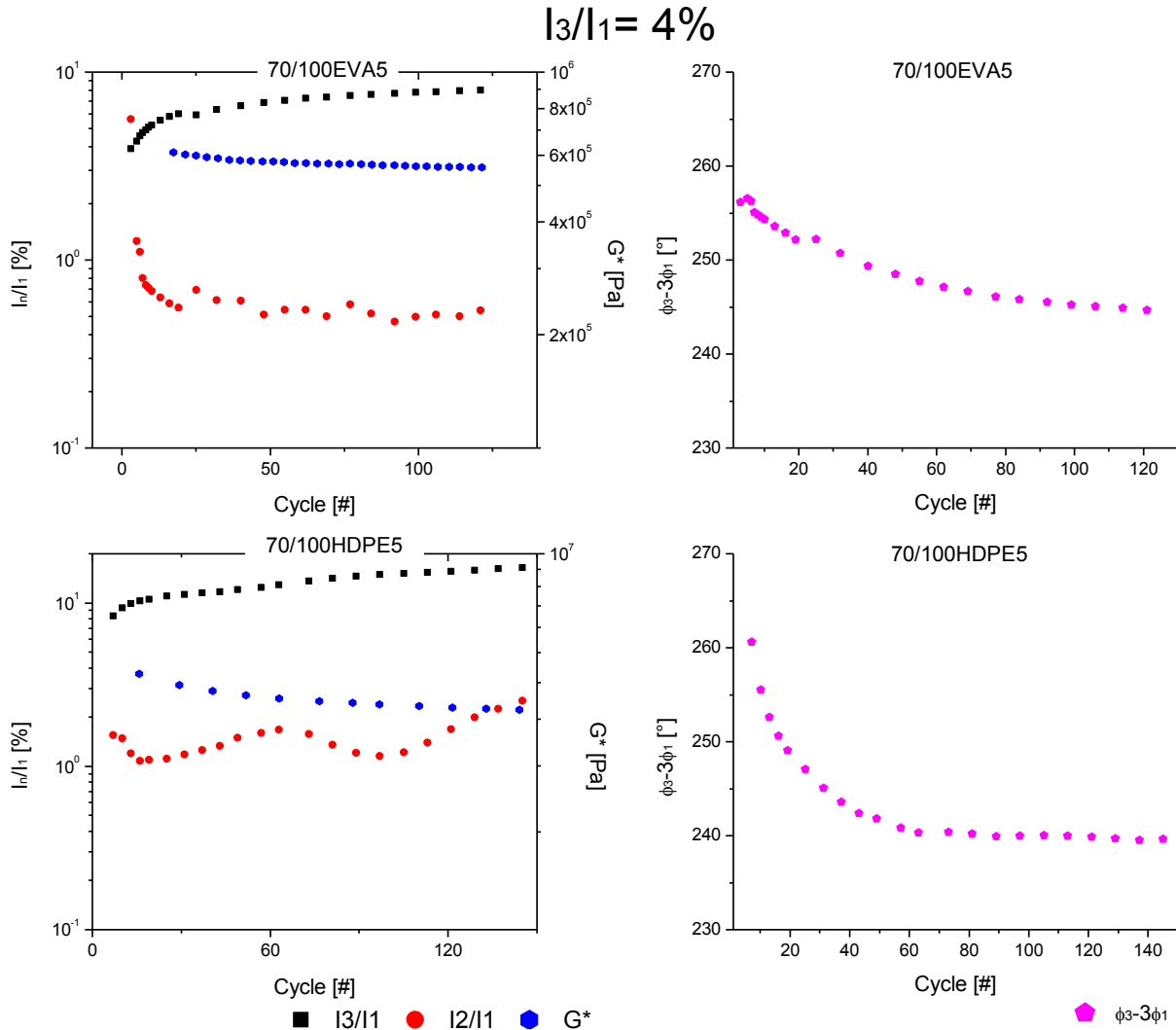


Figure 8-3 Time sweeps at same delta and $I_3/I_1=4\%$ for PMBs.

For all the samples, but for 70/100EVA5 at $I_3/I_1 = 2\%$, these changes went along with a decrease in the phase angle to finally achieve a lower plateau value, which indicated that the binders softened when subjected to a constant cyclic deformation. In the case of 70/100EVA5 at $I_3/I_1 = 2\%$ the value of $\phi_3 - 3\phi_1$ remained constant ($\phi_3 - 3\phi_1 = 247.5 \pm 2.5^\circ$), meaning that the sample only underwent by a transient behavior before stabilizing the nonlinear response. For the rest of the samples the transient behavior was characterized by a change in the I_3/I_1 of more than 50%. The value of I_2/I_1 decreased at the beginning of the test and remained stable for the rest of the test. This initial transient of the I_2/I_1 signal was free from motor noise, first because the cycles for the test started to be counted after the motor signal was stable, and second because the motor signal had $0.02\% < I_2/I_1\% < 0.09\%$ for all cycles and samples tested.

Considering above observations, strictly the changes in nonlinearity could not be correlated to a fatigue phenomenon, because fatigue relates to nonreversible phenomena which in the frame of FTR would be related to an increase in the I_2/I_1 signal, fact that was absent for all the samples. Therefore, in order to explore the possibility to relate fatigue phenomena with I_2/I_1 signal: either other conditions for δ and De can be tested or longer times should be explored. However as per the increase in I_3/I_1 and the decrease in $\phi_3-3\phi_1$, the samples underwent microstructural changes associated to a softening behavior. Based on this, two criteria to quantify nonlinear transient behavior were proposed:

- Cycles number, NC1, corresponding to an increase of 50% in the I_3/I_1 signal.
- Cycles number, NC2, at the interception between the plateau value of I_3/I_1 and the rising of I_3/I_1 , better observed in a log-log representation, shown in Figure 8-4.

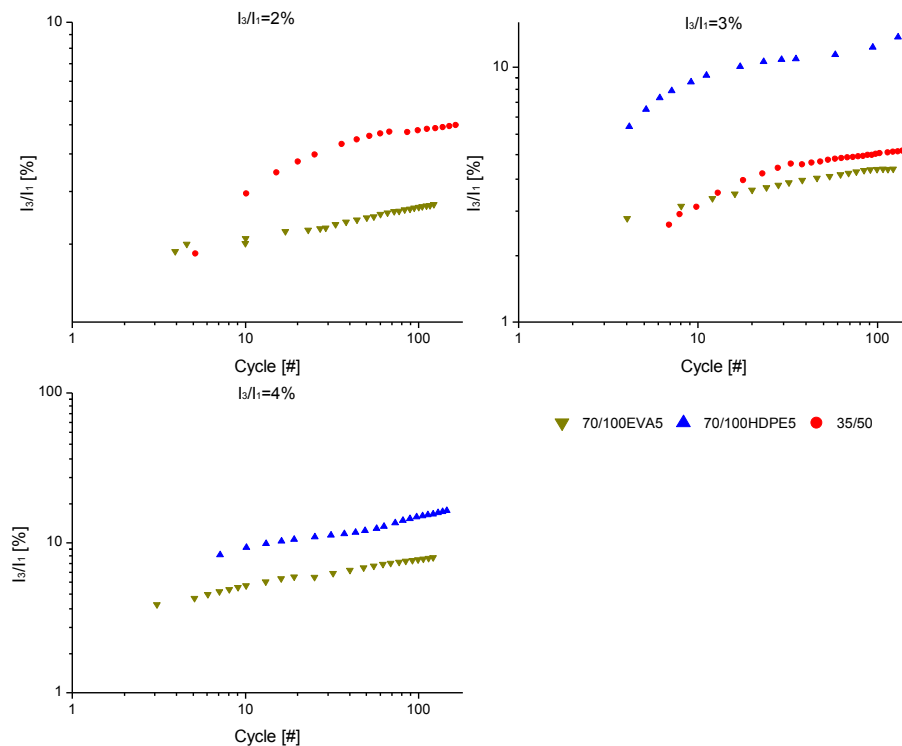


Figure 8-4 I_3/I_1 % signal asaf of cycles number for all binders (log-log representation).

The results are given in Table 8-2. Regarding the number of cycles for fatigue, both methods led to the same trends between the samples. However the second method magnified the differences in cycles between the samples, being therefore more sensitive to small changes between binders.

At $I_3/I_{1,0} \sim 2\%$ sample 35/50 fatigued first while sample 70/100EVA5 needed more than 122 cycles to fatigue. At $I_3/I_{1,0} \sim 3\%$, sample 70/100HDPE5 fatigued first, but this could be because the strain actually gives more $I_3/I_1\%$ than the targeted one, so we cannot compare this result with the other samples. Between the remaining samples, 35/50 binder fatigued first, and being again 70/100EVA5 the last in undergoing fatigue. At $I_3/I_{1,0} \sim 4\%$, no fair conclusion can be drawn because both samples had different values of initial nonlinearity.

Table 8-2 Results summary of time sweep tests

Sample	$I_3/I_{1,0}$ predicted	$I_3/I_{1,0}$ experimental	1.5x $I_3/I_{1,0}$	NC1	NC2
70/100EVA5	2	1.7	2.6	-	-
35/50	2	1.7	2.5	10	58
70/100EVA5	3	2.6	3.8	20	67
70/100HDPE5	3	5.8	8.8	9	11
35/50	3	2.4	3.6	18	32
70/100EVA5	4	3.9	5.8	16	59
70/100HDPE5	4	8.3	12.5	57	302

Respect to each sample, for 70/100EVA5 both methods led to the same conclusion: increasing the strain (or nonlinearity) decreased the number of cycles needed to undergo fatigue. Sample 35/50 also showed that when more strain was applied, NC2 was expectedly smaller as the bitumen fatigues at a faster pace. However, NC1 and thus the method of 50% increase in I_3/I_1 , led to the opposite trend, i.e. as the testing strain is increased, the number of cycles needed to undergo fatigue increased as well. For sample 70/100HDPE5, both NC1 and NC2 showed an increase in number cycles as the strain increased (idem as 35/50 in NC1). However, data for sample 70/100HDPE5 in Table 8-2 do not allow for a comparison of fatigue behavior with the 2 remaining materials as sample 70/100HDPE5 showed results which were not consistent with the predicted and targeted values for initial I_3/I_1 . Thus, probably there was something different with this batch sample. Therefore, no general trend can be concluded respect to an increase in the nonlinearity and the number of cycles to undergo fatigue. Nevertheless, if one excludes the data obtained with sample 70/100HDPE5 and consider only NC2, what was consistent at $I_3/I_{1,0} \sim 2\%$ and 3% was that 70/100EVA5 could resist more cycles than bitumen 35/50 prior to fatigue. However both samples had very different values of De number ($De_{70/100EVA5} = 0.006$ and $De_{35/50} = 0.19$). Therefore to

exclude that this difference in the relaxation state of the materials was not the one triggering the fatigue prediction, then tests at similar D_e conditions should be carried out.

9. Results discussion

In this chapter a discussion of the results presented in the previous chapters will be given.

9.1. Linear viscoelasticity of asphalt binders and morphological characterization

In SAOS measurements differences between the parent 70/100 bitumen and the PMBs were detected. In this regard, the elastic modulus, G' , was more sensitive to the polymer modification, refer to Figure 4-1. This made sense considering that the polymer inclusions were adding interface to the system, which would give an extra elastic component. The lower δ of the PMBs over all the frequency range, refer to Figure 4-2, reflected as well an increase in the elastic nature of the binder. This two differences between 70/100 bitumen and the PMBs were more evident at low frequencies. This can be understood in the frame of emulsion theories (Palierne model) where at low frequencies the effect of the inclusion is evident while at high frequencies the behavior of the matrix and the dispersed phase is reflected [49]. Finally the fact that the ω_c was lower for both PMBs compared to the one of 70/100 binder supported the previous findings: the polymer modification made the binders more solid-like [21, 24]

In regard to the PMBs, at low frequency level-off in δ was detected, Figure 4-2, which is typical of critical materials where a network spanning the entire sample is found [50, 51]. However critical materials do not have a crossover between G' and G'' (infinite relaxation time) [50, 51]. It is evident that any of the PMBs was not a critical material because they both had a crossover, though the constant δ is reminiscent of this behavior.

Binder grades were differentiated at all frequencies, being 35/50 binder stiffer, more elastic and with a higher relaxation time than 70/100 binder. In the case of unmodified bitumen the characteristic relaxation time has been related to its colloidal structure, specifically to the asphaltene aggregates. In the frame of colloidal theories the characteristic relaxation time is related to the particle size of the suspended particles: an increase in particle size increases the relaxation time [52]. However at a constant temperature, not only the size but also the concentration of such particles affects the characteristic relaxation time: an increase in concentration increases the relaxation time [52]. In view that both bitumen grades came from the

same source, the differences in characteristic relaxation time can be more related to an increase in concentration rather than to a difference in particle sizes of asphaltene aggregates [28]. Therefore, the bitumen 35/50 had a higher concentration of asphaltene aggregates than the 70/100 one. To strengthen this finding, and assuming that the concentration range in both binders is low enough as to not modify the shape of the mechanical spectra [52], then both mechanical spectra should overlap by a horizontal shift, ω_{shift} , (change in λ). This is schematically presented in Figure 9-1.

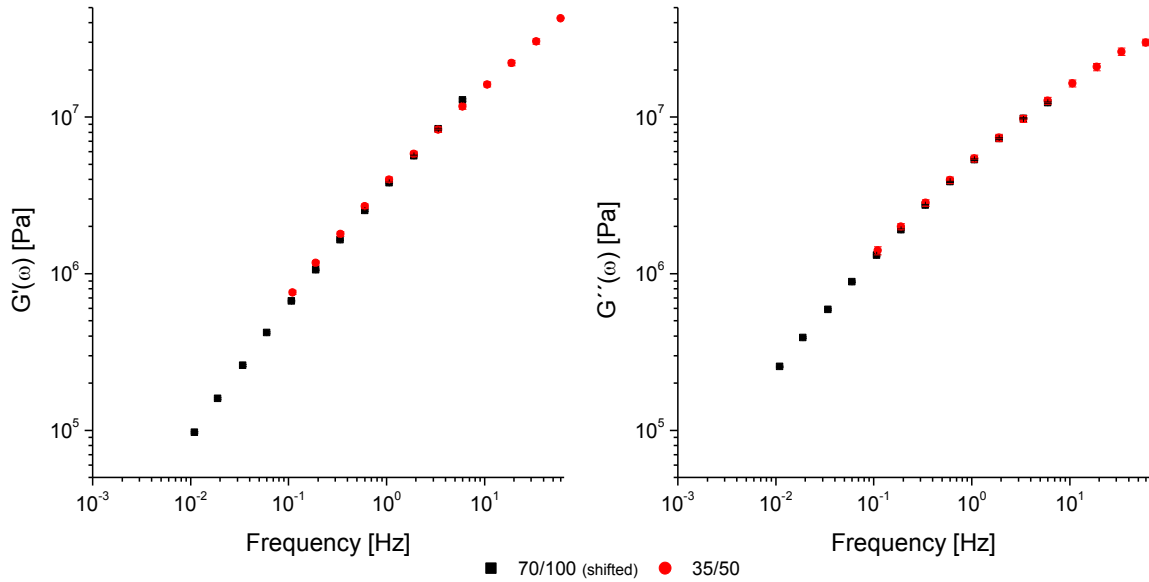


Figure 9-1 Mechanical spectrum of binder grades: data of 70/100 binder were horizontally shifted by 10Hz to overlap the 35/50 data.

The curves fully overlapped in G'' , while for G' there were small deviations at low frequencies. However, the horizontal shift needed was $\omega_{shift} = 10$ Hz and not the $\omega_{shift} = 4.5$ Hz predicted by the ratio of the binders relaxation times. Therefore, according to colloidal suspension theories

$$\lambda(\phi) = \frac{\pi\eta'_{\infty}(\phi)a^3}{k_B T} \quad (9.1-1)$$

where ϕ is the volume fraction, η'_{∞} is the high frequency plateau viscosity (effective medium viscosity), a is the characteristic particle size, k_B is the Boltzmann constant, T is the absolute temperature. It is possible that not only a change in concentration, but also a very small change in particle size may have been present; of the order of $a_{35/50} \sim 1.75 a_{70/100}$.

Modified bitumens had different ω_c : the characteristic relaxation time of 70/100EVA5 was shorter than the one of 70/100HDPE5 (refer to Table 4-1). In the case of the PMBs, λ can be either related to the new interface created (from the emulsions perspective), but also to the increase in concentration, due to the physical distillation process, of the asphaltenes in the asphaltene rich phase (from the colloidal perspective). If the characteristic relaxation time in PMBs would be more related to a change in asphaltene concentration, the characteristic relaxation time of 70/100EVA5 should be shorter than the one of 70/100HDPE5; which is not the case. This supports the idea that for PMBs the characteristic relaxation time (or ω_c) was related to the polymer inclusion. In this regard, the FOM micrographs confirmed that in the PMBs the physical distillation phenomena was present. Furthermore the droplet sizes detected spanned 10-100 microns for both EVA and HDPE modified bitumens, and therefore colloidal concepts cannot be applied. However, it is well documented [53] that for emulsions the relaxation time scales with

$$\lambda_{droplet} \approx a\eta_m/\Gamma \quad (9.1-2)$$

where a is the characteristic droplet size, η_m is the viscosity of the media, and Γ is the interfacial tension between the phases. It has also been reported that EVA copolymer is more compatible with bitumen than HDPE [21, 22], which would lead to lower interfacial tensions and lower particle sizes: decrease in relaxation time. However, this higher compatibility of EVA copolymer greatly enhances the physical distillation phenomena [21], which will consequently increase the medium viscosity: increase in relaxation time. Therefore, the differences detected in relaxation time between the PMBs, Table 4-1, cannot be correlated one to one with morphology data obtained from FOM. Consequently to be able to determine which parameter (a, η_m, Γ) was triggering the differences in λ between the PMBs, extra measurements of η_m, Γ would be needed.

In stress relaxation measurements, some of the conclusions obtained from SAOS tests were strengthened. Considering that $G(t)$ is a measurement of the stiffness of the material as a function of time [8], the modification made the bitumen more rigid, effect that was evident at long times ($t > 1s$). This was congruent with the moduli trends found in SAOS. The $G(t)$ profiles of bitumens and PMBs were different from a qualitative point of view. Bitumens showed the classical response of a VE liquid, on which a $G(t) \rightarrow 0$ at long times. On the other hand PMBs seemed to have the response of a viscoelastic solid, on which $G(t)$ has a finite value at long times, due to the tendency

of $G(t)$ to level-off. However with the data acquired, refer to Figure 4-3, a definite conclusion could not be done. Nonetheless, it is evident that the polymer modification slowed down the relaxation process, which is congruent with the lower relaxation times identified in SAOS.

Nonetheless, it was not expected to see quantitatively the same behavior between $G(t)$ and $G'(1/t)$, because this relationship is valid when $G(t)$ is changing very slowly with time, i.e. in the plateau moduli (G_0 and G_e) [8]. Besides, to make a quantitative comparison between the two moduli it would be needed to Fourier transform the $G(t)$ signal, or made an inverse Fourier transformation of the frequency signal, which is an ill-posed problem [8].

9.2. LAOS characterization of asphalt binders

In order to have some insight of which microstructural aspects of the binders could be studied by means of LAOS-FTR methods, the LAOS fingerprint of the asphalt binders was compared with the one reported of specific material classes: polymer melts, polymer solutions (linear, branched, polysaccharides), suspensions close to the glassy transition, emulsions of Newtonian in Newtonian fluid, rubber with fillers, etc. The binders FTR response could not be correlated one-to-one with any of the above mentioned material classes. However it had some similitudes with some of them. In the following those similitudes will be explained, making a difference on what is general for all binders, unmodified bitumens, and PMBs.

The first and more relevant characteristic of the FTR behavior of asphalt binders was the existence of significant high order harmonics. In the frame of FTR, high order harmonics are characteristic of dispersion systems (suspension or emulsions [1]), i.e. systems where several phases coexist. This, for instance, was in agreement with the colloidal model of bitumen, in which asphaltenes aggregates are dispersed in a maltenes matrix. In the case of PMBs they inherited this colloidal structure and on top a polymer dispersion was formed due to the partial miscibility of the EVA and HDPE in bitumen.

In terms of suspensions all the FTR information found in the literature was for highly filled suspensions close the glassy transition [12], which in fact is not the case for bituminous binders at room temperature for two reasons. First because all bitumens studied were far above their glass transition temperatures (of the order of -20°C). Second, because in binders the glassy transition is

given by the maltenes matrix, refer to Table 2-2, and not by dynamic arrest of the asphaltene aggregates. However, in [12] it was predicted and confirmed that colloidal suspensions close to glassy transition have a I_n/I_1 power law trend as a function of γ at low strains which has a slope lower than two, this reported up to the 9th harmonic. This fact is interesting since all binders, irrespective of modified or unmodified, had this characteristic. It is important to mention that any of the other key characteristics of the FTR behavior of the highly filled suspensions are the same, starting by the fact that G' and G'' had a crossover, because G'' had an overshoot as strain is increased (type III in Figure 2-2). Therefore in order to compare under more similar conditions both FTR spectra, bitumen LAOS-FTR tests should be run at lower temperatures in a regime where the linear conditions from which the binders would depart were similar to the ones of highly filled suspensions, i.e. in the glassy plateau where $G' > G''$.

Regarding emulsion systems it was expected that only PMBs would hold some similarity with such systems. Similar to PMBs, in concentrated emulsions without phase inversion only I_3/I_1 , I_5/I_1 , and I_7/I_1 were detected in a clear power law trend [17, 16]. For these systems it was reported that the ratios I_5/I_3 and I_7/I_5 were correlated with droplet size and droplet size distribution, and also with Ca and p . However, to detect if such correlation was valid for our system in order to predict morphological data, it would be needed to have a series of emulsions of the same PMB (to control as much as possible η_d , η_m , and Γ), but with different morphology to see if such quantifiers were sensitive to droplet size changes in PMBs. The power law predicted for emulsion systems at very low strains [17], see (2.1.5.1), did not hold for PMBs. However experimentally it was found that after this power law the I_n/I_1 tended to level off till reaching a plateau value. Therefore it could be possible that since our analysis was restricted to a very narrow interval of strain we were only able to detect the zone at which the power law has already leveled off. Besides, the noise of the suspension matrix is present in bitumen and PMBs, that is: the aggregates of asphaltene dispersed in the bitumen matrix also generate harmonics. Furthermore, in agreement with emulsion theories [17, 16, 11], when comparing the PMBs with the parent 70/100 binder at the same frequency it was observed that the modification increased the nonlinearity: the interface formed is viscoelastic and therefore an additional source of nonlinearity is brought by the modification [11].

In terms of polymeric systems, the previously described, in section 2.1.5, FTR response of entangled solutions of linear polystyrene (PS) in iso-dioctyl phthalate held several similitudes with

bituminous binders. For instance, for $\delta > 45^\circ$ the I_3/I_1 signal decreased respect to δ and had a clear power law trend asaf of the strain with exponent lower than two, which is in agreement with the results for bituminous binders, see Figure 6-11 and Figure 6-24. Regarding De , it was reported in [13] that for $De < 1$ an increase in De increased the I_3/I_1 signal which is in agreement with the trend found for bituminous binders, as shown in Figure 9-2.

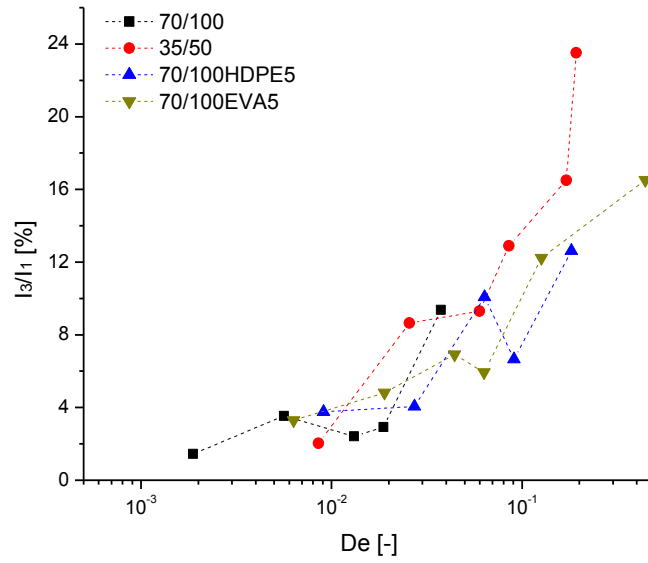


Figure 9-2 I_3/I_1 signal for all binders asaf of De at an arbitrary 20.3% strain

Another characteristic of bituminous binders that was also reported for the entangled solutions of linear polystyrene (PS) was the relationship between $\phi_3 - 3\phi_1$ and $\phi_5 - 5\phi_1$. This relationship was reported to be $\phi_3 - 3\phi_1 < \phi_5 - 5\phi_1$ irrespective the sample type (entanglement density) or delta value. In the case of bitumen a $\phi_3 - 3\phi_1 > \phi_5 - 5\phi_1$ was found for all the samples either at same De or same δ conditions. Therefore, in order to elucidate whether there was a real relationship between the ϕ_n angles and to eliminate any possible arithmetical dependence due to ϕ_1 , a subtraction between relative phase angles was done, by considering $\Phi_3 = \phi_3 - 3\phi_1$ and $\Phi_5 = \phi_5 - 5\phi_1$

$$\frac{5}{3}\Phi_3 - \Phi_5 = \frac{5}{3}\phi_3 - 5\phi_1 - (\phi_5 - 5\phi_1) = \frac{5}{3}\phi_3 - (\phi_5) \quad (9.2-1)$$

Therefore inside the plateaus region, and for the conditions at which Φ_3 and Φ_5 pairs were available, above difference was computed and is given in Table 9-1

Table 9-1 Computed $\frac{5}{3}\Phi_3 - \Phi_5$ to support the existence of a relationship between relative phase angles of binders

Sample	ω [Hz]	δ [°]	De [-]	$\frac{5}{3}\Phi_3 - \Phi_5$ [°]
35/50	0.3	57.7	0.04	269 ± 5
35/50	2.25	52.1	0.19	288 ± 8
35/50	0.7	56.1	0.06	298 ± 6
70/100	2	57.1	0.03	289 ± 7
70/100HDPE5	1	48.7	0.09	280 ± 5
70/100EVA5	1	48.0	0.06	253 ± 11

The values of $\frac{5}{3}\Phi_3 - \Phi_5$ for all the samples vary around $278^\circ \pm 18^\circ$, which is remarkable considering that the error associated to the measurement of ϕ_1 is extrapolated in both Φ_3 and Φ_5 . Only sample 35/50 at 0.3Hz and 70/100EVA5 at 1Hz were significantly different from the rest, and probably a replicate run should be needed to confirm the existence of such difference. However, in view of the data in Table 9-1, it might be possible that there is a correlation between ϕ_3 and ϕ_5 , if so the difference $\frac{5}{3}\Phi_3 - \Phi_5$ may be characteristic of asphalt binders.

Another class of polymer systems that shown some similarity in the FTR spectra with asphalt binders were rubbers loaded with solid particles, described in section 2.1.5. The spectra of such dispersed systems had a bump in the I_3/I_1 signal associated to the presence of the dispersed phase, shown in Figure 2-14. In the case of asphalt samples this bump was present in all samples but only for some testing frequencies, given in Table 9-2 and shown on Figure 9-3.

Table 9-2 Frequencies at which binders shown a bump in the $I_3/I_1\%$ signal

Sample	Bump ω [Hz]	Bump δ [°]	Bump De [-]
70/100	1	61.8°	0.02
35/50	0.7, 2	56.1°, 52.5°	0.06, 0.17
70/100HDPE5	0.1, 0.7, 1	54.2°, 49.9°, 48.6°	0.009, 0.06, 0.09
70/100EVA5	0.1, 0.7	48.2°, 48.7°	0.006, 0.04

The presence of this bump was related to the high interaction between the dispersed phase and the viscoelastic matrix [10]. In the case of asphalt binders strong interactions could be expected between the asphaltene aggregates and the maltenes matrix, which would be the result of Van der

Waals forces and adhesion at the interface. The fact that this bump showed up in not all the frequencies tested can be related to the forces that generate it, which study goes beyond the scope of the thesis.

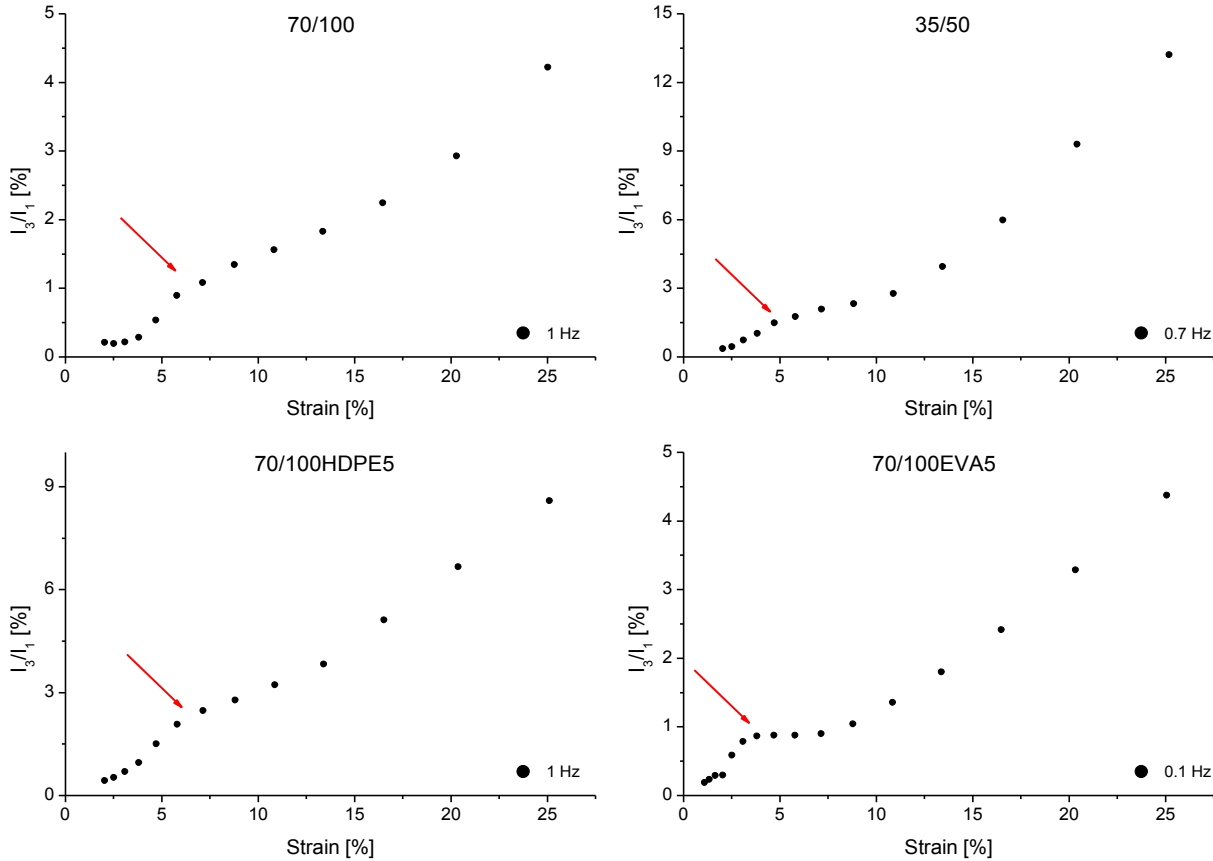


Figure 9-3 Binders I_3/I_1 % response at specific frequencies that shown a bump in the nonlinear signal.

A common characteristic of all the binders was a power law trend of I_3/I_1 as a function of the strain with an exponent value lower than two. In fact it has been reported and derived from theoretical arguments that several materials (polymers [3, 5, 6, 1] and emulsions [16, 17]) displayed such power exponent only in the so called MAOS region. However, deviations from this trend do exist and have been reported [9]. In simple words this is equivalent to detect or not a Newtonian plateau in a flow curve, some materials will have it and some others not, and some others will only have it at specific experimental conditions (temperature, shear rate, etc). Therefore, the fact that in binders this quadratic response was not held is nothing uncommon.

Another quantifier for nonlinear behavior that can be related to the asphalt binders microstructure is the $\phi_3-3\phi_1$ value. In this case almost all the $\phi_3-3\phi_1$ values reflected a strain softening behavior,

given in Table 6-4, which was in agreement with the G' and G'' trend, shown in Figure 6-21. The strain softening behavior reflected that the interactions that gave the initial rheological response were being weakened by means of the strain applied. Furthermore, since all the phase angles varied in a narrow angular interval this was a signal that the polymer modification did not change so much the inner structure of the bituminous binder. This was further confirmed by FOM results given in section 4.3, where no phase inversion was observed, meaning that even if PMBs are a blend, the continuous matrix was still a bitumen-like one.

The fact that the bituminous systems did not fit fully in a specific class of material was not surprising given the complex composition of asphalt binders. Since in unmodified bitumen the nonlinear response could arise from both the glassy matrix as well as from the asphaltene aggregates. In the latter, modification of aggregates would result in a nonlinear signal which is easier to achieve at RT because the Brownian motion (restoring force) is lower at RT than at high temperatures. The glassy matrix is also viscoelastic and therefore prone to give a nonlinear signal, because a viscoelastic system has memory effects of the initial state which could be modified and yield a nonlinear behavior. In a PMB the sources of nonlinearity increased due to the polymeric inclusion and the interface between polymer and bituminous binder. In the former, polymeric systems are source of nonlinearity since they are viscoelastic. Viscoelasticity gives nonlinearity, because by definition a solid is a structured system i.e. has a basal microstructure. Then a viscoelastic system will also have a basic microstructure as well as memory effects, therefore the microstructure can be modified. Considering that at room temperature PMBs can be seen as a complex emulsion, the interface created is an additional source of viscoelasticity and therefore of nonlinearity. In this case the effect of the inclusion will correspond to long time relaxation processes and therefore more feasible to be studied at low frequencies.

9.3. Stress relaxation test of asphalt binders in NLVE region

The objective of the stress relaxation characterization in the nonlinear regime was twofold, first to have a baseline of nonlinear characterization that could be compared with the reported data in bitumen literature, second to compare the nonlinear characterization of asphalt binders in stress relaxation against the LAOS-FTR one.

The nonlinearity in stress relaxation was characterized by means of the damping function, which was valid at short times ($\sim 10^1$ s) for bitumen and PMB samples at room temperature. This contrasted the reported nonlinear stress relaxation characterization of asphalt binders [22, 30, 36], where the damping function was reported to be valid only for unmodified and EVA modified bitumen. Furthermore, in the present work it was found that in the validity region of the damping function the stress relaxation of all the binders showed a power law decay. This finding clearly contradicts the reported trends of $G(t, \gamma)$ for the 3 binder types (unmodified, EVA, and HDPE bitumen), shown in Figure 2-28. Though bitumens used in the present work were of different origin from the ones used by Polacco G. *et al.* [22, 30, 36], the root of the unexpected differences may be in the experimental protocol proposed in this work, i.e. the usage of the rectangular torsion bar to study asphalt binders at room temperature (semisolid materials).

The computed damping function tends to decrease as a function of strain, shown in Figure 7-2, which evidenced the softening response of bituminous binders already found in LAOS tests. By means of this damping function it was found that between PMBs, 70/100HDPE5 was more nonlinear than 70/100EVA5. Meanwhile between binder grades 35/50 was more nonlinear than 70/100. This is in agreement with LAOS-FTR findings (refer to Figure 6-15).

In particular for the stress relaxation tests at long times, it was found that for all samples at low strains $G(t)$ and $G(t, \gamma)$ tended to level off, while at high strains $G(t, \gamma)$ either decreased in a power law fashion or had an abrupt decrease (see in Figure 7-3). The presence of a plateau at long times is characteristic of viscoelastic solids, i.e. of materials that have a network (or solid structure) that inhibits the complete relaxation of the material, see Figure B-5 in Appendix B. On the other hand, a stronger decrease of $G(t, \gamma)$ with time is typical of viscoelastic liquids, i.e. materials that totally relax at long times. Conversely, the power law tendency has been related to critical systems: viscoelastic systems that follow a power law trend in $G(t)$, G' and G'' and that do not have a characteristic relaxation time [54]. In view, that all the studied systems had a characteristic relaxation time, the behavior can be discarded, and longer time measurements would be needed to fully assess the $G(t)$ trend that shown a power law decay. Nevertheless, in perspective the samples changed from a solid-like to a liquid-like behavior. However, since neither a clear plateau nor a pronounced relaxation was found in each of the samples, additional experimental efforts are needed to close this issue.

Even though both nonlinear characterization techniques used in this work (LAOS-FTR and stress relaxation) drew the same general conclusions, they have differences between each other in several aspects. Therefore, in Table 9-3 a comparison between the techniques, for its usage in asphalt binders, is given.

Table 9-3 Comparison between LAOS/FTR and stress relaxation tests for nonlinear characterization

Aspect	LAOS test with FTR	Stress relaxation test
Rheometer	Strain controlled + ADC + external software *	Strain controlled
Experiment	<p>Implementation is more elaborated *</p> <ul style="list-style-type: none"> – Both external and rheometer software have to be synchronized for data acquisition. – Specific details for data acquisition: noise reduction, aliasing, etc. <p>Shorter experimental times and one bar per binder</p> <ul style="list-style-type: none"> – From 3.5 min at $\omega \sim 2$ Hz to 1h at $\omega \sim 0.1$ Hz for 20 experimental points. – One bar needed for comparisons at same δ, De, and ω – Only in a multifrequency study more bars needed. <p>Easy setting of experimental conditions</p> <ul style="list-style-type: none"> – By running SAOS and strain sweep conditions for frequency and strain ranges can be established. 	<p>Implementation is easy</p> <ul style="list-style-type: none"> – All is programmed in the rheometer software. <p>Longer experimental times and at least 6 bars per binder</p> <ul style="list-style-type: none"> – At least 2h (6 bars and 15 min per run) for 6 experimental points in damping function. <p>Difficult setting of experimental conditions</p> <ul style="list-style-type: none"> – Either trial and error or based on dynamic studies (SAOS and strain sweep).
Data analysis	<p>“Complicated” and time consuming *</p> <ul style="list-style-type: none"> – Special software needed (LabView, matlab, mathematica) – FT is done point by point of both stress and strain signal. – At least basic knowledge of FT techniques is needed to interpret spectra 	<p>Relatively easy</p> <ul style="list-style-type: none"> – Done in standard software (excel, origin) – Pre-analysis needed to isolate only valid data – Only basic math and statistics are needed
Results interpretation	<p>Very complete</p> <ul style="list-style-type: none"> – Softening or hardening behavior and balance between them ($\phi_3 - 3\phi_1$) 	<p>Very basic</p> <ul style="list-style-type: none"> – Softening or hardening behavior

	<ul style="list-style-type: none"> – Critical strain and strain sensitivity info of 3rd, 5th, 7th, and total harmonicity – Possible to run comparisons at different conditions either in the viscous or in elastic regime: δ, De, ω. 	<ul style="list-style-type: none"> – Critical strain and strain sensitivity info
Microstructural information	Information available for polymers, emulsions, and suspensions.	Information available only for polymers, as per the author knowledge.

* Many of the experimental “drawbacks” of LAOS-FTR technique can be regarded to the fact that it is a new experimental technique when compared to the stress relaxation one. Therefore, user friendly interfaces are under development, an example of such new generation rheometers is the ARES-G2 Rheometer of TA Instruments.

10. Conclusions

In this closing chapter the conclusions of the present work will be given as well as the possibilities for further work based on this research.

LAOS tests at room temperature ($T \sim 20^\circ\text{C}$) were carried out in asphalt binders and the results were analyzed by the first time using Fourier transform rheology (FTR). However, to obtain a meaningful characterization of asphalt binders in LAOS-FTR, an experimental method was also established. This experimental protocol encompassed:

- to control variations in PMB manufacture, in ATB production, and in sample loading by setting specific conditions for all of them,
- to avoid having interference of binders aging by controlling the storage period of ATB in the freezer to max 4 days prior testing,
- to eliminate experimental pitfalls due to geometry by using a torsion bar geometry and by setting the ATB height to 2.5 cm for all the tests.

The control of these variables and the usage of a torsion bar geometry made possible to characterize the binders' behavior at room temperature in both the linear and the nonlinear regime. As a result, repeatable FTR data were obtained (see table Table 8-2), and the FTR signature of binders in the MAOS regime at room temperature was determined.

The principal characteristics that all binders shared in LAOS-FTR tests were:

- a softening behavior in shear given by both the 1st harmonic trend (both storage and loss moduli decaying with increasing strain) and the value of 3rd relative phase angle ($\phi_3-3\phi_1$ closer to 180°C),
- a reversible nonlinearity given by only significant odd harmonics
- a high harmonicity degree (I_n/I_1 with $n>3$),
- a power law trend asaf of strain in all the harmonic signals and exponent lower than 2 that was a function of the binder type and the frequency used,
- a similar softening to hardening balance given by the $\phi_3-3\phi_1$ signal ($230^\circ < \phi_3-3\phi_1 < 270^\circ$),
- a $\phi_3-3\phi_1 > \phi_5-5\phi_1$ for all the conditions tested,
- an increasing nonlinearity asaf of ω for $De < 1$ and $\delta > 45^\circ$.

Specifically for the modified bitumens, the two studied PMBs showed different nonlinear response. Consistently in all the conditions tested (same De , same δ , and same ω), 70/100EVA5 had a lower level on nonlinearity; meaning that its microstructure was less deformed or affected by strain than the one of 70/100HDPE5. Furthermore, none of the PMBs behaved in the NLVE regime as the benchmark 35/50 binder. However the 70/100HDPE5 binder was more alike.

Regarding binder grades their FTR spectra were similar, however the 35/50 binder had a higher nonlinear degree.

Furthermore, due to the flexibility of conditions that can be attained in a dynamic test, several comparisons of FTR test were performed, and from each of it specific conclusions were drawn.

Same delta condition

At $\delta \sim 57^\circ$, 35/50 binder could withstand more strain than 70/100 sample (75% more γ as per total harmonicity). However, the former was slightly more sensitive to strain than 70/100 in the MAOS region (as per the 5th, 7th, and total harmonicity exponent values).

At $\delta \sim 50^\circ$ done for PMBs and 35/50 binder, consistently sample 70/100EVA5 had the lowest non-linearity based on its highest critical strain values (at least twice higher vs the critical strains of the other binders), and considering that its harmonicity degree was restricted to only the 3rd harmonic. On the other hand, 35/50 binder had consistently the higher values of nonlinearity \therefore at a mechanical equivalence 35/50 deformed more.

Same De condition

At $De=0.06$, between the PMBs, 70/100EVA5 nonlinearity was more affected by changes in strain (as per the exponent value of I_3/I_1 & I_7/I_1 signals) than 70/100HDPE5, but 70/100EVA5 was able to sustain more strain prior to deformation than 70/100HDPE5 (as per the critical strain values). Because of this, the 70/100HDPE5 binder had consistently the higher nonlinearity with respect to 70/100EVA5 in all the signals analyzed, which indicated a higher shear induced microstructural deformation by LAOS.

Frequency dependence of LAOS-FTR response

In this mode it was more difficult to draw general conclusions since not all samples followed the same trends respect to frequency, shown in Figure 6-11 and Figure 6-15, i.e. the nonlinear ranking depended on the frequency at which the samples were tested (viscoelastic nature).

However, in the total harmonicity response there was a frequency at which a steep increase in the signal was detected for all the samples. This allowed a clear differentiation in the FTR-LAOS pattern between modified and unmodified binders. The steep increase was close to 0.3 Hz for 70/100 and 35/50, and it was close to 0.7 Hz for 70/100HDPE5 and 70/100EVA5.

The modification increased the nonlinear nature of the binder (as per the higher PMBs I_3/I_1 and odd sum values) as well as its strain softening nature upon shear (as per the $\phi_3-3\phi_1$ values), the former was evident at all frequencies, shown in Figure 6-12, and the latter was more evident at high frequencies, shown in Figure 6-22. Among PMBs, sample 70/100HDPE5 had the higher nonlinearity (as per the higher I_n/I_1) and less softening nature (as per $\phi_3-3\phi_1$ farther from 180°), which was more obvious at low frequencies $\omega < 1$ Hz. Regarding the binder grades, 35/50 binder had higher nonlinearities and less softening nature, both of them more evident at high frequencies.

The FTR spectra of the binders held similitudes with reported FTR data of other material classes. These findings can give some insights about the kind of microstructural aspects that could be further studied by means of FTR. The principal findings were:

- as in dispersion systems (suspensions and emulsions [1]) all binders had a high number of significant harmonics (high harmonicity degree);
- similar to suspensions [12] all binders had a power law trend with exponent lower than two
- similar to concentrated emulsions [17] without phase inversion the significant harmonics were the 3rd, 5th, and 7th one for PMBs;
- similar to PS solutions in entanglement regime [13, 19] the nonlinear response and the hardening/softening balance increased asaf of ω for $\delta > 45^\circ$ and $De < 1$;

- similar to systems where high interactions existed between the dispersed phase and the matrix [10, 20], a bump in between the power law region was detected at selected frequencies for all binders.

Furthermore, as an alternative to the current protocol to predict fatigue performance by binders testing, LAOS tests in time sweep mode were carried out, and FTR was used to analyze the data. In this regard, FTR shown to be sensitive enough to detect microstructural changes (softening) in a short time frame (15 min). However the detected changes were reversible (i.e. associated to odd harmonics) and not strictly related to fatigue. In the short experimental time proposed ($t < 15$ min), significant changes were detected in the FTR quantifiers (I_3/I_1 and $\phi_3 - 3\phi_1$) while the current criteria of $1/2G_{initial}^*$ was far from happening. Therefore, the proposed methodology has the advantages of being more sensitive and less time consuming. A further study would be needed in order to set the right conditions for its usage, as the outputs of this proposed methodology need to be properly compared with the ones of the current fatigue protocol.

In terms of the stress relaxation characterization in the nonlinear regime, the results reported in this work contradicted the previous findings of Polacco *et al.* [22, 30, 34], because in this work the time-strain separability was valid for all binders (modified and unmodified), and all of them had the same power law decay in the relaxation modulus (type c in Figure 2-28 from Polacco *et al.*), and it was possible to test all the binders at the same temperature ($T \sim 20^\circ\text{C}$). Though bitumens used in the present work were of different origin from the ones used by Polacco *et al.*, the root of the unexpected differences may be in the experimental protocol proposed in this work, i.e. the usage of the rectangular torsion bar to study asphalt binders at room temperature (semisolid materials). The set of the proper experimental protocol, to study binders' rheology at room temperature, allowed to obtain meaningful data of nonlinear stress relaxation modulus. The results of such tests supported the general findings of LAOS test (strain softening behavior of binders, 70/100EVA5 binder less nonlinear than 70/100HDPE5, 70/100 bitumen less nonlinear than 35/50).

However, the stress relaxation test lacked quantitative parameters to make a deeper analysis of the nonlinear behavior of binders. Therefore, the higher number of quantitative outputs (I_n/I_1 , total harmonic, and $\phi_3 - 3\phi_1$), the flexibility of the experimental conditions to be attained (variation of strain and frequency), as well as the high signal sensitivity identified LAOS-FTR technique as a better characterization method for nonlinear rheology of asphalt binders when compared with

stress relaxation tests; setting aside the more elaborated experimental setup needed to perform LAOS-FTR.

The linear rheology of the binders was studied by means of SAOS and stress relaxation. In the present work, it was possible to detect differences between the PMBs in SAOS at low frequencies, in contrast with reported literature [22, 24]. The only difference with reported literature is that in this work the analysis was done not only with respect to G' and G'' , but also in terms of δ . In this regard 70/100HDPE5 was stiffer (higher G' and G'') and 70/100EVA5 was more elastic (lower δ), and both of them were stiffer and more elastic than the parent 70/100 binder. None of the PMBs had the same mechanical spectra as the benchmark 35/50 binder, but 70/100HDPE5 binder was more alike. Nonetheless 70/100EVA5 had a more viscoelastic balanced design since its δ value was more constant over the whole range of frequencies tested ($\Delta\delta_{70/100} \sim 25.3^\circ$, $\Delta\delta_{70/100HDPE5} \sim 20.8^\circ$, $\Delta\delta_{70/100EVA5} \sim 13.1^\circ$ from 0.1 Hz to 60 Hz). Similar to the nonlinear rheology, the stress relaxation test supported the SAOS findings.

In both the linear and nonlinear rheology there were hints of a solid-like behavior at long times. In the linear regime by constant values of δ at low frequencies (for PMBs), and in the nonlinear regime by a plateau in the stress relaxation at long times that disappeared at higher strains (for all binders). However, this apparent solid-like behavior can only be the consequence of very long relaxation processes, not infinite like in a solid, but long enough as to be detected as “solid” in an experimental time frame; for instance the well-known pitch drop experiment. In this regard, long time relaxation processes are better studied in creep experiments.

The FOM study confirmed the presence of the physical distillation phenomena in PMBs (contrast of PRP in fluorescent light). Furthermore, the FOM study strengthened the previous findings that EVA copolymer was more compatible with bitumen than HDPE (70/100EVA5 binder had broader droplet size distribution and higher covered area). Furthermore the droplet sizes detected spanned 10-100 microns for both EVA and HDPE modified bitumens: the PRP droplets did not exhibit a colloidal behavior. However, it was not possible to correlate one to one the morphology data from FOM with the differences in characteristic relaxation time found in SAOS, because in the frame of emulsion concepts the other variables (interfacial tension and matrix viscosity) that also influence the characteristic relaxation time were different between the PMBs. Additionally, in both PMBs phase separation (creaming) was detected. Therefore, in order to correlate the characteristic

relaxation time found in SAOS with the system morphology observed FOM, first it would be needed to modify the samples preparation to avoid the interference of phase separation, and second extra measurements of interfacial tension and matrix viscosity would be needed. In the case of 70/100EVA5 a trend to phase inversion and co-continuous morphology (one out of twenty micrographs) were detected; the co-continuous morphology could be related to the small δ plateau found at low frequencies and the power law trend in $G(t)$ [55, 54]. However, the fact that no phase inversion was observed supported the idea of having very similar $\phi_3-3\phi_1$ values among the binders, meaning that though PMBs are a blend the continuous matrix was still a bitumen-like one.

In summary, all the initially stated goals were accomplished and as expected LAOS-FTR demonstrated to be a very sensitive and flexible technique for the study and characterization of asphalt binders submitted to large deformation at service temperature.

Finally, during the development of this work several findings needed a deeper study in order to be fully addressed:

- Assess whether the quantifiers I_3/I_1 , I_5/I_1 , and I_7/I_1 are sensitive to PMBs morphology (droplet size and size distribution), which was the case for emulsion systems [17].
- Determination of the existence of long time relaxation processes slightly indicated in both linear (delta plateau at low frequencies for PMBs) and nonlinear rheology (apparent yielding from linear to nonlinear stress relaxation modulus trend at long times in all the samples) by means of creep experiment.
- Explore the correlation found between δ and the nonlinear response of PMBs, which was observed inside the plateau in delta at low frequencies: inside the plateau region very few changes in the nonlinear response were detected in the parameters, b , and $\phi_3-3\phi_1$.
- Establish a LAOS-FTR protocol to predict fatigue behavior of asphalt binders. This involves the exploration of other experimental conditions, the comparison with outputs of fatigue tests, fine tune to the experimental protocol including results analysis, etc. This to determine whether differences in De , ω , or ω are triggering the fatigue behavior, and to explore the possibility to correlate I_2/I_1 signal with fatigue.

11. References

- [1] Hyun K. and et. al., "A review of nonlinear oscillatory shear tests: Analysis and application of large amplitude oscillatory shear (LAOS)," *Progress in Polymer Science*, vol. 36, p. 1697–1753, 2011.
- [2] Hyun K., Nam J. G., Wilhelm M., Kyu H. A. and Lee S. J., "Nonlinear response of complex fluids under LAOS flow," *Korea-Australia Rheology Journal*, vol. 15, no. 2, pp. 97-105, 2003.
- [3] Wilhelm M., Maring D. and Spiess H-W., "Fourier-transform rheology," *Rheologica Acta*, vol. 37, p. 399–405, 1998.
- [4] Ramírez R., *The FFT: fundamentals and concepts*, Tektronix, Inc., 1975.
- [5] Wilhelm M., Reinheimer P. and Ortseifer M., "High sensitivity Fourier-transform rheology," *Rheologica Acta*, vol. 38, pp. 349-356, 1999.
- [6] Wilhelm M., "Fourier-Transform Rheology," *Macromolecular materials and engineering*, vol. 287, pp. 83-105, 2002.
- [7] Barnes H.A., Hutton J.F. and Walters K., *An introduction to rheology*, 1st ed., Elsevier, 1989.
- [8] Ferry J. D., *Viscoelastic properties of polymers*, 3rd ed., John Wiley & Sons, 1980.
- [9] Leblanc J. L., "Modeling the strain dependence of torque harmonics as measured through large-amplitude oscillatory shear rheometry," *Journal of Applied Polymer Science*, vol. 126, p. 663–677, 2012.
- [10] Leblanc J. L., "Large amplitude oscillatory shear experiments to investigate the nonlinear viscoelastic properties of highly loaded carbon black rubber compounds without curatives," *Journal of Applied Polymer Science*, vol. 109, p. 1271–1293, 2008.

- [11] Carotenuto C., Grosso M. and Maffettone P. L., "Fourier transform rheology of dilute immiscible polymer blends: a novel procedure to probe blend morphology," *Macromolecules*, vol. 41, pp. 4492-4500, 2008.
- [12] Brader J. M., Siebenburger M., Ballauff M., Reinheimer K., Wilhelm M., Frey S. J., Weysser F. and Fuchss M., "Nonlinear response of dense colloidal suspensions under oscillatory shear: mode-coupling theory and Fourier transform rheology experiments," *Physical review E*, vol. 82, p. 61401, 2010.
- [13] Neidhöfer T., Sioula S., Hadjichristidis N. and Wilhelm M., "Distinguishing linear from star-branched polystyrene solutions with fourier-transform rheology," *Macromolecular Rapid Communications*, vol. 25, p. 1921–1926, 2004.
- [14] Kallus S., Willenbacher N., Kirsch S., Distler D., Neidhöfer T., Wilhelm M. and Spiess H. W., "Characterization of polymer dispersions by Fourier transform rheology," *Rheologica Acta*, vol. 40, pp. 552-559, 2001.
- [15] Carrier V. and Petekidis G., "Nonlinear rheology of colloidal glasses of soft thermosensitive microgel particles," *Journal of Rheology*, vol. 53, no. 2, pp. 45-273, 2009.
- [16] Reinheimer K., Grosso M. and Wilhelm M., "Fourier Transform Rheology as a universal non-linear mechanical characterization of droplet size and interfacial tension of dilute monodisperse emulsions," *Journal of Colloid and Interface Science*, vol. 360, pp. 818-825, 2011.
- [17] Reinheimer K., Grosso M., Hetzel F., Kübel J. and Wilhelm M., "Fourier Transform Rheology as an innovative morphological characterization technique for the emulsion volume average radius and its distribution," *Journal of Colloid and Interface Science*, vol. 380, p. 201–212, 2012.
- [18] Hyun K. and Wilhelm M., "Establishing a New Mechanical Nonlinear Coefficient Q from FT-Rheology," *Macromolecules*, vol. 42, pp. 411-422, 2009.

- [19] Wilhelm M. and Neidhöfer T., "Fourier-transform rheology experiments and finite-element simulations on linear polystyrene solutions," *Journal of Rheology*, vol. 47, no. 6, pp. 1351-1371, 2003.
- [20] Jha V., "Carbon black filler reinforcement of elastomers (thesis)," October 2008. [Online]. Available: <https://www.sems.qmul.ac.uk/research/honours/doc.php?id=335>. [Accessed May 2015].
- [21] Lesueur D., "The colloidal structure of bitumen: Consequences on the rheology and on the mechanisms of bitumen modification," *Advances in Colloid and Interface Science*, vol. 145, p. 42–82, 2009.
- [22] Polacco G., Stastna J., Biondi D. and Zanzotto L., "Relation between polymer architecture and nonlinear viscoelastic behavior of modified asphalts," *Current Opinion in Colloid & Interface Science*, vol. 11, p. 230–245, 2006.
- [23] Haimei Z., *Building Materials in Civil Engineering*, 1st ed., Woodhead Publishing Limited and Science Press, 2011.
- [24] Gallegos C. and García-Morales M., "Rheology of polymer-modified bitumens," in *Polymer Modified Bitumen: Properties and Characterisation*, 1st ed., Woodhead Publishing, 2011, pp. 197-237.
- [25] Mullins O. C., "The Modified Yen Model," *Energy Fuels*, vol. 24, p. 2179–2207, 2010.
- [26] Peralta J., Hillou L. and Silva H., "Rheological quantification of bitumen aging: definition of a new sensitive parameter," *Applied rheology*, vol. 20, no. 6, p. 63293, 2011.
- [27] RoadScience TM, "Distress Guide," [Online]. Available: <http://www.roadscience.net/services/distress-guide/>. [Accessed 10 May 2015].
- [28] Read J. and Whiteoak D., *The Shell bitumen handbook*, 5th ed., Thomas Thelddford Publishing, 2003.

- [29] F. Giuliani and Merusi F., "Advanced Rheological Characterization of Non-Reversible Deformation and Fatigue Behavior in Crumb Rubber Modified Asphalt Binders," *Road Materials and Pavement Design*, vol. 11, no. 1, pp. 197-224, 2010.
- [30] Polacco G., Berlincioni S., Biondi D., Stastna J. and Zanzotto L., "Asphalt modification with different polyethylene-based polymers," *European Polymer Journal*, vol. 41, pp. 2831-2844, 2005.
- [31] Kalantar Z. N., Karim M. R. and Mahrez A., "A review of using waste and virgin polymer in pavement," *Construction and Building Materials*, vol. 33, p. 55–62, 2012.
- [32] Mark J. E. , *Polymer data handbook*, Oxford University Press, Inc., 1999.
- [33] Polacco G., Vacin O. J., Biondi D., Stastna J. and Zanzotto L., "Dynamic master curves of polymer modified asphalt from three different geometries," *Applied Rheology*, vol. 13, no. 3, pp. 118-124, 2003.
- [34] Polacco G., Stastna J., Michalica P., Biondi D., Cantu M. and Zanzotto L., "Memory functions in polymer modified asphalts," *Journal of Applied Polymer Science*, vol. 104, p. 2330–2340, 2007.
- [35] Vlachovicova Z., Stastna J., MacLeod D. and Zanzotto L., "Shear deformation and material properties of polymer-modified asphalt," *Petroleum & Coal*, vol. 47, no. 3, pp. 38-48, 2005.
- [36] Polacco G., Stastna J., Vlachovicova Z., Biondi D. and Zanzotto L., "Temporary networks in polymer-modified asphalts," *Polymer engineering and science*, vol. 44, no. 12, pp. 2185-2193, 2004.
- [37] Vlachovicova Z., Wekumbura C., Stastna J. and Zanzotto L., "Creep characteristics of asphalt modified by radial styrene–butadiene–styrene copolymer," *Construction and Building Materials*, vol. 21, p. 567–577, 2005.

- [38] Merusi F., "Delayed mechanical response in modified asphalt binders. Characteristics, modeling and engineering implications," *Road Materials and Pavement Design*, vol. 13, no. 1, pp. 321-345, 2012.
- [39] Uddin W., "Viscoelastic characterization of polymer-modified asphalt binders of pavement applications," *Applied rheology*, vol. 13, no. 4, pp. 191-199, 2003.
- [40] Botella R., Pérez-Jiménez F.E. and Miró R., "Application of a strain sweep test to assess fatigue behavior of asphalt binders," *Construction and Building Materials*, vol. 36, p. 906–912, 2012.
- [41] Kraus Z. R., "The morphology of polymer modified asphalt and its relationship to rheology and durability," August 2008. [Online]. Available: <https://repository.tamu.edu/handle/1969.1/86003>. [Accessed 15 May 2015].
- [42] Kou C., Kang A. and Zhang W., "Methods to prepare polymer modified bitumen samples for morphological observation," *Construction and Building Materials*, vol. 81, p. 93–100, 2015.
- [43] Wegan V. and Nielsen C., *Microstructure of polymer modified binders in bituminous mixtures*, Denmark: Road Directorate, Danish Road Institute, 2001.
- [44] Costa L., Fernandes S., Silva H. and Oliveira J., "Study of the interaction between asphalt and plastic wastes in new polymer modified binders (PMB)," *Ciência & Tecnologia dos Materiais*, vol. 27, p. 01–80, 2015.
- [45] Tipton C. M., *Hydrocolloids*, Elsevier Science, 2000.
- [46] González O., Muñoz M., Santamaría A., García-Morales M., Navarro F.J. and Partal P., "Rheology and stability of bitumen/EVA blends," *European Polymer Journal*, vol. 40, p. 2365–2372, 2004.

- [47] Van der Vaart K., Rahmani Y., Zargar R. Hu Z. and Bonn D, "Rheology of concentrated soft and hard-sphere suspensions," *Journal of Rheology*, vol. 57, no. 4, pp. 1195-1209, 2013.
- [48] Rolón-Garrido V. H. and Wagner M. H., "The damping function in rheology," *Rheologica Acta*, vol. 48, p. 245–284, 2009.
- [49] Vinckier I., Moldenaers P. and Mewis J., "Relationship between rheology and morphology of model blends in steady shear flow," *Journal of Rheology*, vol. 40, no. 4, pp. 613-631, 1996.
- [50] Winter H.H and Chambon F., "Analysis of linear viscoelasticity of a crosslinking polymer at the gel point," *Journal of Rheology*, vol. 30, no. 2, pp. 367-382, 1986.
- [51] Winter H.H and Chambon F., "Linear viscoelasticity at the gel point of a crosslinking PDMS with imbalanced stoichiometry," *Journal of Rheology*, vol. 31, no. 8, pp. 683-697, 1987.
- [52] Larson Ronald G., *Structure and Rheology of Complex Fluids*, Oxford University Press, 1999.
- [53] Tucker C. and Moldenaers P., "Microstructural evolution in polymer blends," *Annual Review of Fluid Mechanics*, vol. 34, p. 177–210, 2002.
- [54] Winter H. and Mours M., "Rheology of polymers near liquid-solid transitions," *Advances in Polymer Science*, vol. 134, pp. 165-234, 1997.
- [55] Asaletha R. and et.al., "Stress-relaxation behavior of natural rubber/polystyrene and natural rubber/polystyrene/natural rubber-graft-polystyrene blends," *Journal of Applied Polymer Science*, vol. 108, p. 904–913, 2008.
- [56] Bucknell University, "An Introduction To Fourier Analysis," [Online]. Available: <http://www.facstaff.bucknell.edu/mastascu/eLessonsHTML/Freq/Freq4.html>. [Accessed 20 Jan 2015].

- [57] Morrison F., Understanding rheology, New York: Oxford University Press, Inc., 2001.
- [58] White K., Liu P. and Kalindindi S., "Rheological Methods," Society of Plastics Engineers: Texas A&M University, December 2010. [Online]. Available: <http://plastics.tamu.edu/node/270>. [Accessed 8 May 2015].
- [59] Macosko C. W., Rheology: principles, measurements, and applications, New York: Wiley-VCH, 1994.
- [60] Gotro J., "Rheology of Thermosets Part 2: Rheometers," Polymer Innovation Blog, 25 August 2014 . [Online]. Available: <http://polymerinnovationblog.com/rheology-thermosets-part-2-rheometers/>. [Accessed 8 May 2015].
- [61] Hillou L., "Hybrid carrageenans: isolation, chemical structure, and gel properties.," in *Marine Carbohydrates: Fundamentals and Applications, Part I*, Academic Press, 2014, pp. 18-40.

Appendix A. Trigonometric integrals

Properties of sine and cosine integrals used in to calculate the frequency components in a Fourier transformation, [56].

$$\int_0^T \sin(n \omega_0 t) \cos(m \omega_0 t) dt = 0 \quad \forall m \neq n \quad (\text{A-1})$$

$$\int_0^T \sin(n \omega_0 t) \sin(m \omega_0 t) dt = \frac{T}{2} \quad \text{iff } m = n \quad (\text{A-2})$$

$$\int_0^T \cos(n \omega_0 t) \cos(m \omega_0 t) dt = \frac{T}{2} \quad \text{iff } m = n \quad (\text{A-3})$$

Appendix B. Rheology basics

Rheology is the study of deformation and flow of matter. In other words, rheology studies the deformation and the flow of materials that behave in an interesting or unusual manner [57]. Considering this, stress and strain are the basis for rheological characterization. Flow is also an important tool for rheological characterization, and it can be seen as a time dependent form of strain.

There are two major types of deformation used in rheology: shear and elongation. In elongational mode the velocity gradient is parallel to the flow direction. In shear mode the velocity gradient is perpendicular the flow direction.

In the present work the bitumens were studied in shear deformation. Nevertheless, the pavement road deformation is a mixture of bi-axial elongation and shear. Shear deformation is schematically shown in Figure B-1. Hence, for the same change in length, δx , with smaller gaps, h , the deformation achieved is higher than with longer gaps.

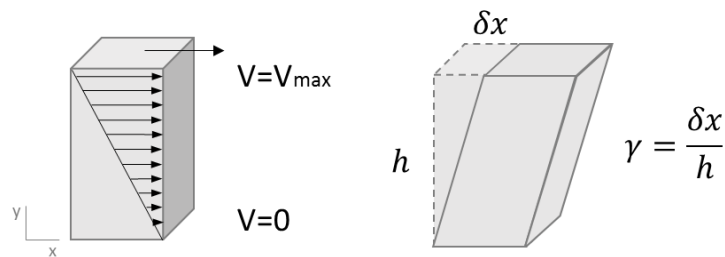


Figure B-1 Schematic representation of simple shear flow (left), and simple shear deformation (right).

There are different ways to achieve shear deformation. The common modes are drag flow and pressure driven flow, shown in Figure B-2. Drag flow was the mode used in this work. In drag flow, shear can be produced either in sliding plates or in rotational movement. The latter is the most commonly used.

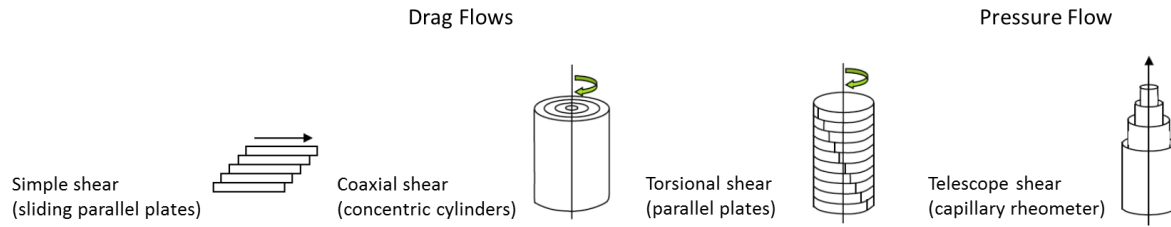


Figure B-2 Schematic representation of drag and pressure flows.

In rotational rheometry several geometries are available, as shown in Figure B-3. These different geometries are needed to avoid experimental pitfalls (slip, sedimentation, fracture, etc), and rheometer damage (overload, compliance, etc.).

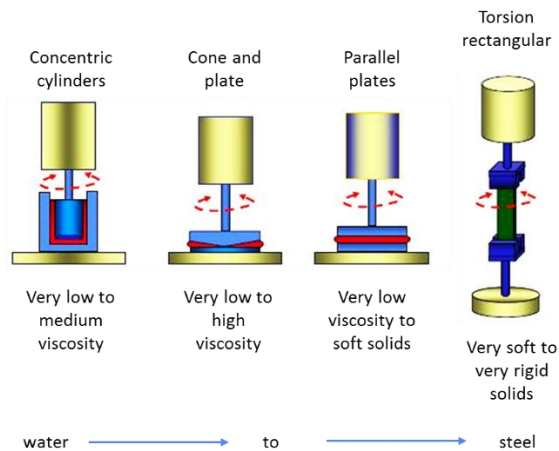


Figure B-3 Geometries available to study shear deformation in rotational rheometers, adapted from [58].

The choice of each geometry depends upon the type of sample to be studied. General guidelines are given in Figure B-3, and a detailed explanation can also be found in [8, 59].

The two parameters for rheological characterization (stress and strain) also set the type of excitation to be used in the sample. In this frame, there are either strain or stress driven shear rheometers, shown in Figure B-4. The choice of each rheometer depends upon the test to be carried out and the accuracy needed.

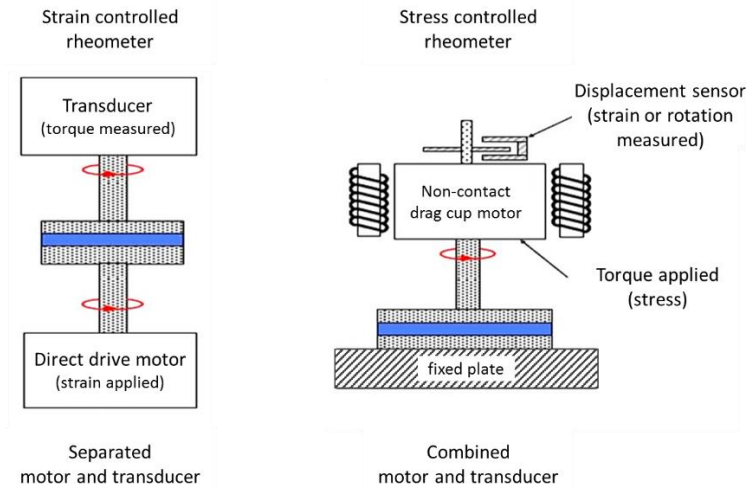


Figure B-4 Schematic representation of strain controlled and stress controlled rheometers, adapted from [60].

In terms of materials, the scope of rheology is located in between the two limiting cases of solid and liquid. An ideal solid is described by Hooke's constitutive equation that in shear deformation is given by

$$\sigma = G\gamma \quad (\text{B-4})$$

where σ is the shear stress, γ is the shear strain, and G is the Hooke modulus.

On the other hand, an ideal liquid is described by Newton's constitutive equation that in shear deformation is given by

$$\sigma = \mu\dot{\gamma} \quad (\text{B-5})$$

where $\dot{\gamma}$ is the shear strain rate, and μ is the Newtonian viscosity.

Nevertheless, most of the materials do not follow any of above equations. Instead, they have an intermediate behavior between solids and liquids, and such materials are called viscoelastic. There are several constitutive equations to describe such behavior nevertheless a common factor in all viscoelastic constitutive equations is the existence of at least one relaxation time, λ . This characteristic time is related to the balance between the viscous and elastic component of the sample, and it sets the limit on time above which the material will fully relax. For $t \gg \lambda$ the material will behave as Newtonian liquid, for $t \ll \lambda$ the material will behave as a Hookean solid. To quantify this balance in the time frame of an experiment the Deborah number was introduced by M. Reiner [7].

$$De = \frac{\lambda}{t} \quad (\text{B-6})$$

where t is the characteristic time of the experiment.

The De number is a dimensionless number that quantifies the state of relaxation of a material and \therefore the behavior it will display, i.e, for $De \gg 1$ the material is unrelaxed and it will have an elastic behavior, for $De \ll 1$ the material is fully relaxed and it will have a viscous behavior, meanwhile for $De \sim 1$ the material will have a viscoelastic behavior.

The relaxation time concept sets that all the rheological parameters ($\eta, J, G, G', G'', G^*, \delta$) of viscoelastic materials depend on time.

Probably the most common constitutive equation for viscoelasticity is the Maxwell model

$$\tau(t) + \lambda \dot{\tau}(t) = \eta \dot{\gamma}(t)$$

or

$$\tau(t) = \int_{-\infty}^t \left[G e^{-\frac{t-t'}{\lambda}} \right] \dot{\gamma}(t') dt' \quad (\text{B-7})$$

where λ, η, G are related by

$$\lambda = \frac{\eta}{G} \quad (\text{B-8})$$

Above equations are valid when either the applied strain or strain rate are small enough (infinitesimal) to not perturb the materials microstructure, and the deformation is said to be in the linear viscoelastic (LVE) regime. Hence, since the material microstructure is the same, in the LVE region it is possible to predict one material function (e.g. G, η, G', G'') from another. Besides, the material functions are geometry independent, i.e. different geometries will yield to the same result. In other words, in the LVE region the rheological parameters are intrinsic material functions of the system, and depend only on time (or frequency). Therefore, in the LVE region it is possible to make a consistency check in between the different measurements carried out, as well as to detect experimental pitfalls (slip, fracture, sedimentation, etc.) due to geometry or measurement conditions. The limiting strain (or stress) for the LVE region is different for each material, since different materials will allow more or less strain (or stress) prior to be deformed microstructurally.

For high enough applied strain (or strain rate) the microstructure is deformed, and the deformation is said to be in the non-linear viscoelastic region (NLVE). This means that the stress and the strain (or strain rate) are no longer linearly proportional, i.e. in LVE region $\sigma \sim \gamma$ or $\sigma \sim \dot{\gamma}$ while in NLVE region $\sigma \sim \gamma^2, \gamma^3, \gamma^4, \dots$. Therefore in the NLVE region the material parameters are strain dependent and can follow very different trends with respect to strain. This is because while the microstructure is being changed a wide variety of deformation modes are possible. While in the LVE region all the material functions are interrelated by means of the relaxation spectrum, in the NLVE region that is not possible anymore [8]. Therefore the predictive power that rheology had is somehow lost. However general trends will stand, i.e. a material that softens upon shear strain in a stress relaxation test will also soften when subjected to LAOS test.

Irrespective of the regime, linear or nonlinear, the viscoelasticity of a material can be studied in different shear deformation modes. In the following sections only shear stress relaxation and oscillatory shear will be described.

Appendix B.1. Shear stress relaxation

In stress relaxation a sudden step shear strain is imposed and kept constant during the test. Ideal elastic solids will respond immediately to the deformation and will generate a constant stress given by equation (B.1). On the other hand, ideal viscous liquids will not generate any stress, since in a liquid a stress is generated by means of flow due to the material's viscosity. Hence in a liquid, in the absence of flow no molecular friction can be generated and therefore no stress occurs.

In reality achieving a step strain is difficult due to motor limitations, as shown in Figure B-5. As a consequence the experiment will start to run from the instant at which a steady value of the deformation is achieved. This problem is less in strain controlled rheometers than in stress controlled rheometers, in which a loop between the stress applied and the strain commanded is needed. For this non-ideal excitation at earlier stages, solids will show a stress increasing in time and liquids will show a stress peak shown in Figure B-5. In between these extremes a viscoelastic material will show a steady stress up until the experiment time is less than the shortest relaxation time. Above that time the stress will decrease, because the material will start to relax. In the case of viscoelastic liquids the stress will decay to zero at $t \rightarrow \infty$, shown in Figure B-5. For viscoelastic solids a residual constant stress will remain even for $t \rightarrow \infty$, shown in Figure B-5. Measuring zero

stress is not feasible, and in most cases the experiment ends when the stress value achieves the resolution limit of the transducer.

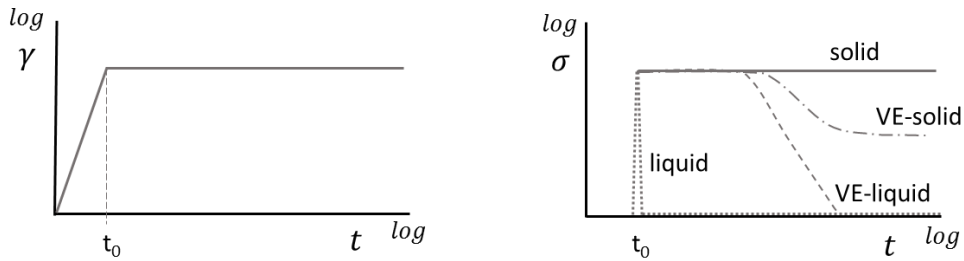


Figure B-5 Schematic representation of a stress relaxation experiment: strain imposed (left), canonical responses per material type (right).

The rheological material function related to the stress relaxation experiment is the linear stress relaxation modulus $G(t)$, defined by

$$G(t) = \frac{\sigma(t)}{\gamma_0} \quad (\text{B-9})$$

In the NLVE region, the rheological material function is the nonlinear stress relaxation modulus

$$G(t, \gamma_0) = \frac{\sigma(t, \gamma)}{\gamma_0} \quad (\text{B-10})$$

and in some cases it is possible to have a strain-time dependence separability which defines the concept of damping function, $h(\gamma_0)$.

$$G(t, \gamma_0) = G(t)h(\gamma_0) \quad (\text{B-11})$$

That accounts changes in the materials microstructure due to deformation [48]. The time strain separability concept implies that the effect of the strain affects equally all the relaxation process of the material.

In the case of polymer systems, it is considered that the time strain separability implies the existence of two independent decay mechanisms. One related to the probability of a polymer strand (Kuhn segment) to remain unrelaxed for a time difference $(t - t')$, and it is described by $G(t)$.

Another related to the probability of a polymer chain and all its strands to withstand a relative deformation without significant microstructural changes and it is assumed to be independent of strand size, and it is described by $h(\gamma)$ [48].

In other words the damping function can be seen as a survival probability that depends on deformation \therefore it is bounded between $1 > h(\gamma) > 0$ for strain thinning materials. Approaching one for very small strains and zero for large enough strains. Therefore departures from one quantify the material nonlinearity. The fitting of damping functions has been commonly done with either exponential or sigmoidal equations,

$$h(\gamma) = f_1 e^{-n_1 \gamma} + (1 - f_1) e^{-n_2 \gamma} \quad (\text{B-12})$$

$$h(\gamma) = \frac{1}{1 + a\gamma^b} \quad (\text{B-13})$$

being the latter the most used because the damping function of the Doi-Edwards model is of that kind [48].

Appendix B.2. Oscillatory shear

In this mode an oscillatory excitation (strain or stress) is input to the material. In the following, the discussion will be restricted to oscillatory strain but is also valid for oscillatory stress.

When an oscillatory shear deformation is input to the material

$$\gamma(t) = \gamma_0 \sin(\omega t) \quad (\text{B-14})$$

an oscillatory stress output is measured. In the linear regime, i.e. in the small amplitude oscillatory shear (SAOS) region, the stress response is sinusoidal

$$\sigma(t) = \sigma_0 \sin(\omega t + \delta) \quad (\text{B-15})$$

The stress measured can be delayed respect to the strain excitation, which is determined by the phase angle, δ (in phase $\delta = 0^\circ$, out of phase $\delta = 90^\circ$).

Analysis of such data can be done by means of a Fourier transform (FT), shown in section 2.1.

By means of FT the material functions of dynamic tests in SAOS are defined, meaning the storage modulus $G'(\omega)$ and the loss modulus $G''(\omega)$.

The stress response in equation (B.13) can be also represented by

$$\sigma(t) = \sigma_0 \sin(\omega t) \cos(\delta) + \sigma_0 \cos(\omega t) \sin(\delta) \quad (\text{B-16})$$

Dividing above equation by the strain amplitude

$$\frac{\sigma(t)}{\gamma_0} = \frac{\sigma_0}{\gamma_0} \cos(\delta) \sin(\omega t) + \frac{\sigma_0}{\gamma_0} \sin(\delta) \cos(\omega t) \quad (\text{B-17})$$

where the first term is in phase ($\sin(\omega t)$) and the second term is out of phase by 90° ($\cos(\omega t)$) with the strain input. The quantity $\frac{\sigma_0}{\gamma_0}$ has units of modulus \therefore in this frame the storage modulus G' and the loss modulus G'' are defined as

$$G' = \frac{\sigma_0}{\gamma_0} \cos \delta \quad (\text{B-18})$$

$$G'' = \frac{\sigma_0}{\gamma_0} \sin \delta \quad (\text{B-19})$$

where the storage modulus is the component in phase with the strain excitation, and the loss modulus is the component out of phase with the strain excitation.

In the FT space an alternative representation is given in terms of the complex modulus, G^* , and the phase angle, δ . All these material functions are related by means of

$$|G^*| = \sqrt{G'^2 + G''^2} \quad (\text{B-20})$$

$$\delta = \text{atan} \frac{G''}{G'} \quad (\text{B-21})$$

The detailed derivation of above equations in the FT space is given in section 2.1.

For a Newtonian liquid $\delta = 90^\circ \therefore G' = 0$ and for a Hookean solid $\delta = 0^\circ$ and $G'' = 0$. However, measuring zero quantities is difficult, therefore as a rule of thumb when δ is close to either 0° or 90° and higher differences than 2 OM between G'' and G' are present the smallest one can be considered as zero. For a VE material $0^\circ < \delta < 90^\circ \therefore$ none of moduli can be regarded as zero.

In dynamic mode there are several tests that can be performed, since frequency and strain amplitude are decoupled. The tests can be carried out either in the LVE region, namely small

amplitude oscillatory shear (SAOS) tests, or in the NLVE region, namely large amplitude oscillatory shear (LAOS) tests. The most commonly used tests are time sweep, strain sweep, and frequency sweep.

In time sweep the frequency and the strain amplitude are kept constant, and the evolution of the sample response over time is recorded. This test is helpful to determine the temporal changes of the sample at the given conditions of temperature, ω and γ_0 . By means of this test, it can be determined the maximum time a sample is stable in oscillatory shear, i.e. free from aging effects, fatigue, evaporation, gelling, etc.

In frequency sweep, the strain is kept constant and the frequency is changed. When the test is performed at strains inside the LVE region, the mechanical spectra of the sample can be determined. The mechanical spectra give information about the intrinsic viscoelastic properties over a wide range of frequencies, thus evidencing the possible relaxation processes which are inherently related to equilibrium structural properties of the quiescent material. It is thus critical to study samples which are not evolving on time, as the record of the spectra down to ω as small as 0.001 Hz can take more than 1000 s [61].

For a Maxwell model (equation (B.4)) the mechanical spectra is shown in Figure B-6. At $\omega \rightarrow \infty$, G' reaches a plateau and G'' tends to zero. At the frequency $\omega_c = 1/\lambda$ $G' = G''$ \therefore the crossover frequency defines the De number in oscillatory shear

$$De = \frac{\omega}{\omega_c} \quad (\text{B-22})$$

which by definition is 1 at the crossover. When $De \ll 1$ $G' \approx \omega^2$ and $G'' \approx \omega$, which in a log-log plot would yield a slope of 2 and 1 respectively. Even though few materials follow to the letter a Maxwellian behavior the limiting behaviors as well as the crossover meaning are good standards for data analysis.

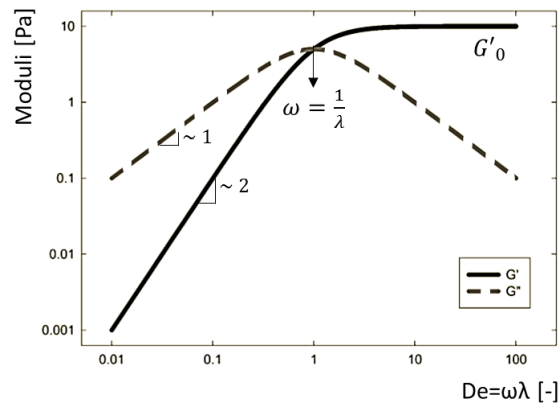


Figure B-6 Schematic representation of a Maxwell model mechanical spectra.

In strain sweep the frequency is kept constant and the strain amplitude is changed. For high enough strains the response will be non-linear. Hence, in the same tests linear and non-linear responses can be captured. Therefore, this test allows for the determination of LVE region. When strain sweep test is performed at high strains the non-linear viscoelastic response can be studied, this is the most common mode of LAOS tests. Nevertheless, in LAOS tests there is a wide variety of possibilities for testing and analysis, this was further discussed in section 2.1.

Appendix C. Extra Lissajous curves

Lissajous curves for $\delta \sim 57^\circ$ condition

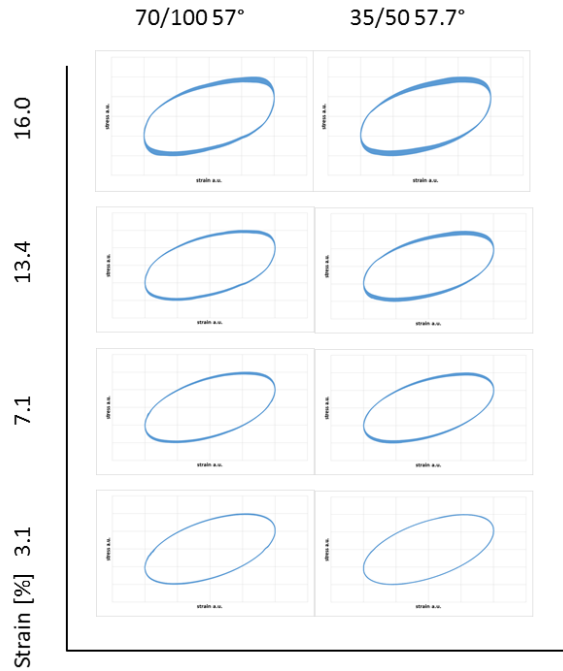


Figure C-1 Lissajous curves for binder samples at $\delta \sim 57^\circ$

Lissajous curves for $\delta \sim 50^\circ$ condition

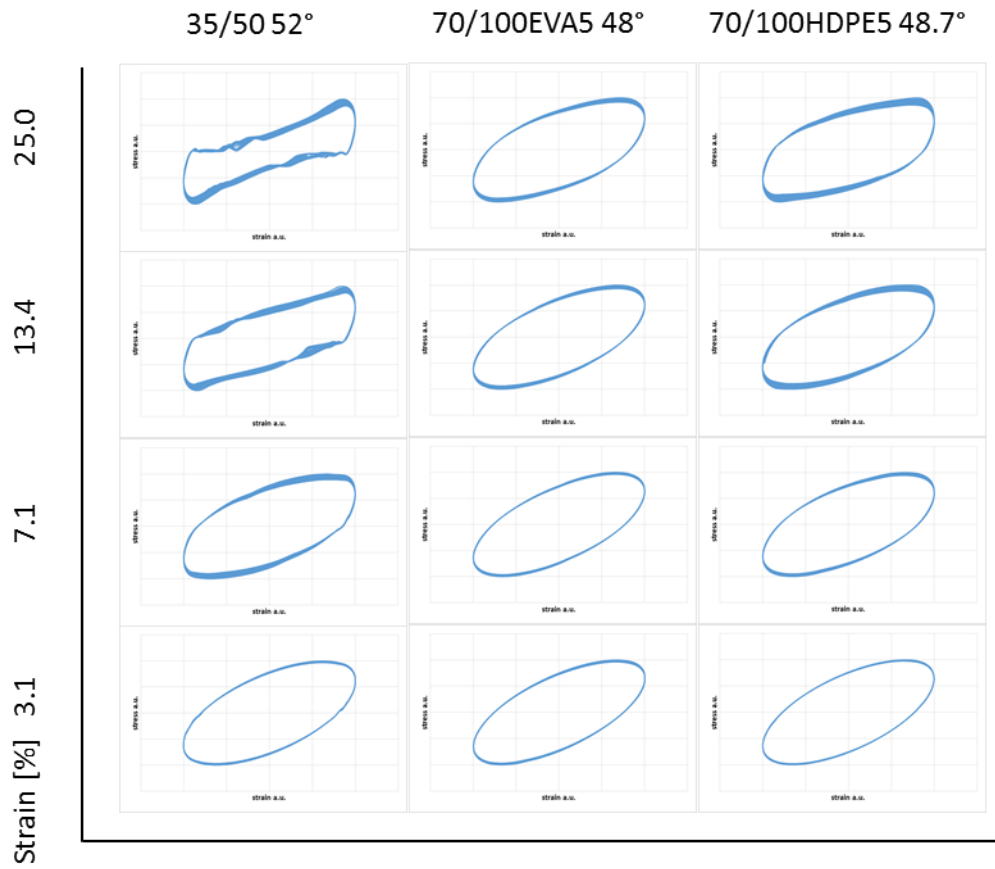


Figure C-2 Lissajous curves for binder samples at $\delta \sim 50^\circ$

Lissajous curves for $De=0.06$ condition

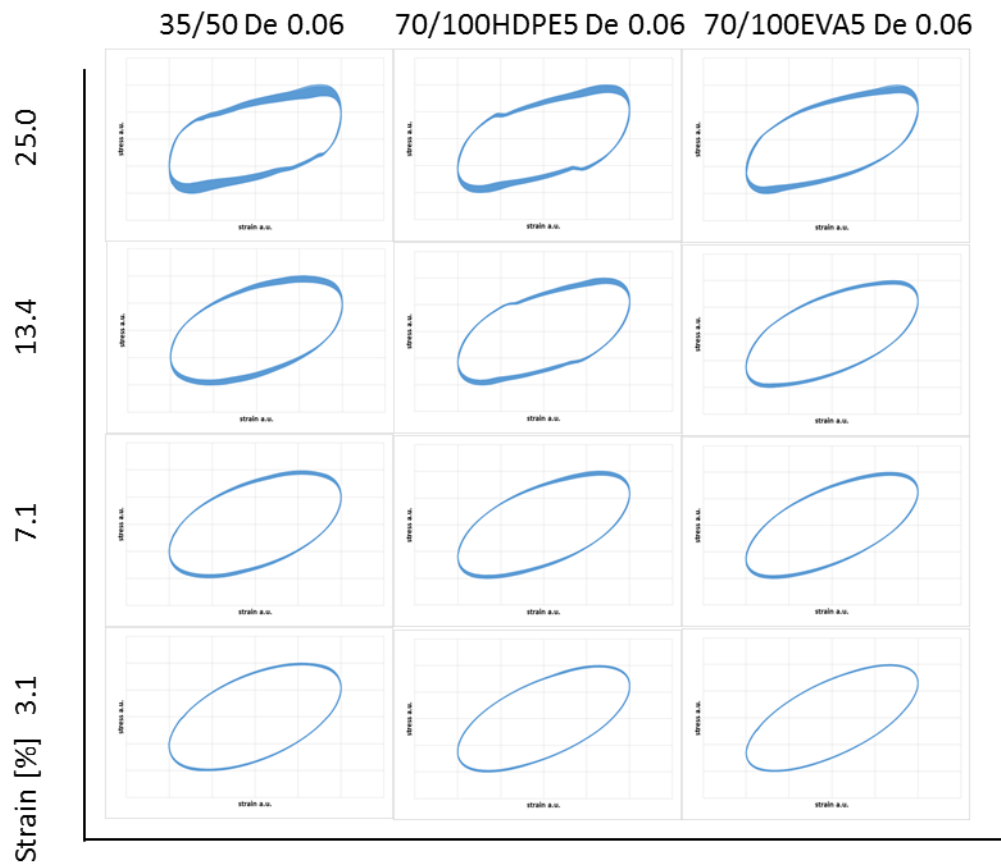


Figure C-3 Lissajous curves for binders at $De \sim 0.06$